Department of Construction Sciences
Solid Mechanics

ISRN LUTFD2/TFHF-15/5197-SE(1-153)

METHODOLOGY FOR MULTIDISCIPLINARY OPTIMIZATION OF VEHICLE SUSPENSION SYSTEMS

Master's Dissertation by

Martin Wollstad and Alexander Sallbring

Supervisor:
Mathias Wallin, Div. of Solid Mechanics

Assistant supervisor:
Pär-Ola Jansell, Altair Engineering

Examiner:
Håkan Hallberg, Div. of Solid Mechanics

Copyright © 2015 by the Division of Solid Mechanics
Altair Engineering, Martin Wollstad and Alexander Sallbring
Printed by Media-Tryck AB, Lund, Sweden
For information, address:
Division of Solid Mechanics, Lund University, Box 118, SE-221 00 Lund, Sweden
Webpage: www.solid.lth.se

Contents

1 Introduction **6**
- 1.1 Presentation of Altair Engineering . . . 6
- 1.2 Thesis Objective . . . 6
- 1.3 Division of Responsibilities . . . 7
- 1.4 Societal and Ethical Aspects . . . 7
- 1.5 Limitations . . . 7
- 1.6 Vehicle Suspension Systems . . . 9
  - 1.6.1 Double Wishbones . . . 9
  - 1.6.2 Strut & Coil Spring . . . 10
- 1.7 Survey of Similar Studies . . . 10

2 Theory **17**
- 2.1 Design of Experiments . . . 17
  - 2.1.1 Classical DOE . . . 19
    - 2.1.1.1 Full Factorial . . . 20
  - 2.1.2 Modern DOE Methods . . . 24
    - 2.1.2.1 Pseudo-Monte Carlo Sampling Methods . . . 24
      - 2.1.2.1.1 Basic pseudo-Monte Carlo . . . 24
      - 2.1.2.1.2 Stratified pseudo-Monte Carlo . . . 24
      - 2.1.2.1.3 Latin Hypercube . . . 25
        - 2.1.2.1.3.1 Latin Hypercube Algorithm . . . 26
    - 2.1.2.2 Quasi-Monte Carlo Sampling Methods . . . 28
      - 2.1.2.2.1 Hammersley . . . 30
        - 2.1.2.2.1.1 Hammersley Algorithm . . . 31
  - 2.1.3 Comparison of Modern DOE Sampling Methods . . . 34
  - 2.1.4 Main & Interaction Effect Calculation . . . 37

3 Method **42**
- 3.1 Multibody Dynamics (MBD) . . . 42
  - 3.1.1 Suspension Model . . . 42
  - 3.1.2 Load Cases . . . 43
    - 3.1.2.1 Kinematic Analysis . . . 44
      - 3.1.2.1.1 Loadcase 1: Parallel Wheel Travel . . . 44
      - 3.1.2.1.2 Loadcase 2: Roll . . . 45
    - 3.1.2.2 Elastokinematic Analysis . . . 46
      - 3.1.2.2.1 Loadcase 3: Lateral Force (WC) . . . 46
      - 3.1.2.2.2 Loadcase 4: Lateral Force (CP) . . . 47
      - 3.1.2.2.3 Loadcase 5: Longitudinal DS Force (WC) . . . 48
      - 3.1.2.2.4 Loadcase 6: Overturning Moment (WC) . . . 49
      - 3.1.2.2.5 Loadcase 7: Aligning Torque (WC) . . . 50
    - 3.1.2.3 Reaction Force Distribution Analysis (NVH) . . . 51
      - 3.1.2.3.1 Loadcase 8-10: Static Loads . . . 51
    - 3.1.2.4 Max Force Analysis (Strength & Weight) . . . 52

3.1.2.4.1 Loadcase 11-13: Max Loads . . . 52
3.1.3 Responses . . . 53
3.1.4 Rating . . . 57
3.1.4.1 Weighted Absolute Mean Deviation . . . 57
3.1.4.2 Design Load Response Target Factor . . . 58
3.1.5 Weighted Sum . . . 59
3.2 Experiment Setup in `HyperStudy` . . . 61
3.2.1 Design Variables . . . 61
3.2.2 Simulation Responses . . . 67
3.2.3 Design of Experiments . . . 69
3.2.3.1 Design Variables . . . 70
3.2.3.2 Design of Experiment Responses . . . 70
3.2.4 System Optimization . . . 71
3.2.4.1 Design Variables . . . 71
3.2.4.1.1 Design Space Reduction Method (DSRM) . . 71
3.2.4.2 Optimization Responses . . . 73
3.2.4.3 Constraints . . . 73
3.2.4.4 Objectives . . . 73
3.2.4.5 Optimization Methods . . . 74
3.2.4.5.1 Global Response Surface Method (GRSM) . . 74
3.2.4.5.2 Multi-Objective Genetic Algorithm (MOGA) 75
3.3 Investigations . . . 76
3.4 Structural Optimization . . . 78
3.4.1 Topology Design Space . . . 78
3.4.2 Finite Element Setup . . . 79
3.4.2.1 Elements . . . 79
3.4.2.2 Materials . . . 80
3.4.2.3 Loads Cases . . . 80
3.4.2.3.1 Stress Constraints . . . 80
3.4.2.3.2 Compliance Constraints . . . 81
3.4.2.4 Objective . . . 83
3.4.2.5 Design Variables . . . 83

4 Results **85**
4.1 Design of Experiments . . . 85
4.2 System Optimization . . . 94
4.2.1 Investigation 1: Constraints . . . 95
4.2.2 Investigation 2: Objectives . . . 98
4.2.3 Investigation 3: Optimization Algorithm . . . 101
4.2.4 Investigation 4: Remove Design Variables . . . 104
4.2.5 Investigation 5: DSRM . . . 107
4.2.6 Investigation 6: Initial Design Space . . . 112
4.2.7 Optimal Designs . . . 117
4.3 Structural Optimization . . . 119

5 Methodology **125**
5.1 Initial Phase . . . 127
5.2 Setup Phase . . . 127
5.2.1 Response Script . . . 127
5.2.2 Experimental Software . . . 128
5.3 Concept Screening Phase . . . 129
5.3.1 Investigate Potential Performance . . . 129
5.3.2 Evaluate Conceptual Design . . . 130
5.4 System Optimization Phase . . . 130
5.5 Structural Optimization Phase . . . 130

6 Conclusion **132**

Appendix A Design of Experiments **135**
A.1 Main Effects . . . 135
A.2 Normalized Main Effects . . . 137
A.2.1 Wheelbase Change . . . 139
A.2.2 Vertical Wheel Travel . . . 140
A.2.3 Roll Steer . . . 141
A.2.4 Roll Camber . . . 142
A.2.5 Lateral WC Compliance . . . 143
A.2.6 Lateral TP Compliance . . . 144
A.2.7 Lateral TP Steer . . . 145
A.2.8 Lateral TP Camber . . . 146
A.2.9 Longitudinal Compliance . . . 147
A.2.10 Longitudinal Steer . . . 148
A.2.11 Longitudinal Camber . . . 149
A.2.12 Overturning Moment Steer . . . 150
A.2.13 Overturning Moment Camber . . . 151
A.2.14 Aligning Torque Steer . . . 152

Appendix B `MATLAB` Scripts **153**
B.1 MATLAB Code: Static 1 - stat1.m . . . 153

Acknowledgement

Pär-Ola Jansell (Altair Engineering) and his team for supervising this master's dissertation. Krister Olsson (Department of Energy Sciences) for providing technical papers on the subject. Lucas Börjesson and Oscar Eklund (LeanNova) for providing expertise on suspension analysis.

Abstract

A manual iterative process is often used in the design process of vehicle suspension systems. This thesis aim to develop a methodology for multidisciplinary optimization of vehicle suspension systems, which can be used to introduce an optimization driven process into the design process of vehicle suspension systems.

A Multibody Dynamics (MBD) model of a Strut & Coil Spring suspension system will be used as a test subject.

The methodology developed includes concept screening of suspension systems, multi-objective system optimization and weight reduction using structural optimization. The initial concept screening will provide guidance to selection of important design variables. Ride comfort, handling performance, and noise, vibration, and harshness (NVH) are optimized in the multi-objective system optimization, using the Multi-Objective Genetic Algorithm (MOGA) combined with a Design Space Reduction Method (DSRM).

1 Introduction

1.1 Presentation of Altair Engineering

Altair Engineering was founded in 1985 and is headquartered in Troy, Michigan, with regional offices in 22 countries and more than 2000 employees world wide. The Swedish regional offices are located in Lund, Gothenburg, and Stockholm, with main focus on software support, consulting business and sales. Over the years Altair has developed simulation software to assist engineers in different fields when it comes to simulate and optimize designs, processes and decisions. Altairs software suite HyperWorks can be used in a wide range of applications and is built with an open-architecture that is designed to easily interact with other simulation software on the market.

1.2 Thesis Objective

The main objective of this master's thesis is to develop a CAE[1]-methodology for incorporating optimization into the development process of vehicle suspension systems. Nowadays the development process for suspension systems consist of a trial and error approach with aid of the CAE software. In other words, a design is generated with help of engineers' experience and good guesses, and then simulated and validated with the CAE software. If the generated trial design fails to meet the requirements the process must start over again. This process is iterative and continues until the suspension meet the established requirements. By introducing a CAE-methodology that incorporates optimization into the design process the costs and development time can be reduced as well as the performance improved.

The methodology developed in this thesis will be tested on a multibody dynamics model (MBD) of a strut & coil spring suspension system. Brief descriptions of the strut & coil spring suspension system and the double wishbones suspension system, which is commonly used in similar studies, are given in Section 1.6. The optimal solution for the suspension system is to be found by finding the optimal positioning of the attachment points and the optimal stiffnesses in the bushings. These are the design variables to be used. A variety of load cases will be simulated and a set of responses will be recorded at each load case. These responses are the ones to be optimized, and their data needs to be converted into a format suitable for the optimization algorithms. The responses are divided into the objectives Ride, Handling, and NVH[2].

[1] Computer-Aided Engineering.
[2] Noise,Vibration and Harshness.

The first step is an analysis of the suspension system, using Design of Experiment (DOE) methodology, which will be used for a suspension concept screening and an investigation of the importance of the design variables. The second step is the system optimization where different optimization methods and approaches will be investigated. The last step is a structural optimization of a suspension component. Together these steps aim to satisfy the multidisciplinary requirements of ride comfort, handling performance, reduced NVH, and low weight.

The main goals of this master thesis are to:

- Develop a methodology for integrating system Optimization into the design process of vehicle suspension systems.
- Establish a method for analysing the response data and converting it into a suitable format.
- Establish a method for weighting and combining a large quantity of objectives into a single objective.
- Perform a concept screening and investigate the importance of the design variables.
- Perform a system optimization.
- Perform a structural optimization.

1.3 Division of Responsibilities

Most sections where written by both authors. However, Sallbring surveyed similar studies and researched Design of Experiments theory. Sallbring was responsible for extracting the results from the Design of Experiments results. Wollstad was responsible for the multibody dynamics model and running the system and the structural optimizations.

1.4 Societal and Ethical Aspects

No societal and ethical aspects have been identified in this Master's thesis.

1.5 Limitations

This master's thesis will be limited to a non driven rear axle strut & coil spring suspension. The developed methodology will not be tested on other suspension systems.

The volume of the suspension components and the rear axle are not taken into account, thus it will be possible to place some attachment points in a way that would lead to intersection between these components. The design space is mainly limited by

the vehicle's chassis and the wheels.

The vehicle body and suspension components will be treated as rigid bodies, thus deformation will not be taken into account during the simulation. One can assume the deformation of the vehicle body and suspension components are much smaller than those experienced in the bushings. The error introduced by this assumption will be investigated.

The joints in the MBD model will be assumed to be frictionless, hence there will be no energy losses during the simulations.

The loads are applied slow enough for damping to have no effect, and thus are static in practice. The damping of the bushings and the damper are therefore neglected and are not used as design variables.

The spring stiffness is much lower than the bushing stiffnesses and is therefore assumed to have little effect on the results. The spring stiffness is neglected and is not used as a design variable.

1.6 Vehicle Suspension Systems

A vehicle's wheel suspension transmit forces from the road to the chassis while at the same time constraining the wheel's degrees of freedom to two or three. The wheel suspension's purpose is to give the vehicle good driving performance and comfort with a minimum of transmitted vibrations and noise. At the same time the suspension must be light in weight, cost effective, robust, easy to mount and maintain, and have an adequate life-span.

1.6.1 Double Wishbones

The double wishbones is an independent suspension system. The wheels can move independent of each other and disturbances are not directly transmitted between the wheels. The double wishbones provides more free design parameters than the strut & coil spring suspension system. It is very common on sports and racing cars, such as Formula 1 cars, since it's relatively easy to tune the suspension kinematics. Due to the many components the service time is long and the weight is heavy. Figure 1 shows a typical double wishbones suspension setup [6].

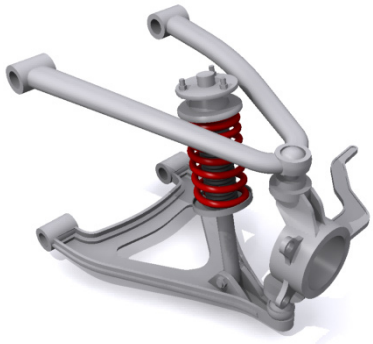

Figure 1: Double Wishbones suspension system [10].

1.6.2 Strut & Coil Spring

The strut & coil spring suspension system is a variation of the MacPherson strut suspension. The advantage of this independent suspension system is its simplicity. It is similar to the double wishbones in construction but require less space and weight less but provides slightly less control over the design parameters. This type of suspension is common in modern passenger cars. Figure 2 shows a typical MacPherson suspension setup [6].

Figure 2: MacPherson suspension systems [10].

1.7 Survey of Similar Studies

The problem formulation in [13] is basically a Multi-Objective Optimization of a MacPherson front suspension. Typical kinematic and compliance (K&C) characteristics for the suspension system are optimized. A set of load cases are simulated where the rate of change in the MBD outputs for steer angle, roll center height, lateral- and longitudinal stiffness is measured. These objectives are chosen since they have a great impact on the ride and handling performances. The attachment points of the MacPherson suspension are used as design variables in the optimization. In total six attachment points are used and each point have three translational coordinates, in total 18 design variables.

The problem is initially approached by conducting a sensitivity analysis of the system in order to get a better understanding of the characteristics and a hint on how to improve the suspension system. The sensitivity analysis requires a DOE to be performed. The chosen DOE method is the orthogonal array in three levels. The design space is defined as the baseline value $\pm 10\,\mathrm{mm}$ for each design variable. The results from the sensitivity analysis indicates that it would be possible to divide the problem into two sub-problems where simulations for kinematic and compliance characteristics can be separated. The design variables which have a great impact on the kinematic characteristics does not effect the compliance characteristics and vice versa.

The next step in the process is the optimization, and the setup of the objectives and the constraints. Since it is a multi-objective optimization it is vital to find a way to normalize the different responses and capture them in a good manner with an objective function. One of the difficulties is the different responses, which should either be minimized, maximized or reach a target value. [13] use different functions to normalize the responses dependent on the behavior. The different target values used in the objective formulation are found by benchmarking of competitor's vehicles.

Two separate optimizations are performed, one which optimizes the kinematics in the suspension and one which optimizes the compliance. These optimizations use different sets of objectives and constraints. The optimization algorithm used is the Sequential Two-point Diagonal Quadratic Approximate Optimization(STDQAO). The STDQAO is suited for nonlinear problems and uses a sequential approximate optimization technique. The computation time for the MBD model was affordable and therefore a RSM[3] was not used.

The results from the optimization in [13] is shown in Table 1. Real values are not published due to confidentially. Target Values, Optimized Result, and Final Design are presented in reference to the initial design.

Nbr.	Initial	Target	Optimized Result	Final Design
1	100%	200%	167%	200%
2	100%	154%	157%	185%
3	100%	0-37%	37%	-1%
4	100%	155%	162%	214%
5	100%	>100%	100%	98%
6	100%	>100%	97%	115%
7	100%	<93%	93%	98%
8	100%	minimize	50%	84%

Table 1: Final result.

The main objective for this research was to find out if it was possible to improve both K&C characteristics in a suspension system. Previous work done in this field has, according to [13], only treated the kinematics characteristics in the optimizations. Previous work has also been limited when it comes to the number of kinematics objectives. Is is clear that the K&C characteristics of the initial design can be improved by utilizing a multi-objective optimization.

[1] optimizes a few kinematic characteristics in two load cases. As in [13] the suspension to be optimized is a MacPherson front suspension, however the problem is approached somewhat differently. [1] investigates the under-steer and over-steer characteristics using two load cases which treats the cornering behavior of a full vehicle.

[3]RSM = Response Surface Method

The turning radius is constant and the velocity is increased in the first load case, while the velocity is constant and the turning radius is tightened in the second load case. A complete vehicle model in `Adams` is used. This model includes the steering system and front and rear suspension systems. In most MBD model bodies are treated as rigids, but in [1] FEM models for the rear axle and the anti-roll bar in the front suspension are imported in order to be able to treat them as flexible parts.

The design variables in this investigation are the coordinates for some of the attachment points, the stiffness for the anti-roll bar, the spring, some connector bushings and tires, and the damping for the dampers. In total 15 design variables are used. Eight responses which are tightly connected to a cornering manoeuvre of a vehicle is used in the investigation. The responses are:

$\mathbf{R}_1 =$ Yaw velocity overshoot

$\mathbf{R}_2 =$ Yaw velocity rise time

$\mathbf{R}_3 =$ Lateral acceleration overshoot

$\mathbf{R}_4 =$ Lateral acceleration rise time

$\mathbf{R}_5 =$ Roll angle steady state response

$\mathbf{R}_6 =$ RMS of the under-steering coefficient

$\mathbf{R}_7 =$ RMS of the steering torque

$\mathbf{R}_8 =$ RMS of the steering sensitivity

In the optimization one objective function is used, which is a linear combination of the eight responses. The objective function represent the handling behavior of the vehicle and is given by:

$$F = \sum_{i=1}^{8} W_i R_i \tag{1}$$

where W_i is a weight value for each response R_i. In [1] 0.5 is used for W_{1-4} and 1 for W_{5-8}, the weight value is an indication of the importance of one response for the handling behavior. The higher value the of the objective function the better is the handling behavior.

A sensitivity analysis is performed using the DOE method fractional factorial design. The main effects from the sensitivity analysis indicates that only 10 out of 15 design variables have a great influence on the responses. For the optimization a Response Surface Method (RSM) model with the 10 most influential design variables is used. By using a second-order approximation an optimized design which had the objective value of $y_{optimal_{RSM}} = 4.2412$ is found. The approximated result is validated against a real MBD simulation where an objective value of $y_{optimal_{MBD}} = 4.2373$ is obtained.

Hence, the objective values show conformity. The initial value for the objective was $y_{initial} = 2.6469$, and it is evident that the handling performance was increased.

A lot of research has been devoted to the design optimization of vehicle suspension systems, and there are several papers in this area that suggests different techniques and approaches for finding the optimal design. However, according [4] most of these approaches are based on deterministic optimizations. By introducing robust design in the optimization process of the vehicle suspension system it would be possible to ensure the overall quality of the suspension design due to manufacturing errors etc. [4] merges the robust design and vehicle suspension optimization together. The results are promising and the robustness and performance of the design was improved. The improvement in robustness became larger if greater manufacturing errors were introduced in the simulation.

Robust design is introduced for a Double Wishbone suspension system. In a Double Wishbone design it is vital that the attachment point coordinates and the angles between different points are setup in a correct manner for the guiding mechanism, to ensure good performance of the suspension system. The suspension is modelled and simulated in the `ADAMS` software with the following limitations:

1. The composition members of the suspension are rigid body and the elastic deformation is ignored.
2. Rigid connection between the various components is used and ignores internal clearance and friction.
3. Only consider the ground roughness, without regarding the dynamic factors.
4. Add an incentive on the test platform to simulate the unevenness of the ground; the tires are always in contact with the test bench.

In the robust design optimization the position of twelve attachment points are optimized. Since each attachment point has three translational coordinates, the total number of design variables then becomes 36. The optimal position for these points are found for one load case, namely a displacement in the lateral direction at the tire patch. During the lateral displacement two responses are evaluated, which are the toe angle and wheel center displacement.

A sensitivity analysis is performed using the Latin Hypercube DOE method. The main effects from the sensitivity analysis indicates that 12 of the design variables have great influence. These design variables are used to create a Kriging RSM model. The Kriging model is fitted to the Latin Hypercube data and verification of the model yields a r-square value[4] of 0.87, thereby the RSM can be used instead of the MBD

[4] r-square is a measure of the conformity between the RSM model and random points in the design space and take values in the range of [0 1], values close to 1 indicate that a good conformity exist.

model in the robust design optimization.

For the robust design the 12 most significant design variables are used, manufacturing errors are introduced and the mean and variance of the two responses is studied. The algorithm used in the optimization is the PSO [5] that utilize an evolutionary technique. In comparison to other evolutionary algorithms the PSO generations do not compete in order to survive to the next step in the optimization. The PSO is based on the social behavior of a flock of birds. The algorithm moves the whole generation in the direction of the best solution, the direction and velocity are calculated from the objective function. As mentioned before the optimization showed promising results, the maximum deviation of the responses was reduced with 52 percent.

According to [2] the typical design process for vehicle suspension systems contains some issues. In the first stage of the design process one normally set the performance targets for the suspension system by benchmarking existing vehicles. The performance targets are typically the steer, camber, and caster angles of the wheel. These characteristics have a great influence on how the vehicle behave when driven. In other words, they define the handling stability, ride comfort, and life time of the tires. These targets are set individually for the front and rear suspension without considering how they perform in a unified vehicle system. [2] point out that the targets for the suspensions should be set in the perspective of the whole vehicle. In the end, it is the vehicle dynamics that should be optimized, and the vehicle dynamics are dependent on both the front and rear suspensions.

[2] introduced the "Target Cascading Method" into the vehicle suspension design process. This method is supposed to combine the ordinary suspension design with vehicle dynamics design by utilizing multi-level simulations. It is divided into the following steps:

Step 1: Design targets for vehicle
Define design targets for the vehicle system, typically Ride, Handling, NVH, and durability are considered.

Step 2: Optimization vehicle level
At vehicle level the design variables are typical suspension characteristics such as camber, toe, caster, wheelbase change, and track-width change. The objectives in the optimization is to find suitable design variable values that satisfy the target values defined in step 1 for the vehicle system.

Step 3: Optimization suspension level
At suspension level the design variables are the attachment point coordinates and bushing stiffnesses. The design target at suspension level are the design variables values from step 2, the typical suspension characteristics. The objective in the optimization is to minimize the discrepancy of the design variable values at vehicle level and the design target at the suspension level.

[5] PSO = Particle Swarm Optimization

Step 4: Construct vehicle model

In the fourth step a complete complete vehicle model is constructed by assembling the front&rear suspension that was found in step 3.

Figure 3 visualizes how the target values are cascaded between system levels. With this approach the target values for the next level are defined by the design variables in the previous level, as described in the steps above. The optimized front & rear suspension are ensured to work together in a complete vehicle when the Target Cascading Method is utilized.

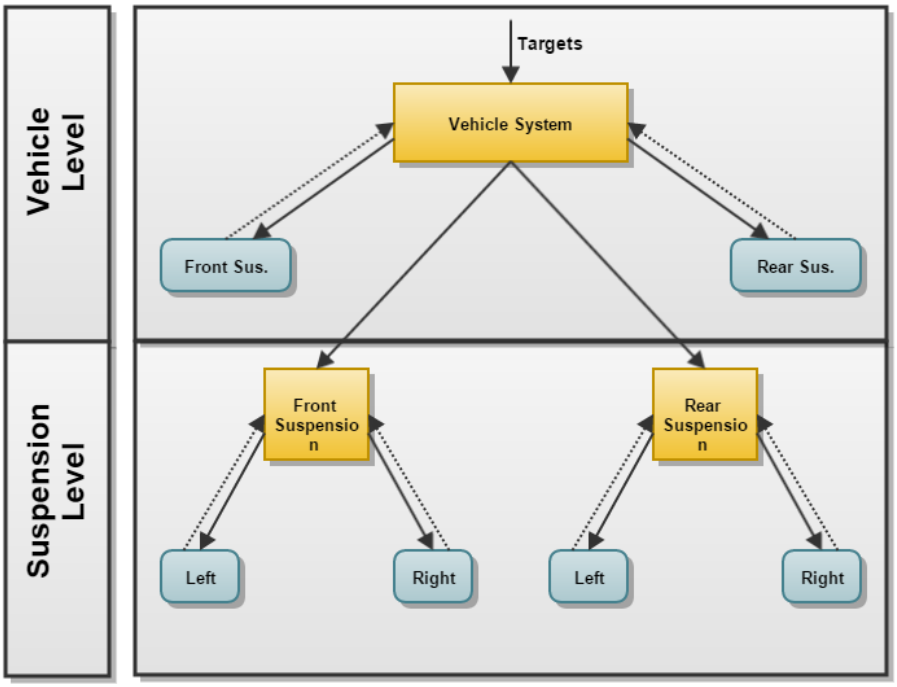

Figure 3: Target Cascading Method for vehicle suspension design.

When it comes to modeling the vehicle system [2] implements a method known as TEKS[6], the TEKS model use the kinematic and compliance characteristics of the suspension instead of actual kinematics data from the MBD model at suspension level. The TEKS model is based on the assumption that the characteristics of the suspension can be modeled as an elastic system which connects the wheel body to the wheel carrier. The TEKS model can therefore be modeled as a component that has 2, respectively 3, degrees of freedom (DOF) for translation and rotation. The vehicle body is modeled as a rigid body with 6 DOF and the complete vehicle model end up with 15 DOF.

At the suspension level the goal is to find a geometrical design which fulfill the suspension characteristics cascaded from the vehicle system. Therefore it is necessary

[6]TEKS = Tabular Elastic-Kinematic Suspension

to be able to change the geometrical setup of the suspension in terms of attachment point coordinates and bushing stiffnesses, and at the same time be able to evaluate the suspension characteristics for each design. This is solved by using a `ADAMS` MBD model. In the investigation a Double Wishbones suspension system is used for the front and a Multi-link suspension system for the rear suspension. The total number of design variables for the two different suspensions systems ends up at 54 respectively 73. The design space range for the design variables is set to $\pm 20\%$ from the initial design. The systems are subjected to four different load cases, bump and roll, which treats kinematics, and lateral and longitudinal force, which treats compliance characteristics for the suspensions.

A DOE is performed and RSM models are created for the different systems at vehicle and suspension level. The RSM models was used in the Target Cascading Method approach described above, and the end results are promising. The handling and ride performance was improved by 37% respectively 16% from the initial design. [2] conclude that the suggested design method is both effective and systematic.

2 Theory

2.1 Design of Experiments

Engineers and scientists frequently conduct experiments and simulations in order to get a basic understanding of how things work. The subjects to these studies are called systems. A general system consist of design variables, inputs that are allowed to change, and controllable and uncontrollable noise factors. The measured results of a conducted experiment are called responses. These responses are influenced by the design variables and the noise factors. Figure 4 shows a general system. The design variables can be changed in order to find a certain desired response. As more experiments are conducted, the understanding of the influence on the responses by the design variables grows. In order to find the true relationship between the design variables and responses, it is necessary to reduce the influence of the noise factors. A typical uncontrollable noise factor is the relative humidity in the experiment environment, hence it is necessary to measure the relative humidity and thereafter find the influence it has on the responses and adjust the measured values. The influence of a controllable noise factor is reduced by using proper experimental planning. For example, in a metallurgy experiment a typical controllable noise factor would be the difference between batches of raw material. The possible variance of material properties in the batches is controllable if a proper experiment plan is used.

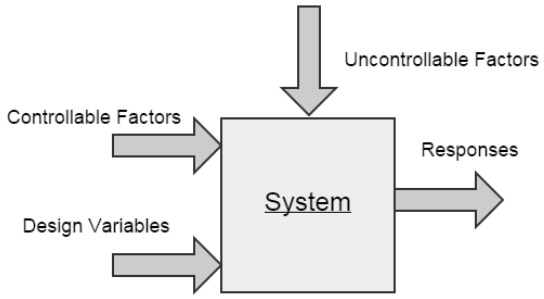

Figure 4: A general system.

Thus, the question arise; how should one generate a plan for the experimental setups, called sampling points, in order to minimize the influence of the controllable noise factors? Moreover, how can one ensure that the results from the experiments contain the correct information about the system if a certain set of sampling points are used? And at the same time, one would like to use the fewest number of sampling points as necessary to find this information. The methodology of how to generate the sampling points is known as Design of Experiments (DOE). The appropriate way to use this methodology is dependent on the system that is investigated. Nowadays, several methods exist and each method is suited for different tasks. At first a brief introduction of common mistakes regarding DOE will be presented below, thereafter the differences between the classical and modern DOE methods are explained.

Without any prior knowledge of how to design plans for experiments it is easy to begin using the ”best-guess” or the ”one-factor-at-time” method without knowing the drawbacks and pitfalls. According to [11] these two methods have been widely used by engineers in the industry with the result that incorrect conclusions have been drawn. For instance the ”best-guess” DOE method is based on the engineer's prior knowledge and experience of the system. This method can work reasonable well but the engineer will have to keep on guessing until an appropriate experiment setup which yield the desired results is found. This method is an iterative process that can be very time consuming and it is difficult to estimate the time needed beforehand. Another drawback is that the whole design space, all possible combinations of the design variables, is not explored properly. There might be unexplored solutions which perform better than the found ”best-guess” solutions. When it comes to the ”one-factor-at-a-time” method the main idea is to establish a baseline model for the system. Thereafter, one design variable is changed in each experiment whilst the others are held constant. By doing so it is possible to extract the main effects, how one design variable is effecting a certain response. However, the interaction effects can not be found with this method. An interaction effect is the combined effect of two or more design variables on a certain response. In other words, the design variables are dependent and might have no effect on the response unless they are both changed in a certain way. Without the interaction effects it is likely that the conclusions drawn are incorrect.

The aforementioned methods are not effective when it comes to fully exploring the design space and getting a complete understanding of the system. The DOE methods that are generally accepted by the research community nowadays are based on the principle that all design variables are varied at the same time. Hence, the interaction effects are taken into account in these methods. However, the means by which these methods generate the sample points in the design space differ greatly [11]. Although, it is possible to divide the different methods into two categories, classical and modern DOE methods. The first has a tendency to place the sample points at the boundaries of the design space, whilst the latter place sample points in the interior of the design space. The classical DOE methods were developed for laboratory and field experiments that possesses random error sources, whilst modern DOE methods are specifically designed for use with deterministic computer simulations. Another feature that distinguish the modern from the classical DOE methods are that they allow the design variable values to not be uniformly distributed. The classical methods are based on the assumption that the likelihood of a design variable to take on any value between the lower and upper bound is identical, whilst the modern methods can be used with different probability distributions, not only the uniform. The classical and modern methods share common ground, in the sense that they generate independent sample points. Hence, they allow simultaneous evaluation of several sample points, which is advantageous in modern computer simulations where parallel processing can be utilized [3].

2.1.1 Classical DOE

Most classical DOE methods are based on the assumptions that the general trend of the true response is known and a measured response quantity contain a random error term,

$$y_m(x) = y_t(x) + \varepsilon \tag{2}$$

where x is the design variable, y_m is the measured response, y_t is the true response and ε is the random error term. The influence of the random error terms ε_1 and ε_2 at the measured responses $y_m(x_1)$ and $y_m(x_2)$ is visualized in Figure 5.

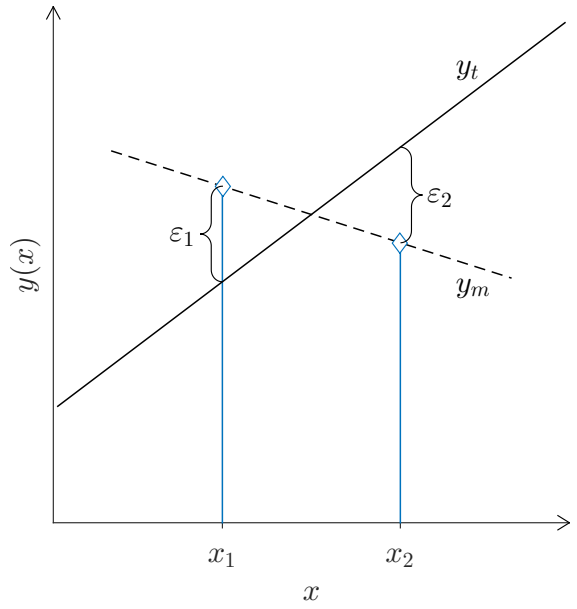

Figure 5: Influence of the random error terms ε_1 and ε_2.

The classical DOE methods are designed to place a fixed number of sample points in the design space in such a way that the influence of the random error term at each sample point is minimized in the subsequent computations, where the trends in the response data are estimated. A generic approximation of the response value is given by:

$$\hat{y}(x) = f\big(\mathbf{x}_s, y_m(\mathbf{x}_s)\big) \tag{3}$$

where $\mathbf{x}_s$ is a vector of the sample points, $y_m(\mathbf{x}_s)$ is the measured response at the sample points, f is some function, and $\hat{y}(x)$ is the approximate response value at an arbitrary design point x. The influence of the random error term in the approximation model (Eq. (3)) is minimized by placing the sample points as far away from each other as possible. Thus, they are placed at the boundaries of the design space. Figure 6 shows how the influence of the random error terms ε_1 and ε_2, with maintained magnitudes, is reduced by placing x_1 and x_2 far away from each other.

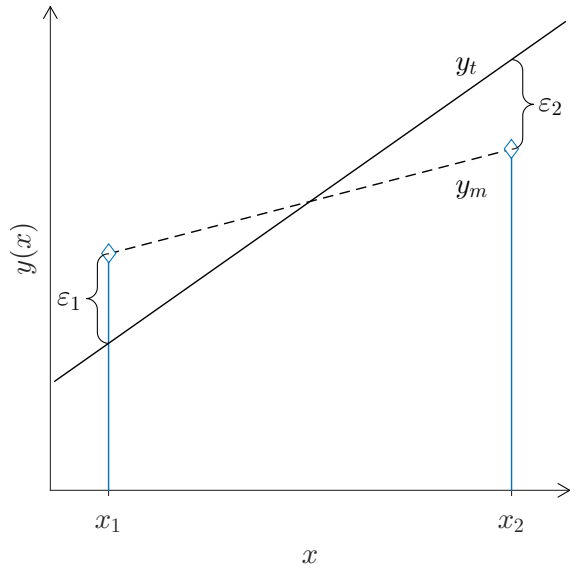

Figure 6: Reduced influence of the random error terms ε_1 and ε_2.

Another feature of the classical DOE methods is replicated sampling. Each time a sampling is repeated with an identical design variable value a slightly different y_m is measured. By placing multiple, identical, sample points in the design space it is possible to perform a lack-of-fit statistical analysis, and measure the magnitude of the random error term in Equation (2) [3].

2.1.1.1 Full Factorial

The full factorial sampling method is a classic DOE method that is used to completely explore the boundaries of a design space. This method tests all possible combinations of the design variables and therefore resolve all effects and interactions. The total number of samples N depend on the number of design variables n and the number of sample values per design variable L, known as levels. For instance, if $L = 2$ for a design variable with the range [0 1], then the design variable will take on the values 0 and 1, whilst for $L = 3$ a center point at 0.5 is added to the evaluation. In the most common setup the levels are equal for all design variables, the number of sample points is then:

$$N = L^n$$

Note that it is possible to have different number of levels for the design variables. For instance:

$$N = 2^3 \cdot 3^2 \cdot 4^1 = 288 \qquad \text{if} \begin{cases} 3 \text{ design variables have } L = 2 \\ 2 \text{ design variables have } L = 3 \\ 1 \text{ design variable have } L = 4 \end{cases}$$

In a case with two design variables at two levels, the total number of combinations is four. The sample point values are shown in Table 2.

i	$\mathbf{x}_1$	$\mathbf{x}_2$
1	0	0
2	1	0
3	0	1
4	1	1

Table 2: Full Factorial sampling: $n = 2$ and $L = 2$.

It is possible to visualize the sample points for the design variables by plotting them against each other, for the case shown in Table 2 see Figure 7. Note that the sample points are placed on the corners of a square. Figure 8 shows the sample points for a Full Factorial sampling where the levels are increased to three for the two design variables.

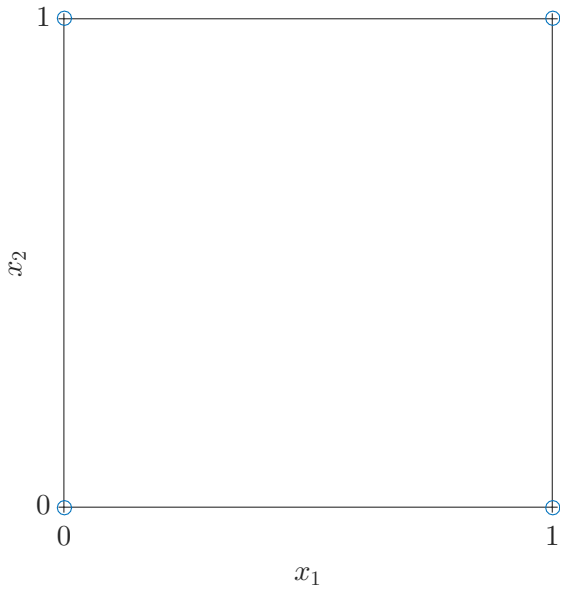

Figure 7: Full Factorial sampling: $n = 2$, $L = 2$ and $N = 4$.

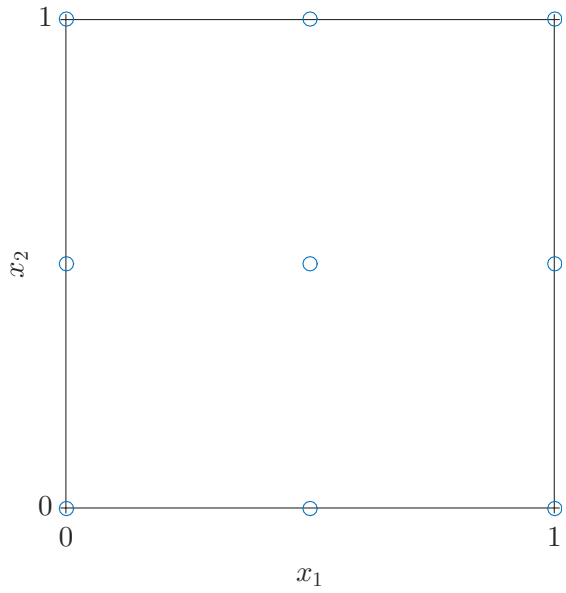

Figure 8: Full Factorial sampling: $n = 2$, $L = 3$ and $N = 9$.

If the number of design variables are increased to three at two levels the plot of the sample points takes the appearance as shown in Figure 9. Note that this time the sample points are placed on the corners of a cube. In higher dimensions the sample point will continue to be placed at the corners, although, it is quite troublesome to visualize dimensions higher then three.

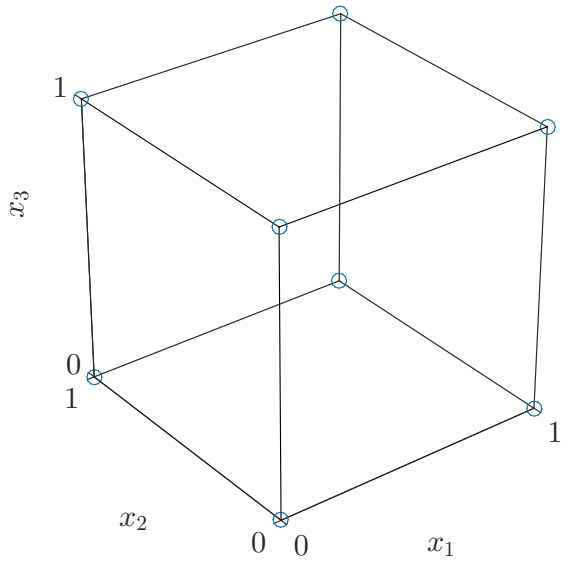

Figure 9: Full Factorial sampling: $n = 3$, $L = 2$ and $N = 8$.

In conclusion the full factorial method is great when it comes to fully explore the boundaries of the design space and get a complete understanding of a system regarding the main and interaction effects. Although the number of samples depend greatly on the number of design variables and therefore the method is only suitable if a few

design variables are investigated in a study. Some other classical methods are based on the full factorial but has different techniques to systematically reduce the number of samples without losing to much information of the system. These methods will not be investigated further, the interested reader is referred to [11].

2.1.2 Modern DOE Methods

Modern DOE methods are based on the assumptions that there are no random errors in the deterministic computer simulations and that the true response trend is unknown. The modern DOE methods are also known as ”space-filling” methods, since they tend to place sample points in the interior of the design space. This is an effort to minimize the bias error that occur when there is a difference between the true response trend and the estimated response trend. According to [3], placing the sample points close to each other reduce the bias error compared to placing the sample points at the boundaries of the design space.

2.1.2.1 Pseudo-Monte Carlo Sampling Methods

The Monte Carlo sampling methods are named after the casinos of Monte Carlo as they utilizes random values in order to perform stochastic simulations [8]. The pseudo-Monte Carlo sampling methods use pseudo-random number generators to mimic a truly random natural process in order to perform a random sampling.

2.1.2.1.1 Basic pseudo-Monte Carlo

In the basic pseudo-Monte Carlo sampling method the samples are randomly distributed in the design space. The sample points are placed independent of each other and large regions are often left empty in the design space. Figure 10 shows how a basic pseudo-Monte Carlo algorithm distributes 16 sample points in the design space for the design variables x_1 and x_2 [3].

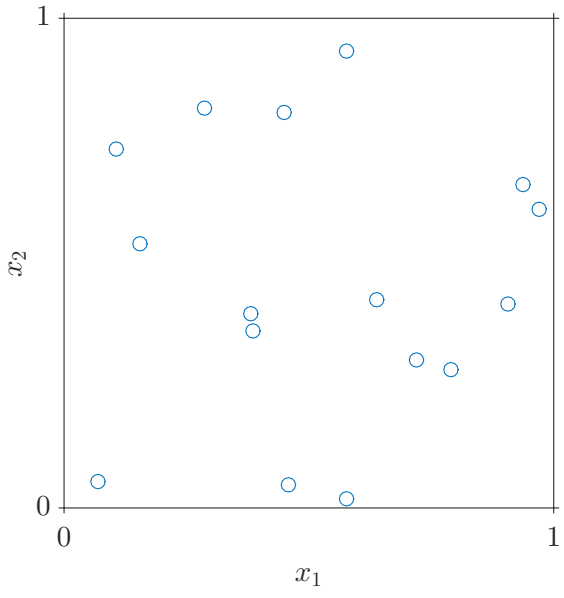

Figure 10: Basic pseudo-Monte Carlo sampling.

2.1.2.1.2 Stratified pseudo-Monte Carlo

The stratified pseudo-Monte Carlo sampling method was developed to provide a more uniform sampling of the design space. The design space is divided into sub-intervals

called bins, of equal probability and, if the probability distribution is uniform, equal size. A sample point is randomly selected in each bin. This sampling method is very computationally expensive as the number of samples equals to B^n, where B is the number of bins, by which the design range of each design variable is divided into, and n is the number of design variables. Even when only two bins are used for each design variable the computation of $\mathcal{O}(2^n)$ samples quickly becomes expensive when there are many design variables. Figure 11 show how the 4^2=16 sample points are distributed by a stratified Monte Carlo algorithm when the design space for x_1 and x_2 is divided into 4 bins each [3].

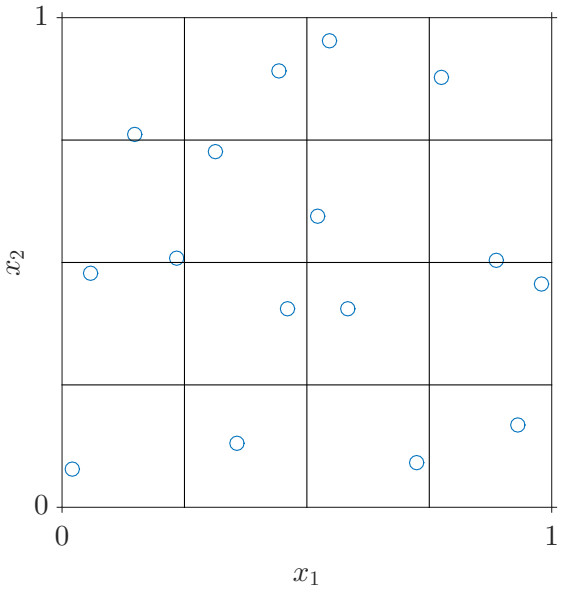

Figure 11: Stratified Monte Carlo sampling.

2.1.2.1.3 Latin Hypercube

The Latin Hypercube sampling method is an alternative to the previously discussed pseudo-Monte Carlo sampling methods and let the user tailor the number of samples N to the available computational budget. For N samples the design range of each design variable is divided into N bins of equal probability. Thus, the design space is divided into N^n bins. The N samples are randomly placed inside a bin such that for all one-dimensional projections of the bins there will only be one sample in each bin. There is however more than one possible arrangement of the samples that meet the projection criteria and the design space is poorly covered. The Latin Hypercube sampling provides a more accurate mean value of the response than the previously discussed pseudo-Monte Carlo sampling methods does [3]. Figure 12 show how a Latin Hypercube algorithm distributes 4 sample points in 4^2=16 bins for the design variables x_1 and x_2.

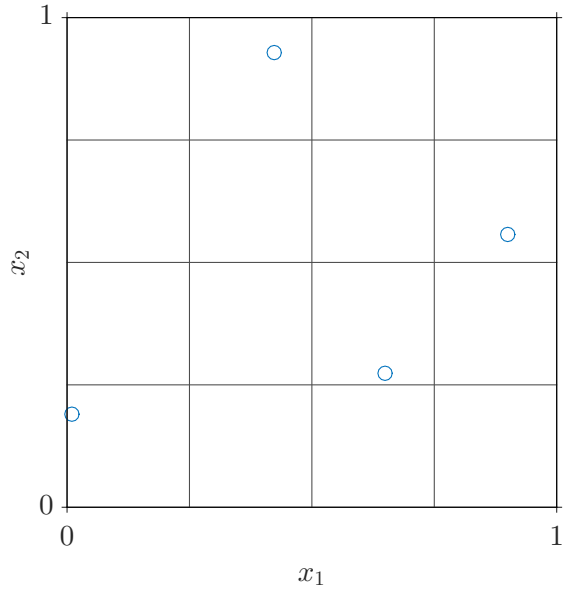

Figure 12: Latin Hypercube sampling (two design variables).

Figure 13 show how the design space from Figure 12 is extended to include the design variable x_3, without increasing the number of samples or changing their x_1 and x_2 distribution. The 4 samples are now distributed in 4^3=64 bins.

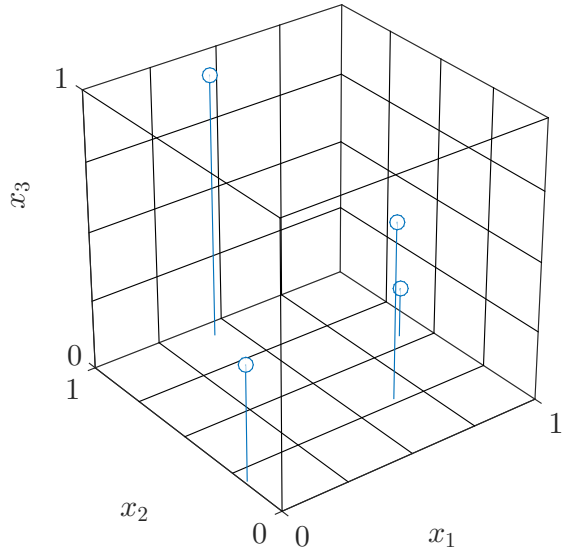

Figure 13: Latin Hypercube (three design variables).

2.1.2.1.3.1 Latin Hypercube Algorithm

The Latin Hypercube algorithm generate the placement of the sample points $\mathbf{x}$, using index notation, where i denotes design variable index number and j denotes sample point number, by:

$$\mathbf{x}_{ij} = \frac{\boldsymbol{\pi}_{ij} + \mathbf{U}_{ij}}{N}, \tag{4}$$

for $i = 1 : N$ and $j = 1 : n$, where $\boldsymbol{\pi}_{:j}$ is a random permutation of the sequence of integers $0, 1, \ldots, N-1$, that determine the order in which the bins are selected for the design variable $\mathbf{x}_i$, and $\mathbf{U}_{ij}$ is a uniform random value on [0 1], which determine the placement within that bin. Equation (5) shows how the sample points in Figure 12 where calculated [3].

$$\mathbf{x} = \frac{1}{4}\left(\overbrace{\begin{bmatrix} 3 & 0 \\ 2 & 3 \\ 0 & 1 \\ 1 & 2 \end{bmatrix}}^{\boldsymbol{\pi}} + \overbrace{\begin{bmatrix} 0.1966 & 0.2511 \\ 0.4733 & 0.3517 \\ 0.5853 & 0.5497 \\ 0.2858 & 0.7572 \end{bmatrix}}^{\mathbf{U}}\right) = \begin{bmatrix} \overbrace{0.7991}^{\mathbf{x}_1} & \overbrace{0.0628}^{\mathbf{x}_2} \\ 0.6183 & 0.8379 \\ 0.1463 & 0.3874 \\ 0.3215 & 0.6893 \end{bmatrix} \tag{5}$$

2.1.2.2 Quasi-Monte Carlo Sampling Methods

Quasi-Monte Carlo sampling methods use a deterministic algorithm to generate unique sample points with low-discrepancy in the design space. Low-discrepancy is a quantitative measure of how much the distribution of samples deviates from an ideal uniform distribution. These methods aim to distribute sample points in the design space as uniformly as possible without using a regular Cartesian lattice. Quasi-Monte Carlo methods differ from the pseudo-Monte Carlo methods in the sense that they do not use random number generation algorithms. However, they share common ground in the way that they were developed for multidimensional numerical integration [3].

According to [12] the Monte Carlo methods was developed in the 1940s because of the phenomenon "curse of dimensionality" that appears in multidimensional numerical integration when classic integration methods are utilized. Typical classical integration methods are the Trapezoidal rule and Simpson's rule. The Trapezoidal rule applied on a one dimensional integral in the unit interval of [0 1] is approximated as,

$$\int_0^1 f(u)\,\mathrm{d}u \approx \sum_{n=0}^{m} w_n f\left(\frac{n}{m}\right)$$

where m is a positive integer and w_n the weights that is given by

$$w_n = \begin{cases} \frac{1}{2m} & \text{if} \quad n = 0 \quad \text{or} \quad n = m \\ \frac{1}{m} & \text{else} \quad 1 \leq n \leq m-1 \end{cases}$$

The error obtained with this approximation is $\mathcal{O}(m^{-2})$ if the function f has a continuous derivative in the unit interval. It is possible to use the Trapezoidal rule in multidimensional cases by using Cartesian products with the one-dimensional integration rules, for more details see [12]. [12] shows that the obtained integral error for s dimensions is given by $\mathcal{O}(N^{-2/s})$. To obtain an error value be below 1%, the number of integration points N must be at least 10^s. Note how the number of integration points increases exponentially with dimensions s, this is known as the "curse of dimensionality".

As mentioned earlier the "curse of dimensionality" was the reason for the development of the Monte Carlo methods. The Monte Carlo methods can be described as numerical methods based on random sampling that can be used in many applications, not only numerical integration. However in numerical integration the methods are favorable since the value of the integration error do not depend on the number of dimensions but only on the number of integration point used. [12] shows that the obtained integral error can be estimated as $\mathcal{O}(N^{-1/2})$ during the right circumstances regarding the random sample points. The error is actually probabilistic and the above error term only holds for one regularity condition, that it is a square-integral integrand. There are ways to reduce the error and improve the efficiency of the Monte Carlo methods and they are based on variance reduction and one such method is the stratified Monte Carlo method. Another drawback with the Monte Carlo methods are that the sample

points are supposed to be truly random and independent. It is common that the sample points are generated as pseudorandom numbers and this effect the obtained results from the Monte Carlo methods. Pseudorandom number generation is actually a deterministic generation of random samples and thus not truly random.

To overcome the drawbacks with the Monte Carlo methods in numerical integration, the quasi-Monte Carlo methods was introduced in the 1950s. As mentioned earlier the quasi-Monte Carlo methods generate the sample points in a deterministic manner. Since the sample points are generated deterministically the error bound in numerical integration also becomes deterministic, hence the drawbacks of the Monte Carlo methods are removed. [12] performed a study on the error bounds and concluded, that it is not the true randomness of the sample points that decrease the error, but rather how uniformly the sample points are spread in the integration space. In other words, in order to reduce the error in the numerical integration, it is of interest to find a deterministic algorithm that places the sample points as uniformly as possible in the integration space. For the quasi-Monte Carlo methods the deterministic error bound can be approximated as $\mathcal{O}(N^{-1}(\log N)^{s-1})$, if the sample points are chosen in a suitable way, note that the error term depends on how uniformly distributed the sample points are.

So far a brief explanation has been given to why the quasi-Monte Carlo methods are widely used in numerical integration, but not the connection to DOE. According to [12] the quasi-Monte Carlo methods can be applied to computational physics and structural mechanics. The use of quasi-Monte Carlo methods in these areas has contributed to the refinement of the methods and made the methods known to a wider public than before. Quasi-Monte Carlo methods are used in DOE since they both reduce the bias error and thoroughly explore the design space by distributing the sample points uniformly.

In the end, it is the uniformity of the sample points that determines how much information that can be extracted. Since the uniformity is that essential, it is important that a qualitative measure can be used to compare the uniformity of different sets of sample points. As mentioned earlier in this section the discrepancy is the qualitative measure that is used, the lower discrepancy value, the better is the uniformity. In practice the discrepancy can be calculated with different methods, each method has it's pros and cons. Some of the methods that can be found in the literature are the star L_p-discrepancy, modified L_2-discrepancy, the centered discrepancy and the wrap-around discrepancy. According to [5] the star L_p-discrepancy has been essential to the use of quasi-Monte Carlo methods. Apparently the star L_p-discrepancy is quite difficult to calculate, hence other methods have been developed. For more details about various discrepancy methods see [12] and [5].

Furthermore on the subject uniformity, [5] states that several studies from the 1990s have found a connection between uniformity and classical design criteria for Factorial Design. The design criteria in question are the orthogonality, aberration, design iso-

morphism, estimation capacity, model robustness, and supersaturated design. More details about the connection and the design criteria can be found in [9]. Hence these design criteria will be fulfilled in the most cases if the uniformity is optimized. In other words, DOE methods which generate uniform sample points are desirable. These DOE methods can be used in the following situations according to [9],

- for unknown models as Factorial Design
- for space filling design in computer experiments
- for robust design with model specifications
- for design of experiments with mixtures

2.1.2.2.1 Hammersley

A well known Quasi-Monte Carlo sampling method is the Hammersley sampling method. The Hammersley algorithm is based on bit-reversal permutation on integers that are converted between positional numeral systems.

In the Hammersley algorithm, the positional notation of the integer i, representing the sample number $i = 1 : N$, is converted to the positional numeral system with the number at the j:th position in the $\mathbf{r}$ vector as its radix[7], where the integer j represents the design variable number $j = 1 : n$. The $\mathbf{r}$ vector is populated by a number sequence starting with 10, followed by the prime numbers:

$$\mathbf{r} = [10, 2, 3, 5, 7, 11, \ldots]$$

Thus, the positional systems used for the design variables are:

$$\mathbf{r} = [\text{decimal}, \text{binary}, \text{ternary}, \text{quinary}, \text{septenary}, \text{undecimal}, \ldots]$$

The sample number i is thereby represented in a unique prime number radix for each design variable. The exception is the first design variable where the decimal numeral system is kept. The representations of i in the prime number radixes are bit-reversed and converted back into the decimal numeral system. The result of this operation is a fraction unique for each numeral system used. These fractions are used to place the sample points in the design space. Figure 14 shows how the Hammersley sampling method place 4 sample points in a design space with 2 design variables.

[7]The radix, or base, is the number of unique digits used to represent numbers in a positional numeral system.

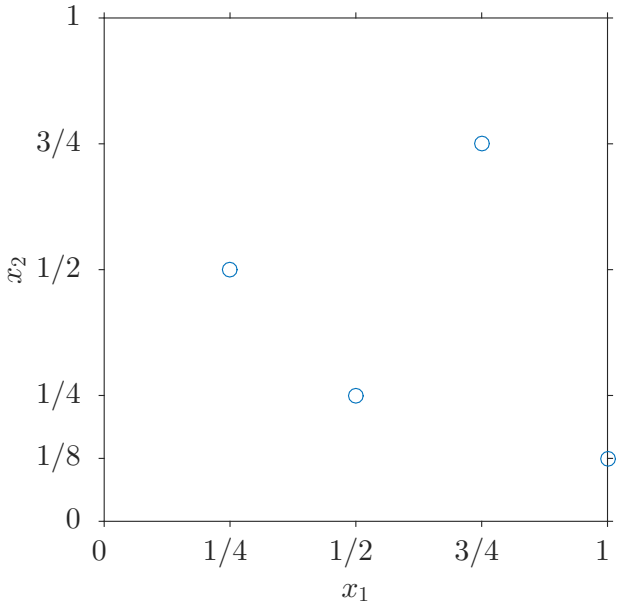

Figure 14: Hammersley sampling (two design variables).

Figure 15 shows how the Hammersley sampling method places 4 samples in a design space with 3 design variables.

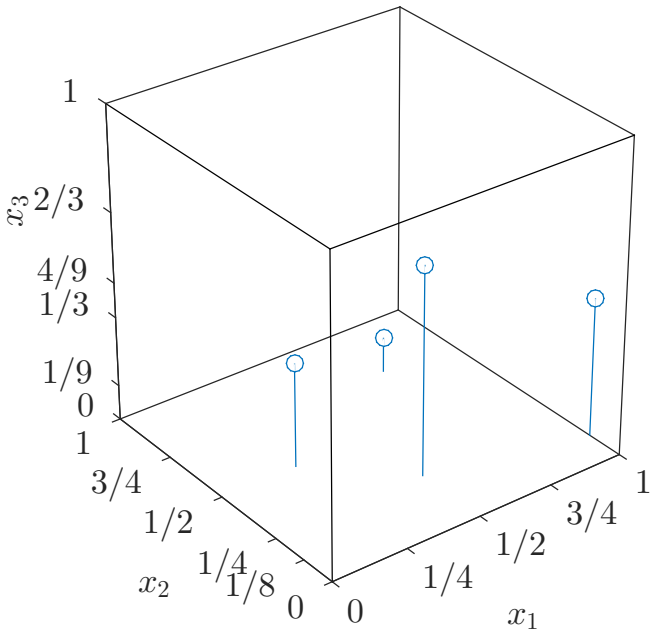

Figure 15: Hammersley sampling (three design variables).

Note that the sample point values for the first two design variables do not change when a third design variable is added [3].

2.1.2.2.1.1 Hammersley Algorithm

The integer $(i)_{10} \in \mathbb{Z}$ is converted from the decimal numeral system into the integer $(a)_r \in \mathbb{Z}$ in the numeral system whose radix is r. The digits of a are denoted as:

$$a = a_{(m)}a_{(m-1)} \dots a_{(2)}a_{(1)}a_{(0)} \tag{6}$$

where the number of digits, $m + 1$, in a is given by:

$$m = \left\lfloor \log_r(i) \right\rfloor$$

The $\lfloor\ \rfloor$ symbols denote the floor function, which performs a rounding to the largest previous integer.

The digit values of a are calculated using Euclidean division (7) and assembled using Equation (6).

$$\begin{array}{rclll rcll}
q_m & = & \left\lfloor \frac{(i)_{10}}{r} \right\rfloor & \text{(quotient)}, & (a_{(0)})_r & = & (i)_{10} - r \cdot q_m & \text{(remainder)} \\
q_{m-1} & = & \left\lfloor \frac{q_m}{r} \right\rfloor & \text{(quotient)}, & \left(a_{(1)}\right)_r & = & q_m - r \cdot q_{m-1} & \text{(remainder)} \\
\vdots & & & & \vdots & & & \\
q_1 & = & \left\lfloor \frac{q_2}{r} \right\rfloor & \text{(quotient)}, & \left(a_{(m-1)}\right)_r & = & q_2 - r \cdot q_1 & \text{(remainder)} \\
q_0 & = & \left\lfloor \frac{q_1}{r} \right\rfloor & \text{(quotient)}, & \left(a_{(m)}\right)_r & = & q_1 - r \cdot q_0 & \text{(remainder)}
\end{array} \tag{7}$$

$(a)_r$ can be converted back into $(i)_{10}$ in the decimal numeral system using the radix function:

$$i = f(a, r) = \sum_{k=0}^{m} a_{(k)} \cdot r^k \tag{8}$$

A bit-reversal permutation reverse the sequence in which the digits of a number are positioned. In a bit-reversed permutation of a, the real number $b \in \mathbb{R}$, the digits of a are positioned as:

$$b = 0.a_{(0)}a_{(1)}a_{(2)} \dots a_{(m-1)}a_{(m)}$$

The digits of b are denoted as:

$$b = b_{(0)}.b_{(-1)}b_{(-2)} \dots b_{(-m+1)}b_{(-m)}$$

b inherits the numeral system of a, and can be converted back into the decimal numeral system using Equation (8). Since b is not an integer the value will be a fraction that differ from the bit-reversed value if i. Thus, by converting the integer i into a new numeral system and bit-reversing the result, a fraction unique to the numeral system used is obtained when the bit-reversed result is converted back into the decimal numeral system. The values of these fractions range from [0,1] and are therefore suitable to be used for sampling the design space. This is the deterministic algorithm

that the Hammersley sampling method utilizes to place sample points.

The bit-reversal of a can be skipped if the inverted radix function is used, since it performs the conversion of an integer as if it was bit-reversed:

$$\varphi = f_{\text{inv}}(a, r) = \sum_{k=0}^{m} \frac{a_{(k)}}{r^{k+1}}$$

Using index notation to describe the matrix operations, the Hammersley algorithm place the sample points $\mathbf{X}$ by:

$$\mathbf{M}_{ij} = \left\lfloor \log_{\mathbf{r}_j}(i)_{10} \right\rfloor$$

$$(\mathbf{A}_{ij})_{\mathbf{r}_j} = (i)_{10}$$

$$\mathbf{\Phi}_{ij} = f_{\text{inv}}(\mathbf{A}_{ij}, \mathbf{r}_j) = \sum_{k=0}^{\mathbf{M}_{ij}} \frac{\mathbf{A}_{(k)\,ij}}{\mathbf{r}_j^{k+1}}$$

$$\mathbf{X}_{ij} = \begin{cases} \frac{i}{N} & \text{if} \quad j = 1 \\ \mathbf{\Phi}_{ij} & \text{else} \end{cases}$$

where $\mathbf{A}_{ij}$ is the representation of i in the $\mathbf{r}(j)$ numeral systems as calculated by Equation (7).

Equation (9) shows the values assigned to $\mathbf{M}$, $\mathbf{A}$, $\mathbf{\Phi}$, and $\mathbf{X}$, in the Hammersley algorithm durring the computation of the sample points shown in Figure 15 [3].

$$\begin{aligned} \mathbf{M} &= \begin{bmatrix} 0 & 0 & 0 \\ 0 & 1 & 0 \\ 0 & 1 & 1 \\ 0 & 2 & 1 \end{bmatrix} & \mathbf{A} &= \begin{bmatrix} (1)_{10} & (001)_2 & (01)_3 \\ (2)_{10} & (010)_2 & (02)_3 \\ (3)_{10} & (011)_2 & (10)_3 \\ (4)_{10} & (100)_2 & (11)_3 \end{bmatrix} \\ \mathbf{\Phi} &= \begin{bmatrix} 0.1 & 0.500 & 0.333 \\ 0.2 & 0.250 & 0.666 \\ 0.3 & 0.750 & 0.111 \\ 0.4 & 0.125 & 0.444 \end{bmatrix} & \mathbf{X} &= \begin{bmatrix} 1/4 & 1/2 & 1/3 \\ 2/4 & 1/4 & 2/3 \\ 3/4 & 3/4 & 1/9 \\ 1 & 1/8 & 4/9 \end{bmatrix} \end{aligned} \tag{9}$$

2.1.3 Comparison of Modern DOE Sampling Methods

Figure 16 to 18 show the distribution of sample points for two design variables in the design space for the modern DOE sampling methods Basic psuedo-Monte Carlo, Latin Hypercube, Hammersley and Uniform Latin Hypercube. Research on new more uniform methods is currently conducted. One such method currently being developed is the Uniform Latin Hypercube method. Sample points generated using an experimental version of this method are presented below for comparison to the existing methods discussed earlier.

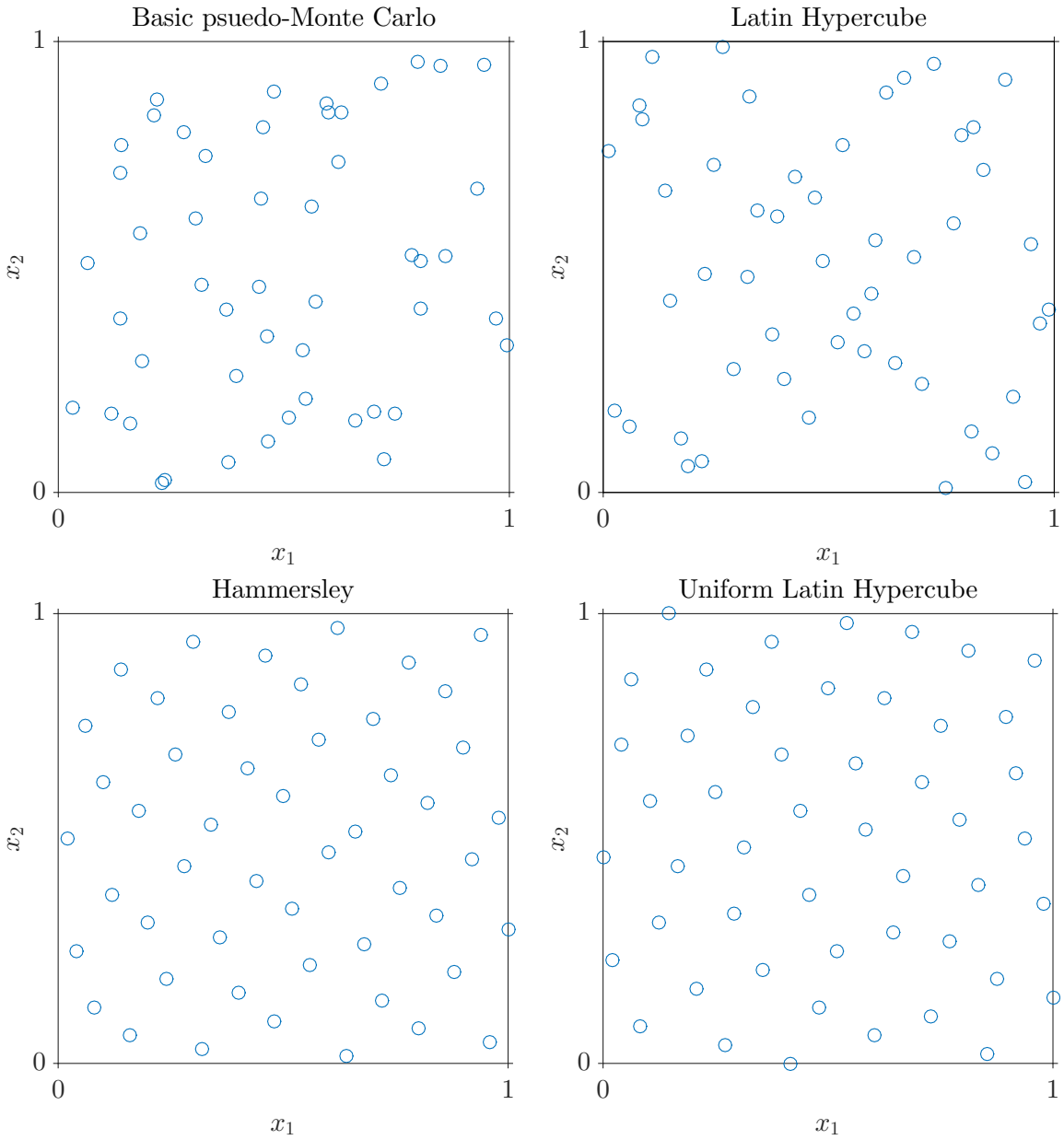

Figure 16: Comparison for 50 samples.

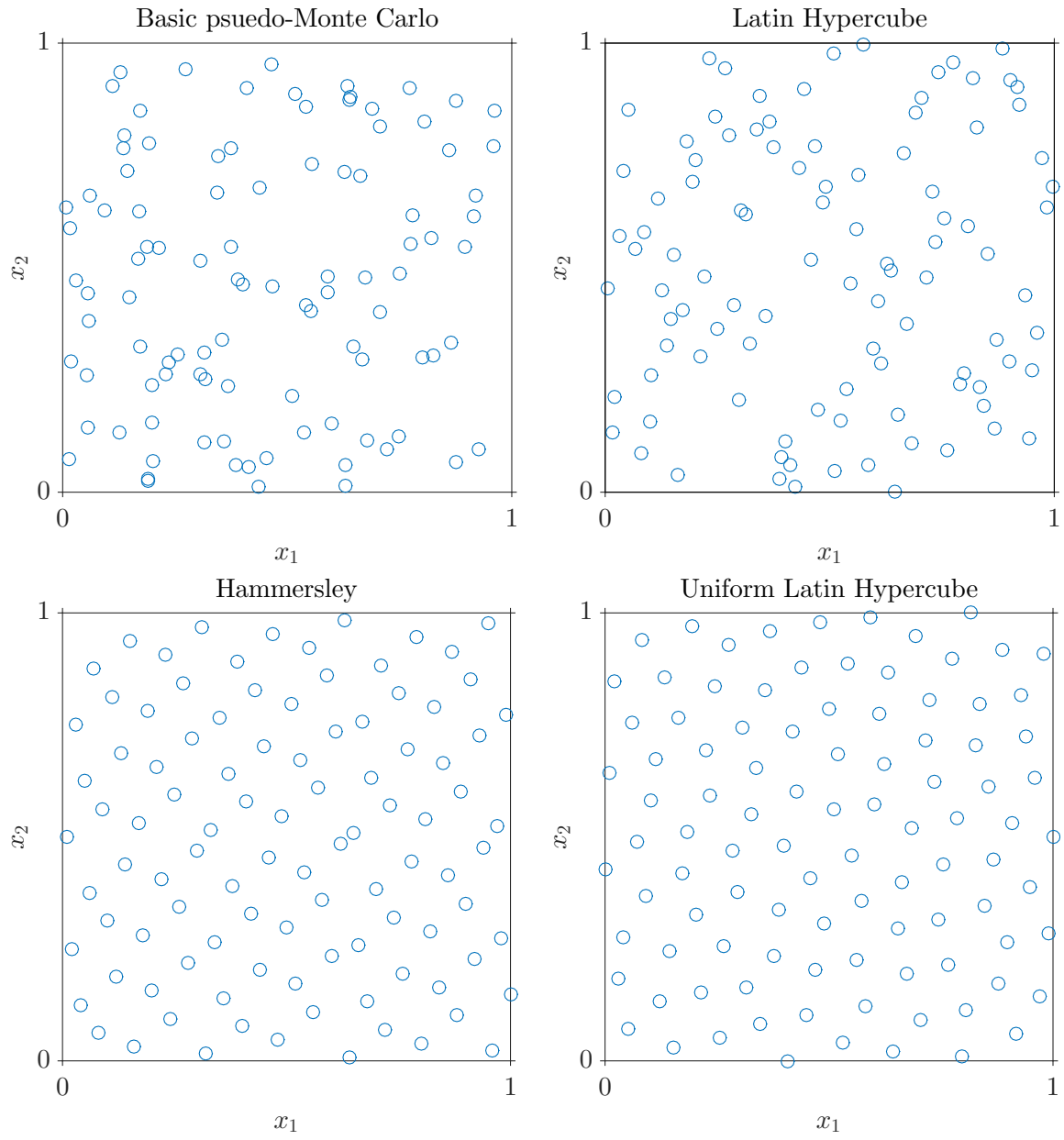

Figure 17: Comparison for 100 samples.

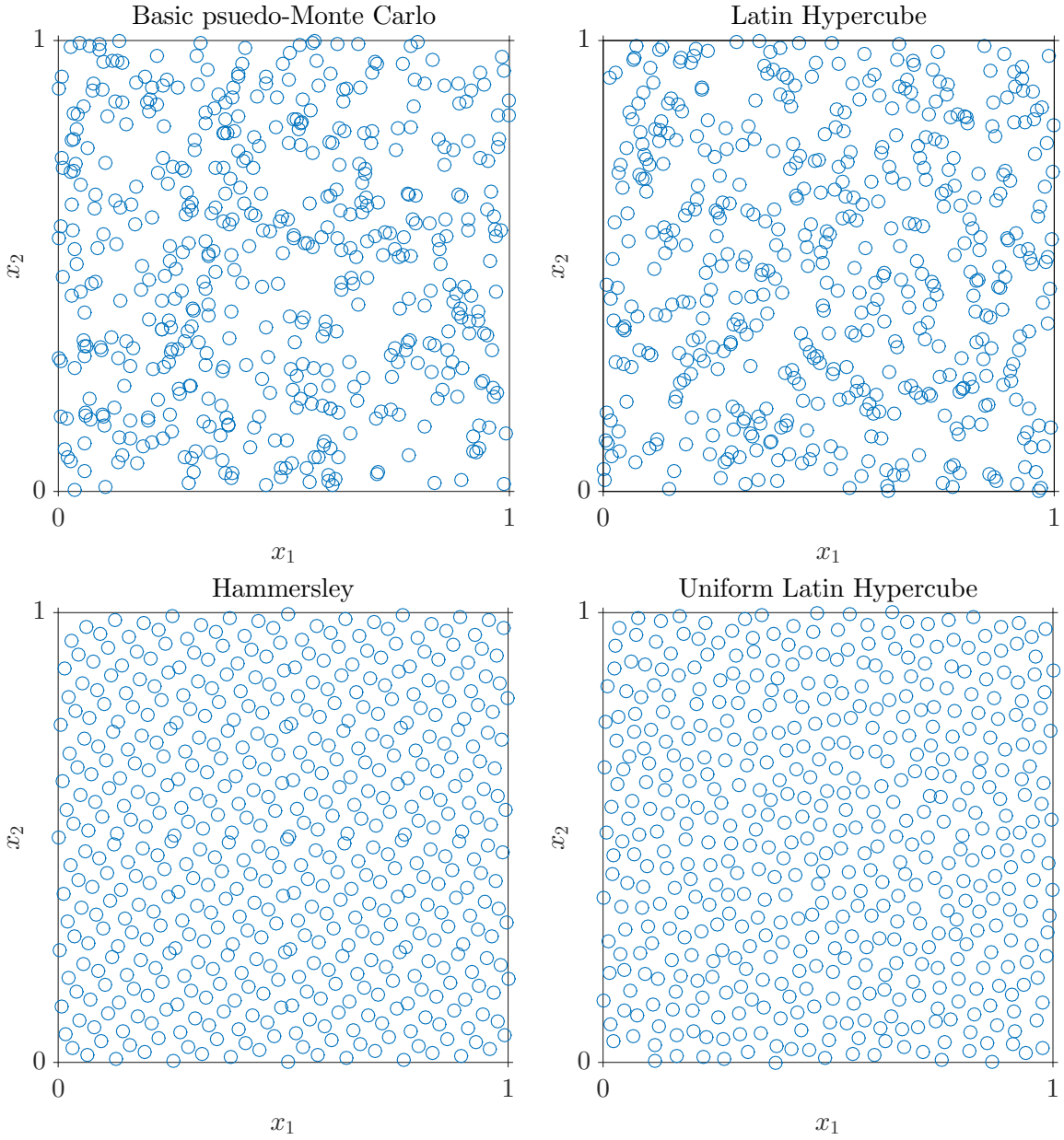

Figure 18: Comparison for 500 samples.

The Hammersley sampling is close to a uniform distribution. The patterns that appear as certain x_n values are used repeatedly to place the samples. Due to the projection rule the Latin Hypercube algorithm will never place more than one sample in each bin for each design variable x_n. The sample points are not as uniformly distributed in the design space as in the Hammersley sampling, but each sample point has a unique x_n value which is never repeated.

2.1.4 Main & Interaction Effect Calculation

A brief introduction to the main & interaction effects was given in the beginning of this chapter in order to explain some important concepts in DOE. Therefore, a more thorough explanation of the effects and the calculations will be presented here. First of, the effects are vital in the sense that they reveal by which magnitude the design variables influence the system responses. The sole purpose of the DOE approach is to find out more about the system and how to improve it for the better, hence the effects are vital to succeed in this matter. Keep in mind that the experimental setups, sample points, need to be properly planned, otherwise the information extracted from the calculated effects may be misleading.

For the calculation example, the sample points have been generated according to a Full Factorial setup with two design variables at two levels, where the response values are fabricated. With this setup, four sample point are generated and the design variables can take a low or a high value. The experimental setup and the fabricated response values are shown in Table 3. It might be easier to use Figure 19 in order to understand the setup and the calculations described later on.

DV		Sample Combination	Response	Response Value
$\mathbf{x}_1$	$\mathbf{x}_2$			
0	0	x_1 low, x_2 low	$r_1 r_2$	20
1	0	x_1 high, x_2 low	r_1	30
0	1	x_1 low, x_2 high	r_2	15
1	1	x_1 high, x_2 high	$R_1 R_2$	40

Table 3: Full Factorial design example.

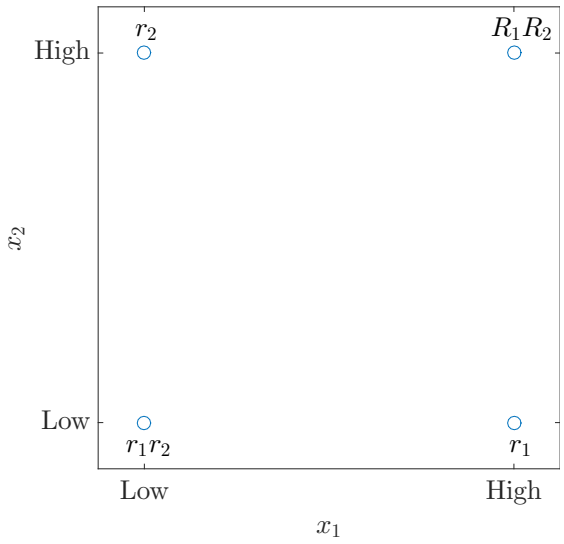

Figure 19: Full Factorial design example

Note that the calculations presented below only holds for an experimental setup in two levels, if more levels are used the calculations needs to be modified, the same goes for the number of design variables. In this thesis the general approach is presented to give a basic understanding of the effects. For more details the reader is referred to [11]. From here on the main effects of the design variables will be denoted as $\mathbf{E}_1$, $\mathbf{E}_2$ and the interaction effect as $\mathbf{E}_1\mathbf{E}_2$.

One way to describe the calculations of the main effect would be the difference of the average response change at high and low level of a design variable. If this approach is applied to the design variable x_1, the main effect $\mathbf{E}_1$ is given by:

$$\mathbf{E}_1 = \frac{R_1R_2 + r_1}{2} - \frac{r_2 + r_1r_2}{2}$$

Another way to describe the main effects calculation would be the average change in response of x_1 at low and high levels of x_2. If this approach is applied to the design variable x_1, the main effect $\mathbf{E}_1$ is given by:

$$\mathbf{E}_1 = \frac{R_1R_2 - r_2}{2} + \frac{r_1 - r_1r_2}{2}$$

Note that both approaches consist of identical terms in the expressions, the difference is just rearrangement of the terms within. If the latter approach is applied to the design variable x_2, the main effect $\mathbf{E}_2$ is given by:

$$\mathbf{E}_2 = \frac{R_1R_2 - r_1}{2} + \frac{r_2 - r_1r_2}{2}$$

The calculations of the main effects is straightforward and the results are rather easy to comprehend. In general, the higher the effect value the greater the impact a certain design variable has on the system. The sign of the effect value is an indication on how the response value is changed when the value of the design variable is increased. Hence, a negative effect value yields a decreased response value if the design variable value is increased. If the response values from Table 3 are inserted into the main effect expressions they would yield the following main effects for this example:

$$\mathbf{E}_1 = \frac{40 - 15}{2} + \frac{30 - 20}{2} = 17.5$$
$$\mathbf{E}_2 = \frac{40 - 30}{2} + \frac{15 - 20}{2} = 2.5$$

The calculations from above yields effect values and sometimes it can be tedious to interpret these values especially if there are more than two design variables and one response. In other words a graphical presentation of the effects would be useful to interpret the large amount of data one could acquire. This graph is constructed by using some of the calculations from the first approach that was presented above. For each design variable a line is drawn between the effect at low respectively high level, such a graph has been generated for this example and can be found in Figure 20. The Y-axis corresponds to the mean response value whilst the X-axis the levels of the

design variables. Note that the y-distance between the points for each line corresponds to the main effect values.

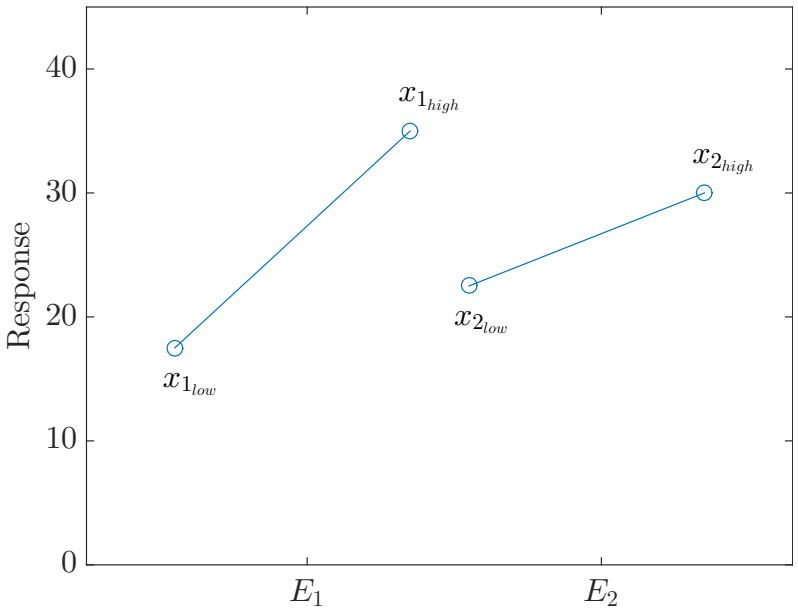

Figure 20: Graph of the main effects $\mathbf{E}_1$&$\mathbf{E}_2$.

In this example one can conclude that the design variable x_1 has a greater impact on the system, because the main effect value $\mathbf{E}_1$ is much greater than $\mathbf{E}_2$. Note that if more than one response is of interest, the main effect value for the different responses might not be comparable, since the main effect value scales according to the response values. Although in this example such considerations are not necessary since there is only one response present. However, one can not yet conclude that design variable x_2 can be rejected in further studies to improve the system response, since the interaction effect has not been taken into consideration.

To find out if there is an interaction effect influencing the system one could compare the effect values of a design variable at high and low levels of the other design variable. In other words it is possible to find out if the interaction needs to be taken into account if there is a big difference between the two effect values. The difference indicate that the value of one design value is influenced by the change of level in the other one. In this example this kind of evaluation is done by looking at the effect of the design variable x_1 at low and high levels of x_2, and numerically this is

$$\mathbf{E}_{1,low} = r_1 - r_1 r_2 = 30 - 20 = 10$$
$$\mathbf{E}_{1,high} = R_1 R_2 - r_2 = 40 - 15 = 25$$

This result indicates that there is an interaction effect present in the problem, since $\mathbf{E}_{1,low} \neq \mathbf{E}_{1,high}$, hence the levels of x_2 influence the effect of x_1. Another way to find out if a interaction effect is present, is by illustrating it in a graph with two lines. In this graph the X-axis is the levels of design variable x_1 and the Y-axis the

response value. Then the two lines are drawn between the points at high levels of x_2 respectively low levels of x_2. If the two lines in the graph are not parallel it is an indication that there is an interaction effect present. Such graph has been generated for this example and is shown in Figure 21, note that the lines are not parallel.

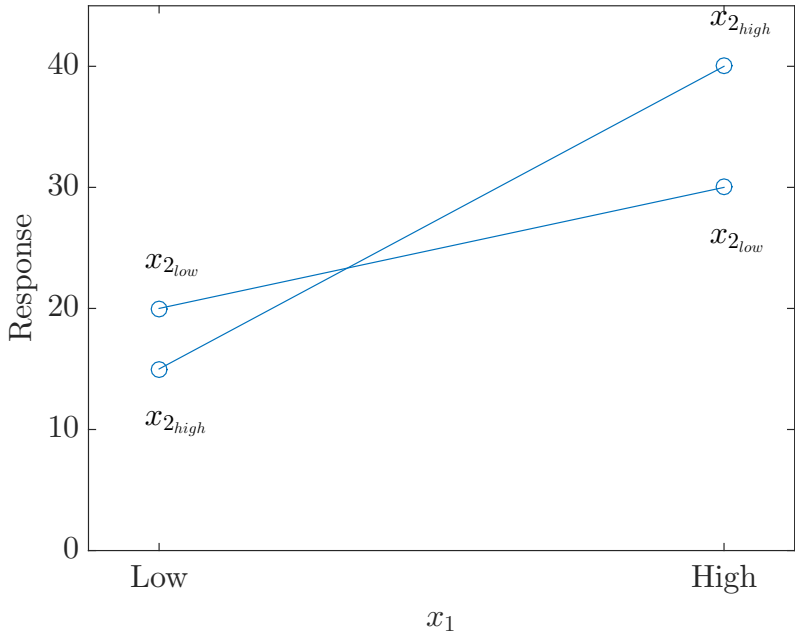

Figure 21: Interaction effects at low respectively high levels of x_2.

So far, the conclusion is that an interaction effect is present, although its value has not been calculated. The interaction effect, $\mathbf{E}_1\mathbf{E}_2$, is calculated by taking the average difference of the effect of x_1 at low respectively high levels of x_2, and in this example it can be expressed as

$$\mathbf{E}_1\mathbf{E}_2 = \frac{R_1R_2 - r_2}{2} - \frac{r_1 - r_1r_2}{2}$$

If the response values from Table 3 is inserted into the expression the interaction effect $\mathbf{E}_1\mathbf{E}_2$ is given by

$$\mathbf{E}_1\mathbf{E}_2 = \frac{40 - 15}{2} - \frac{30 - 20}{2} = 7.5$$

The value of the interaction effect $\mathbf{E}_1\mathbf{E}_2$ indicates that the interaction effect influence the system, hence the second design variables should not be neglected if the system response is to be improved. This conclusion can be drawn by comparing the magnitude of the interaction effect $\mathbf{E}_1\mathbf{E}_2$ to the main effects $\mathbf{E}_1$ and $\mathbf{E}_2$, in this example $\mathbf{E}_2 < \mathbf{E}_1\mathbf{E}_2 < \mathbf{E}_1$. However, one might wonder how much smaller the magnitude of an effect must be in order to be able to neglect a design variable. In the end it is up to the experimenter to interpret the result and draw a conclusion. It is rather difficult and non-statistical to compare these effect values manually but in general a good indication to which design variables that are vital in the system. Although, there

is a statistical approach to confirm the interpretation of the effects, this approach is known as analysis of variance (ANOVA). For more details see [11].

3 Method

3.1 Multibody Dynamics (MBD)

3.1.1 Suspension Model

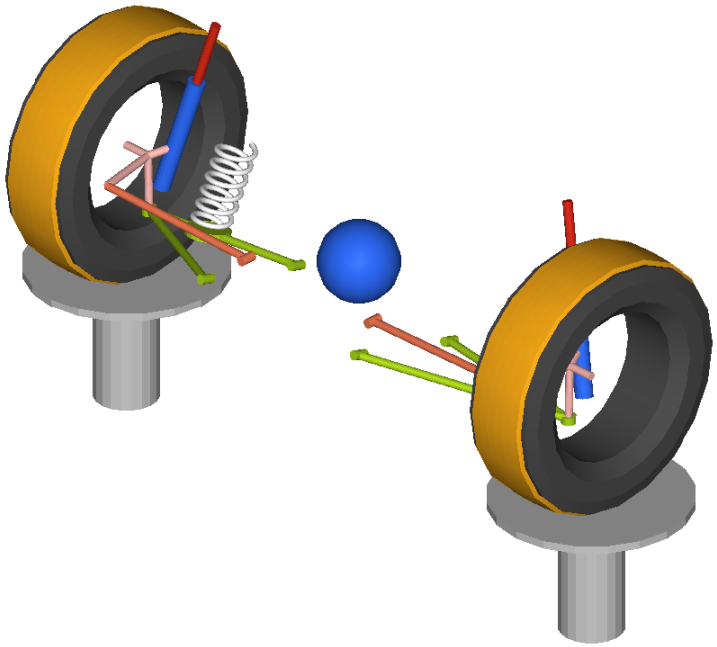

Figure 22: Strut & Coil Spring suspension system model.

The multibody dynamics model is built in `MotionView` using rigid bodies. These are the control arm (green), toe link (orange), knuckle (pink), spring (white), damper (blue and red), wheel (orange and black), and test rig (gray). The blue sphere is a point mass at 680 kg. It represents the part of the mass of the car, the driver, and a passenger in the front seat, which is suspended by the rear axle. The attachment points, by which the suspension is attached to the vehicle body, are rigidly connected to this point mass via bushings. The spring connects directly to the control arm and the vehicle body.

This model setup does not take elasticity in the suspension parts into account as they are all modeled as rigid bodies. It is possible to model elasticity using flex bodies and advanced wheel models, but this greatly increases the simulation time. The mass of the suspension parts is fixed at 1 kg each as all simulations in this setup are static, where mass have no effect.

3.1.2 Load Cases

A set of driving situations, drive cases, are analysed. The resultant forces and motions of these drive cases are divided into a set of load cases. Each load case is applied in a quasistatic manner onto the multibody dynamics model in turn, and a set of outputs are measured. The loads are applied as approximations of single sinus waves[8] at 0.1 Hz in order to avoid dampening effects. Thereby, inertial effects are negligible. Table 4 shows the drive cases and their corresponding load case.

Nr.	Drive Case	Load Case
1	Speed Bump (Two Wheels)	Parallel Wheel Travel
2	Speed Bump (One Wheel)	Roll
3	Cornering	Lateral Force (WC)
4	Cornering	Lateral Force (CP)
5	Speed Bump	Longitudinal Force (WC)
6	Speed Bump (One Wheel, Offset)	Overturning Moment (WC)
7	Cornering	Aligning Torque (WC)
8	Pothole/Bump (NVH)	Static Vertical Force (CP)
9	Cornering (NVH)	Static Lateral Force (CP)
10	Braking (NVH)	Static Longitudinal Force (CP)
11	Pothole/Bump (Max)	Max Vertical Force (WC)
12	Cornering (Max)	Max Lateral Force (WC)
13	Braking (Max)	Max Longitudinal Force (WC)

Table 4: Load cases (WC = Wheel Center, CP = Contact Patch[9]).

[8] The approximation of a sinus wave is explained in Section 3.1.3.

[9] The contact patch is the portion of the tire that is in contact with the road surface.

3.1.2.1 Kinematic Analysis

All loads in the kinematic analyses are applied as displacement controlled motions. Load cases 1 and 2 are kinematic analyses.

3.1.2.1.1 Loadcase 1: Parallel Wheel Travel

The parallel wheel travel load case simulates the car driving over a speed bump with both wheels. Both wheels are displaced ±100 mm vertically. The longitudinal displacement in the wheel center and the lateral displacement in the contact patch are measured. Figure 23 shows the input motion and the measured output displacements. Table 5 summarize the measured responses in this load case.

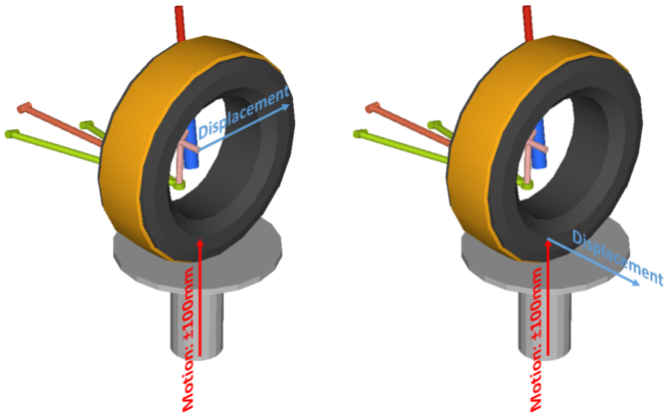

Figure 23: Load Case 1: Input (red) and outputs (blue).

Resp. Nr.	Input	Output
1	±100 mm Vertical Wheel Travel	Wheelbase Change (WC)
2		Track Width Change (CP)

Table 5: Load Case 1: Responses.

3.1.2.1.2 Loadcase 2: Roll

The roll load case simulates the car driving over a speed bump with one wheel. The wheels are displaced vertically in opposite directions in order to simulate a ±4° roll. The toe and camber angles are measured. Figure 24 shows the input motion and the measured output angles. Table 6 summarize the measured responses in this load case.

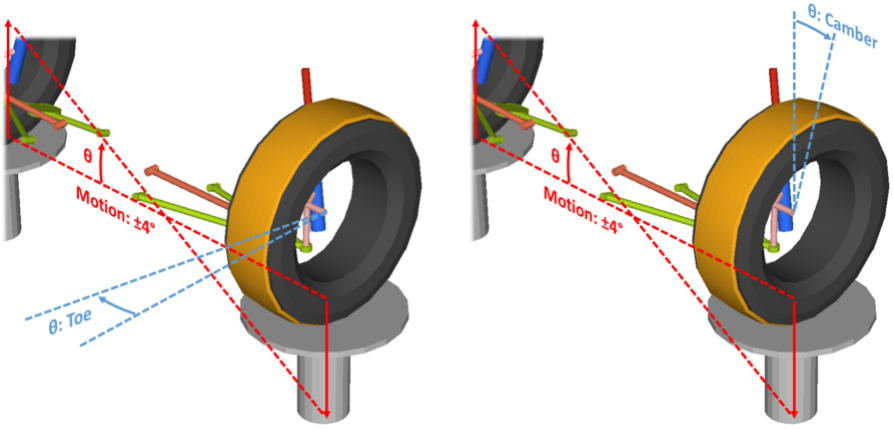

Figure 24: Load Case 2: Input (red) and outputs (blue).

Resp. Nr.	Input	Output
3	±4° Roll	Steer
4		Camber

Table 6: Load Case 2: Responses.

3.1.2.2 Elastokinematic Analysis

All loads in the elastokinematic analyses are applied as forces. Load cases 3 and 8 are elastokinematic analyses.

3.1.2.2.1 Loadcase 3: Lateral Force (WC)

The Lateral Force (WC) load case simulates the car taking a corner. A lateral force at ±20 kN is applied at the wheel center. The lateral displacement in the wheel center is measured. Figure 25 shows the input force and the measured output displacement. Table 7 summarize the measured response in this load case.

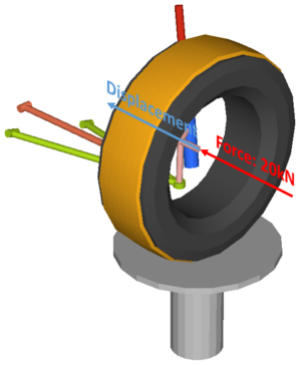

Figure 25: Load Case 3: Input (red) and output (blue).

Resp. Nr.	Input	Output
5	±20 kN Lateral Force (WC)	Compliance (WC)

Table 7: Load Case 3: Response.

3.1.2.2.2 Loadcase 4: Lateral Force (CP)

The Lateral Force (CP) load case simulates the car taking a corner. A lateral force at ±20 kN is applied at the contact patch. The lateral displacement in the contact patch, and the toe and camber angles are measured. Figure 26 shows the input force and the measured output displacement and angels. Table 8 summarize the measured responses in this load case.

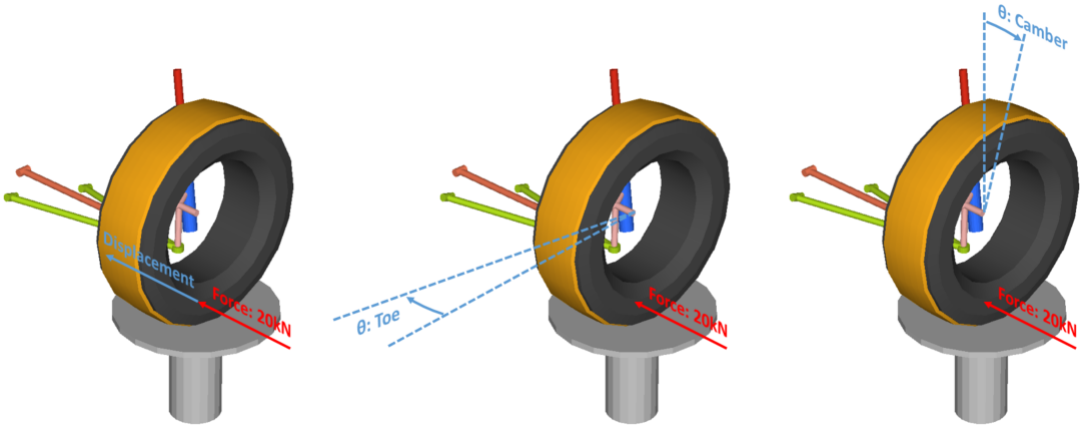

Figure 26: Load Case 4: Input (red) and outputs (blue).

Resp. Nr.	Input	Output
6		Compliance (CP)
7	±20 kN Lateral Force (CP)	Steer
8		Camber

Table 8: Load Case 4: Responses.

3.1.2.2.3 Loadcase 5: Longitudinal DS Force (WC)

The Longitudinal Force (WC) load case simulates the car driving over a speed bump with both wheels. A longitudinal force at ±5 kN is applied at the wheel center. The longitudinal displacement in the wheel center, and the toe and camber angles are measured. Figure 27 shows the input force and the measured output displacement and angels. Table 9 summarize the measured responses in this load case.

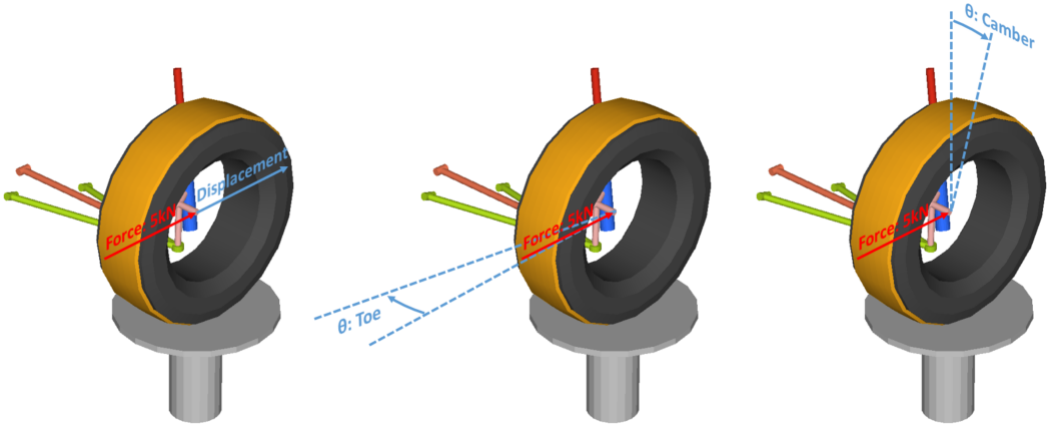

Figure 27: Load Case 5: Input (red) and outputs (blue).

Resp. Nr.	Input	Output
9		Compliance (WC)
10	±5 kN Longitudinal Force (WC)	Steer
11		Camber

Table 9: Load Case 5: Responses.

3.1.2.2.4 Loadcase 6: Overturning Moment (WC)

The Overturning Moment (WC) load case simulates the car driving over a speed bump with one wheel offset. A lateral torque at ±1 kNm is applied at the wheel center. The toe and camber angles are measured. Figure 28 shows the input torque and the measured output angels. Table 10 summarize the measured responses in this load case.

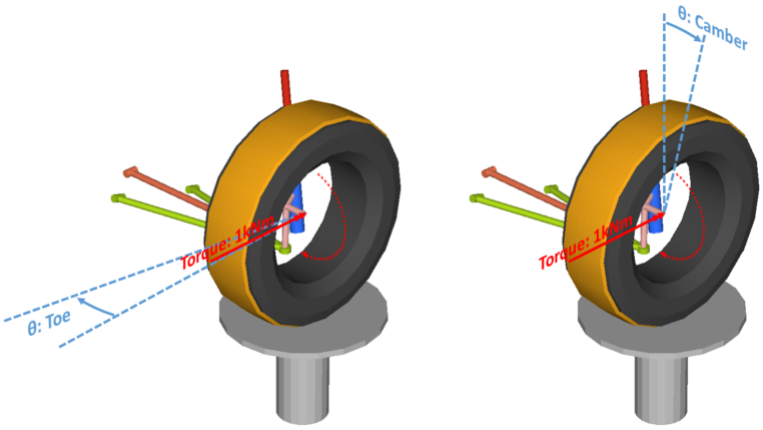

Figure 28: Load Case 6: Input (red) and outputs (blue).

Resp. Nr.	Input		Output
12 13	±1 kNm	Overturning Moment (WC)	Steer Camber

Table 10: Load Case 6: Responses.

3.1.2.2.5 Loadcase 7: Aligning Torque (WC)

The Aligning Torque (WC) load case simulates the car taking a corner. A vertical torque at $\pm 1\,\mathrm{kNm}$ is applied at the wheel center. The toe angle is measured. Figure 29 shows the input torque and the measured output angel. Table 11 summarize the measured response in this load case.

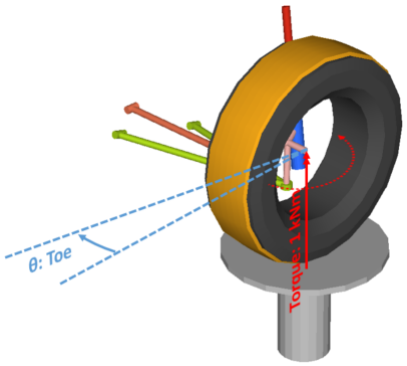

Figure 29: Load Case 7: Input (red) and output (blue).

Resp. Nr.	Input	Output
14	$\pm 1\,\mathrm{kNm}$ Aligning Torque (WC)	Steer

Table 11: Load Case 6: Response.

3.1.2.3 Reaction Force Distribution Analysis (NVH)

In the force distribution analysis the loads are applied as static forces. The distribution of the reaction forces in the bushings is to be evened out in an attempt to improve the noise, vibration, and harshness (NVH) performance. The damper is locked and is not allowed to be compressed in order to simulate an impact. Load cases 8-10 are included in the force distribution analysis.

3.1.2.3.1 Loadcase 8-10: Static Loads

Load case 8 simulates the car driving into a pothole or over a speed bump. A vertical force at $\pm 1\,\mathrm{kN}$ is applied at the contact patch. Load case 9 simulates the car taking a corner. A lateral force at $\pm 1\,\mathrm{kN}$ is applied at the contact patch. Load case 10 simulates the car braking. A longitudinal force at $\pm 1\,\mathrm{kN}$ is applied at the contact patch. The magnitude of the max forces in the bushings are measured at each load case. Later on, in the system optimization, the distribution of these max forces are evened out by minimizing the standard deviation of the max forces. Figure 30 shows the input forces and the bushings where the reaction forces are measured. Table 12 summarize the measured response in the reaction force distribution analysis load cases.

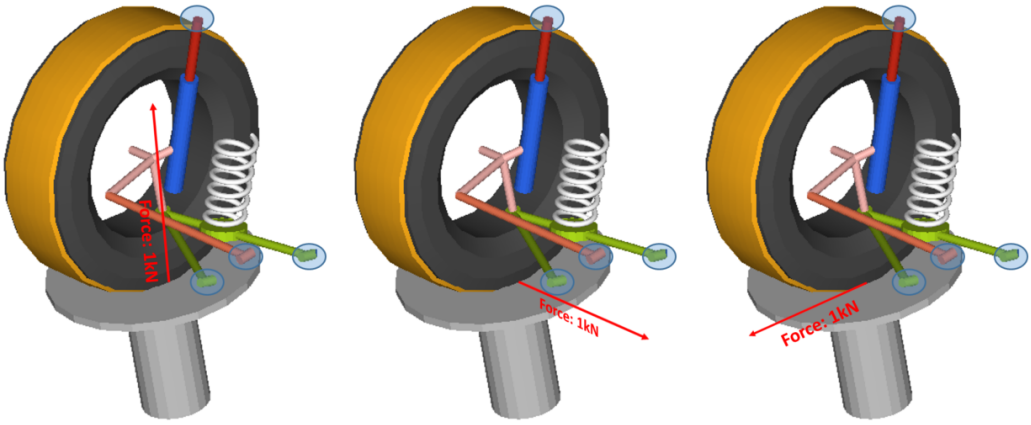

Figure 30: Loadcase 8-10: Inputs (red) and bushings (blue).

Resp. Nr.	Input		Output
15	$\pm 1\,\mathrm{kN}$	Vertical Force (CP) Lateral Force (CP) Longitudinal Force (CP)	Standard Deviation of Max Forces (Bushings)

Table 12: Load Case 8-10: Response.

3.1.2.4 Max Force Analysis (Strength & Weight)

The max loads are used in the topology optimization on the control arm later on. The damper is locked and is not allowed to be compressed in order to simulate an impact. Load cases 11-13 are included in the max force analysis.

3.1.2.4.1 Loadcase 11-13: Max Loads

Load case 11 simulates the car driving into a pothole or over a speed bump. A vertical force at $\pm 3.5\,\mathrm{m{\cdot}g}$ is applied at the wheel center, where m denotes the design load mass of the vehicle which is supported by the rear axle. Load case 12 simulates the car taking a corner. A lateral force at $\pm 1.2\,\mathrm{m{\cdot}g}$ is applied at wheel center. Load case 10 simulates the car braking. A longitudinal force at $\pm 1.2\,\mathrm{m{\cdot}g}$ is applied at the wheel center. The max forces in the connection points of the control arm are measured at each load case. These forces are used later on in the topology optimization on the control arm. Figure 31 shows the input forces and the connection points where the forces are measured. Table 13 summarize the measured response in the max force analysis load cases.

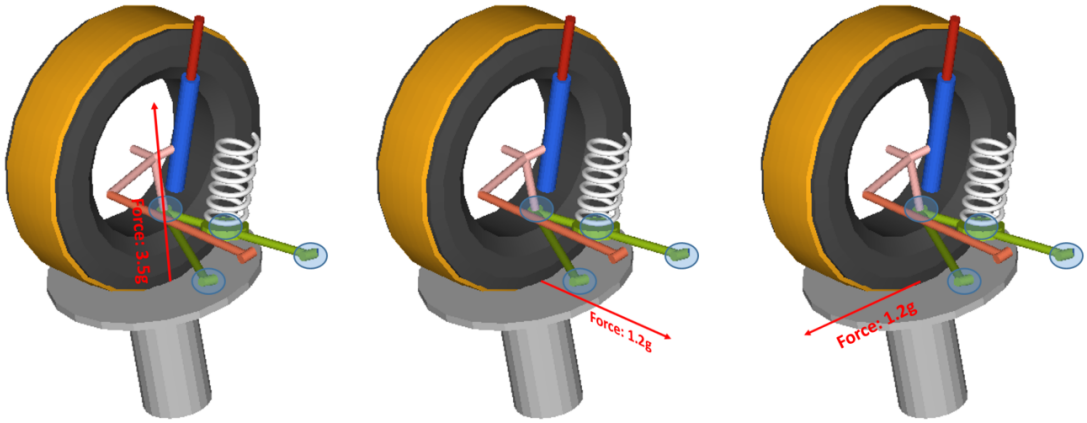

Figure 31: Loadcase 11-13: Inputs (red) and control arm connection points (blue).

Resp. Nr.	Input		Output
16	$\pm 3.5\,\mathrm{m{\cdot}g}$	Vertical Force (WC)	Max Forces (Control Arm)
	$\pm 1.2\,\mathrm{m{\cdot}g}$	Lateral Force (WC)	
		Longitudinal Force (WC)	

Table 13: Load Case 11-13: Response.

3.1.3 Responses

For each load case simulation, a load is applied as an approximation of a sinus function[10], performing one oscillation, with the amplitude A equal to the max load. Figure 32 shows how the input load is applied as an approximation of a sinus function.

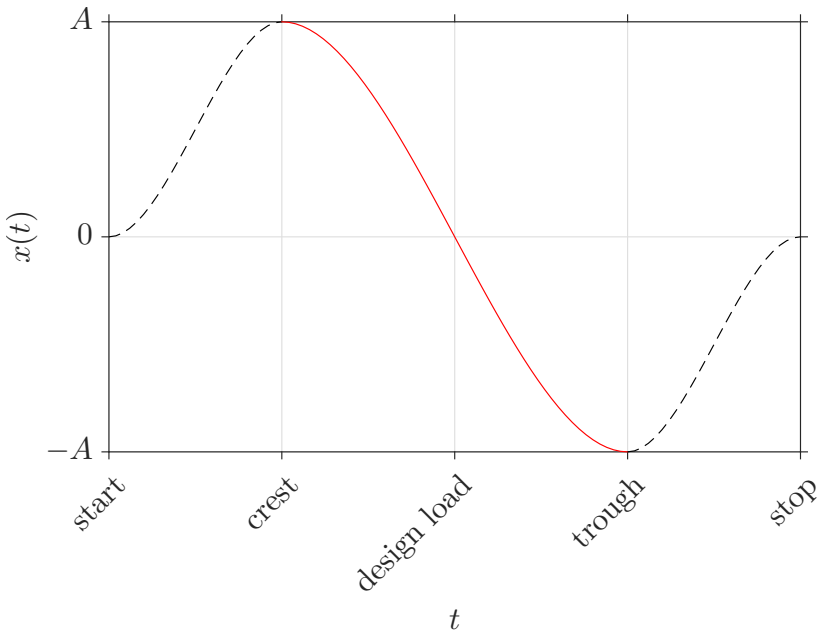

Figure 32: Variation of the input load over time during a load case simulation.

The magnitude of the load at the time steps which marked in red are stored in the input vector $\mathbf{x}$. Thus, data from the entire range of the input load is collected without duplicate samples.

[10]The `MotionSolve` function `STEP` [7] outputs a smooth transition between two points, and is used to approximate a sinus function in order to ensure that the input attain specific values at specific time steps.

A set of translational and rotational displacements are measured at each time step during the load case simulations, and stored in the output vectors $\mathbf{y}_1, \mathbf{y}_2, \mathbf{y}_3, \ldots, \mathbf{y}_n$. Each of these displacements, $\mathbf{y}$, is an output of the function f, the multibody model, with the load $\mathbf{x}$ as the input, Equation (10).

$$\mathbf{y} = f(\mathbf{x}) \tag{10}$$

Figure 33 shows the measured displacement $\mathbf{y}$ during a load case simulation.

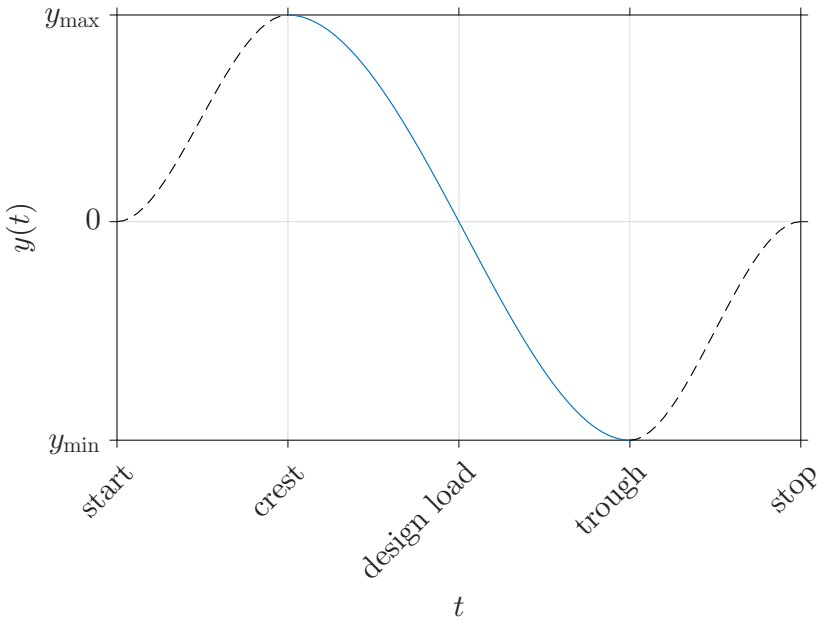

Figure 33: The measured displacement over time during a load case simulation.

The response $\mathbf{r}$ is the derivative of the multibody model f, with respect to the load $\mathbf{x}$. The derivative of f is approximated as the rate of change between the input $\mathbf{x}$, and the output $\mathbf{y}$, Equation (11).

$$\mathbf{r} = f'(\mathbf{x}) = \frac{\mathrm{d}\mathbf{y}}{\mathrm{d}\mathbf{x}} \approx \frac{\Delta\mathbf{y}}{\Delta\mathbf{x}} \tag{11}$$

Figure 34 shows the variation of the response $\mathbf{r}$ and its limits during a load case simulation.

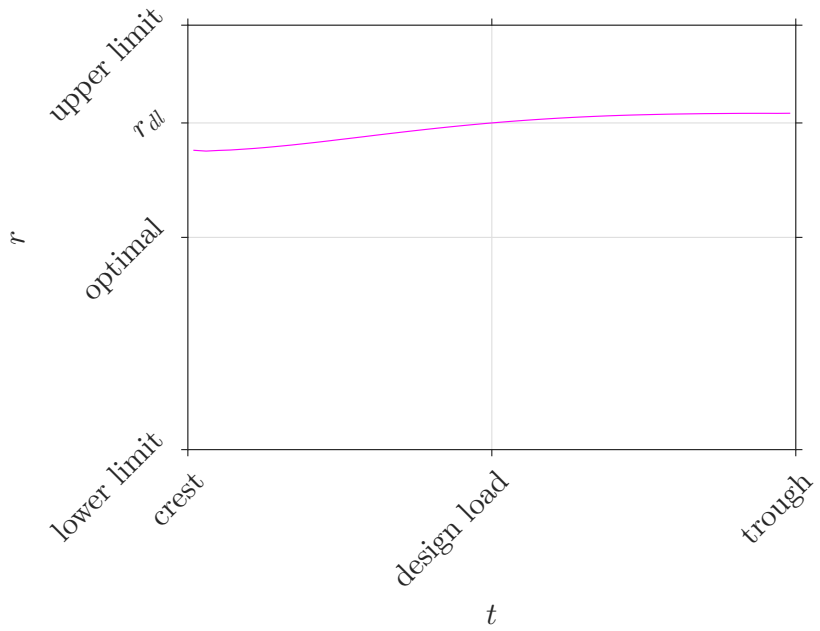

Figure 34: Variation of the response $\mathbf{r}$ during the load case simulation.

The response recorded at the design load, r_{dl}, is called the design load response. It is this response to which the response limits apply.

Table 14 summarize the responses presented in Section 3.1.2 with their limits and the objective they belong to.

Nr.	Response Input		Output	Limits Lower	Optimal	Upper	Unit	Objective
1	±100 mm	Vertical Wheel Travel	Wheelbase Change (WC)	–*	–*	–*	$^{mm}/_{100mm}$	Ride
2			Track Width Change (CP)	–*	–*	–*		Handling
3	±4°	Roll	Steer	–*	–*	–*	$^{deg}/_{deg}$	Handling
4			Camber	–*	–*	–*		
5	±20 kN	Lateral Force (WC)	Compliance (WC)	–*	–*	–*	$^{mm}/_{kN}$	Handling
6	±20 kN	Lateral Force (CP)	Compliance (CP)	–*	–*	–*	$^{mm}/_{kN}$	Handling
7			Steer	–*	–*	–*	$^{deg}/_{kN}$	
8			Camber	–*	–*	–*		
9	±5 kN	Longitudinal Force (WC)	Compliance (WC)	–*	–*	–*	$^{mm}/_{kN}$	Ride
10			Steer	–*	–*	–*	$^{deg}/_{kN}$	Handling
11			Camber	–*	–*	–*		
12	±1 kNm	Overturning Moment (WC)	Steer	–*	–*	–*	$^{deg}/_{kNm}$	Handling
13			Camber	–*	–*	–*		
14	1 kNm	Aligning Torque (WC)	Steer	–*	–*	–*	$^{deg}/_{kNm}$	Handling
15	±1 kN	Vertical Force (CP) Lateral Force (CP) Longitudinal Force (CP)	Standard Deviation of Max Forces (Bushings)		Min		N	NVH
16	±3.5 m·g ±1.2 m·g	Vertical Force (WC) Lateral Force (WC) Longitudinal Force (WC)	Max Forces (Control Arm)				N	Mass Reduction

Table 14: MBD responses. *confidential

3.1.4 Rating

The responses presented in the previous sections are to be optimized in such a way that they yield their optimal target value, or at least a value within their limits, shown in Table 14. These limits describe a limited response range with an optimal response value in the middle or at one side of the range. The nature of these responses cause some problems that need to be dealt with.

In a traditional optimization the objectives are normally set to be maximized or minimized. For instance, if one would like to reduce the mass of a component, one could set the objective to minimize the mass response. This kind of setup is straightforward in the sense that the lower the response value is, the better the result is. The traditional optimization approach is not viable when the responses are supposed to approach a certain value within a given range. The optimization algorithm will only know to minimize or maximize the responses, regardless of their current values. The algorithm does not know when it has reached an optimal target value.

The responses use various units and the magnitudes of their variations vary greatly. This inhomogeneity of the responses may bias the optimization algorithm into a certain direction for the solution as some responses are more compliant than others.

These problems are solved by finding an appropriate rating method, which mathematically transforms the response values into a new one-sided rating range [0 ∞], where less is always better, and converts the response values into dimensionless quantities. In this thesis the two rating methods `Weighted Absolute Mean Deviation` and `Design Load Response Target Factor` where developed to handle these conversions.

3.1.4.1 Weighted Absolute Mean Deviation

A weighted absolute mean deviation of the response, D, is computed for the measured response $\mathbf{r}$ using Equation (12), with the optimal response e as the expected value, and the difference between the optimal response e and the active response limit l at each time step as the tolerable variance $\boldsymbol{\sigma}$.

$$D = \frac{1}{n} \sum_{t=1}^{n} \frac{|\mathbf{r_t} - e|}{\boldsymbol{\sigma}_t} \tag{12}$$

D is a dimensionless quantity since it is the mean of the ratios between the observed response deviation and the tolerable deviation at each time step. Thus, it is comparable between different responses. Since D is a mean value it is also independent of the number of time steps n used in the simulation. Thus, load cases using different number of time steps are comparable, with the exception that the accuracy for D decreases with less time step.

Equation (13) shows how either the lower limit l_{l}, or the upper limit l_{u}, is selected as the active limit l, in the tolerable variance $\boldsymbol{\sigma}$, at each time step t during the load case

simulation, depending on which side of the expected value the response is measured.

$$\boldsymbol{\sigma}_t = \begin{cases} |l_u - e| & \text{if} \quad \mathbf{r}_t \geq e \\ |l_l - e| & \text{else} \end{cases} \tag{13}$$

Figure 35 shows how D varies if the measured response $\mathbf{r}$ is a straight line with the slope $\nabla\mathbf{r}$.

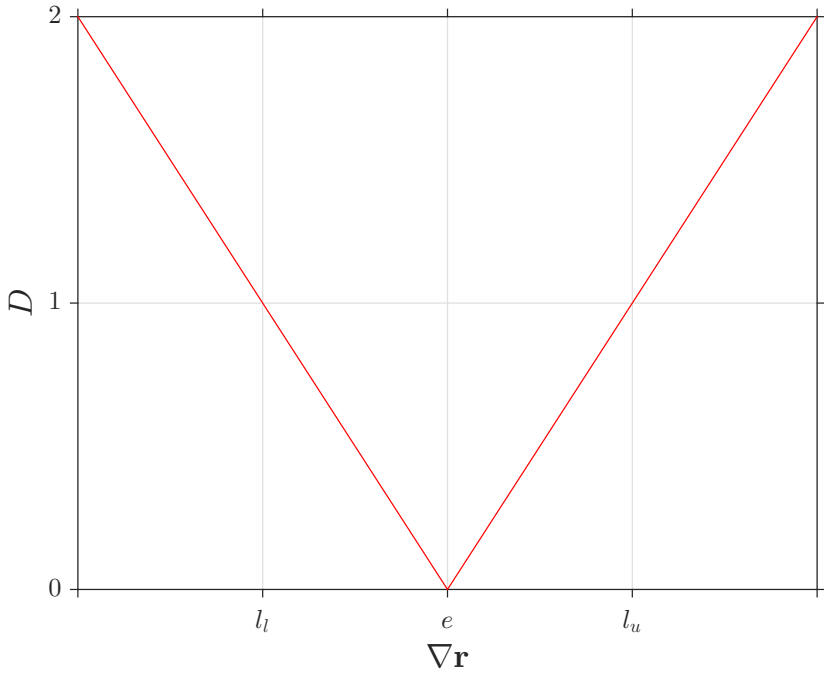

Figure 35: Weighted Absolute Mean Deviation.

3.1.4.2 Design Load Response Target Factor

The target values and limits for the responses, shown in Table 14, are set to apply at the design load. The design load is the rear axle load of the car with a driver and a passenger in the front seats. The time step at which the design load occur during a load case simulation is marked in the Figure 34.

The response measured at the design load, r_{dl}, is extracted from the response data, and the factor by witch it violates its target limits, T, is calculated using equation 14.

$$T = \frac{|r_{\text{dl}} - e|}{\sigma_{\text{dl}}}, \qquad \sigma_{\text{dl}} = \begin{cases} |l_u - e| & \text{if} \quad r_{\text{dl}} \geq e \\ |l_l - e| & \text{else} \end{cases} \tag{14}$$

If $T \leq 1$ then the response is within the target limits at the design load.

3.1.5 Weighted Sum

The responses presented in Section 3.1.3 are divided into the Ride, Handling, and NVH objectives, as shown in Table 14. The Ride and Hanling objectives consist of multiple responses. Each are to be given a mean rating value of the responses belonging to them.

A problem occurs when the responses are non-linear. The `Weighted Absolute Mean Deviation` algorithm punishes the non-linear responses by giving them big weighted absolute mean deviation D values. When these responses are improved their D values drop significantly. This variation in the D values of the non-linear responses may even be greater than the total sum of the other D values of the responses belonging to the same objective. The non-linear responses would thereby dominate the objectives and drown the other responses with their variation ratio.

This problem is solved by normalizing the D values into a range of [0 1] using Equation (15).

$$D_N = 1 - \frac{1}{1 + D} \tag{15}$$

Figure 36 shows how R varies as a function of D.

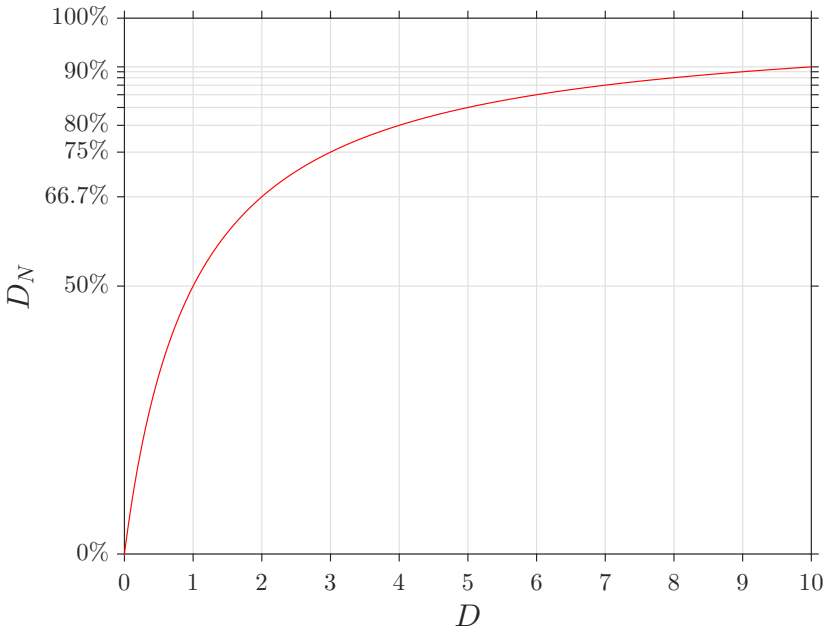

Figure 36: Normalized Weighted Mean Deviation rating.

An optimal response, with $D = 0$, will result in $D_N = 0$, while an infinitely poor response, with $D = \infty$, will result $D_N = 1$. The entire response range is thereby compressed into the range of [0 1], with a response matching one of the response limits at $D_N = 0.5$. The D_N values of the responses make it possible to compare improvement in very nonlinear responses to the improvement of those which are close

to optimal. At the same time, responses far of from their optimal values are punished by compressing them into the upper segment of the weighted value. Each objective is assigned the mean value of its responses D_N values.

It would be possible to give the responses individual weight, but all of the responses under each objective are considered to be of equal importance. The objectives are also considered to be of equal importance.

3.2 Experiment Setup in `HyperStudy`

`HyperStudy` is a multi-disciplinary design exploration, study and optimization software [7].

3.2.1 Design Variables

The design variables in the multibody dynamics model are the coordinates of the attachment points and the stiffnesses of the bushings in the attachment points which connect the suspension to the vehicle body. There are no bushings in the attachment points which internally connect the parts of the suspension system. Figure 37 shows the attachment points and bushings which are used as design variables.

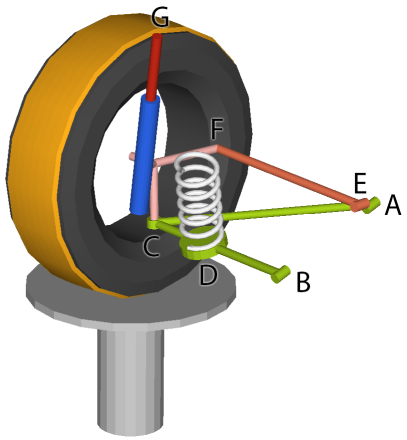

Figure 37: Design variables.

The attachment points have three design variables each, one for each degree of freedom as they are allowed to translate in the room. The bushings initially have six degrees of freedom as they have both translational and rotational stiffnesses in all respective degrees of freedom. We have assumed cylindrical symmetry for the bushings and reduced the number of design variables to four using axial and radial translational stiffnesses, and axial and radial rotational stiffnesses. Table 15 summarize the attachment points and their respective bushings and the total number of degrees of freedom used as design variables at each location.

Location	Name	Attachment Point	Bushing	Sum of Variables
A	Control Arm to Body Front	Yes	Yes	7
B	Control Arm to Body Rear	Yes	Yes	7
C	Control Arm to Knuckle	Yes	No	3
D	Control Arm to Spring	Yes	No	3
E	Toelink to Body	Yes	Yes	7
F	Toelink to Knuckle	Yes	No	3
G	Strut to Body	Yes	Yes	7
		7	4	37

Table 15: Design variables.

In similar studies, presented in Section 1.7, the design range for the attachment points are set in varying ways. In some studies, a fixed range from the initial value is used, such as $x \pm 20\,\text{mm}$, and in others a percentage of the initial value, such as $x \pm 10\%$. In this study the design range for the attachment points will be a fixed range, however much greater then the similar studies, namely a range of $x \pm 100\,\text{mm}$. Although, for some attachment points the range has been limited in order to avoid intersection of the suspension bodies. In reality this range should be set by a designer, and would probably be narrowed down since the space for the suspension parts is limited as well as the possibilities to move the attachment points on the vehicle body. Since the goal of this thesis is not to find a working design for an existing vehicle, it is possible to use such a great range in order to investigate the potential of the suspension without any limitations.

Figure 38 shows the local Cartesian coordinate system for a bushing. The axial translational and rotational stiffnesses is assigned to the z-directional stiffnesses. The radial translational and rotational stiffnesses are assigned to both the x and y-directional stiffnesses. Note that a true radial value would be $\sqrt{(x^2 + y^2)}$, but this is not of importance when two suspension simulations are compared.

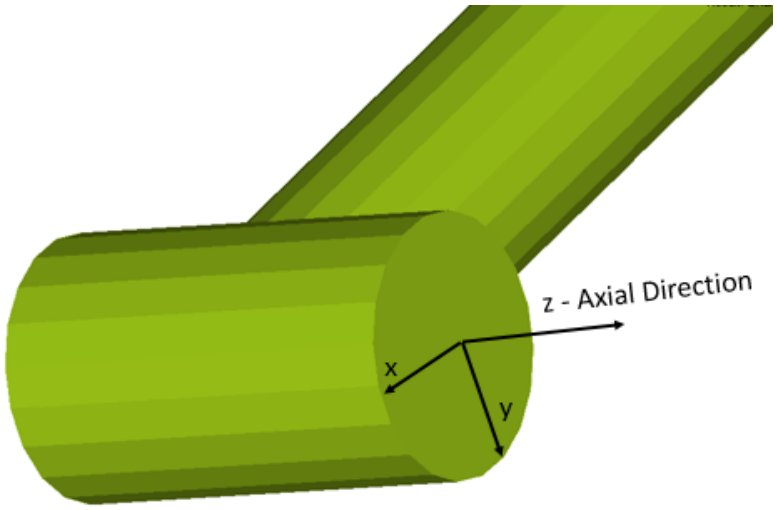

Figure 38: Bushing with Cartesian coordinate system.

Table 16 shows the design range for the bushings, based on data on typical stiffness values provided by Altair.

Direction	Translational Stiffness [N/mm]		Rotational Stiffness [Nmm/deg]	
	Lower	Upper	Lower	Upper
Axial (z)	100	10000	1000	10000
Radial (x,y)	1000	25000	1000	30000

Table 16: Typical range of bushing stiffnesses for a rear suspension.

The design variables that determine the Control Arm to Spring position, point D in Figure 39 below, are set in a bit different manner. Initially, six design variables with ranges similar to those of the other attachment points where used to describe the attachment points to the control arm and to the vehicle body. However, this initial approach was not suitable since it often yielded designs where the spring was positioned in such a way that it did not function properly.

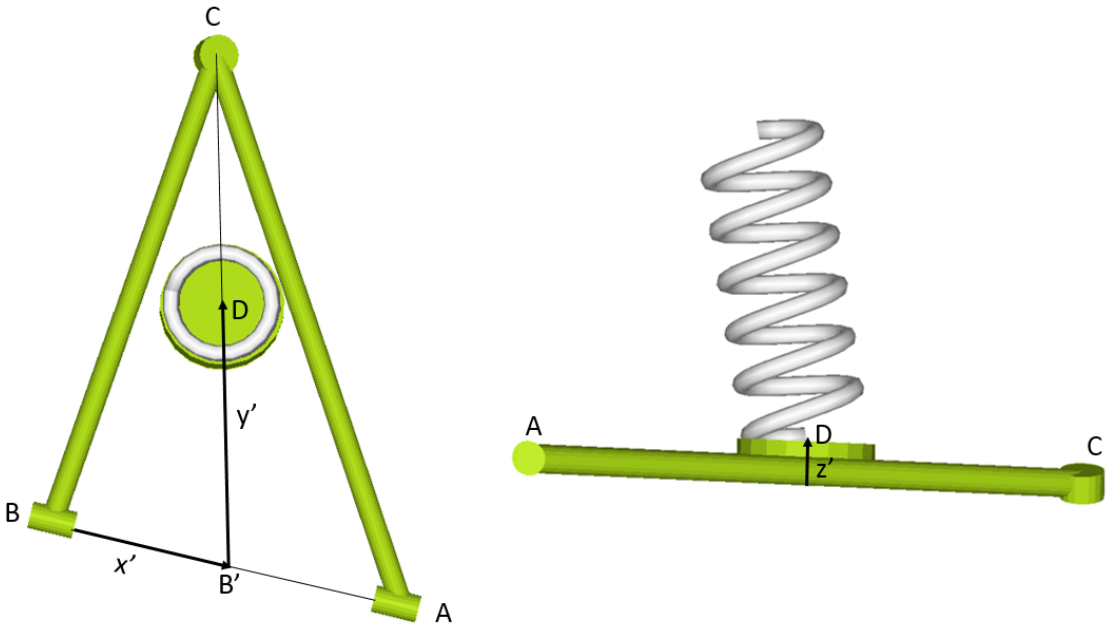

Figure 39: Definition of spring coordinates.

By examining the placement of the spring in the nominal model it was found that the positioning of the spring was dependent on the geometry of the control arm. The plane of the control arm is given by the points A B and C, regardless of how they are positioned in the global coordinate system. The attachment point of the spring to the control arm needs to be constant relative to this plane. In the vertical wheel travel load case the point C is elevated 100 mm in the global z-direction. The point attaching the spring to the vehicle body must be placed in such a way that the compressed spring is perpendicular to the elevated control arm.

This problem is solved in four steps. First, the design variable x′ determines by which fraction [0 1] point D is to be placed between the arms AC and BC. This determines the position of B′ between B and A in Figure 39 above. Secondly, the design variable y′ determines by which fraction point D is to be placed between B′ and C. Intersection between the spring seat and other geometry is avoided by limiting the range of y to [0.2 0.8]. Thirdly, the design variable z′ determines the offset of the point D from the ABC plane by ±40 mm. The position of the control arm to spring attachment point is now defined in all dimensions. Fourthly, the appropriate position for the spring to body attachment point is calculated such that it fulfills the requirements stated above. The positioning of the spring is now defined using totally three design variables. In Figure 39 above the x′ and y′ design variables are both set to 0.5 and the z′ design variable to 10 mm.

This approach solves the problem with non-feasible designs. Constant x′ y′ and z′ design variables always yield geometrically similar designs, independently of how the points A B and C are set. For instance, the point D will always be placed in the center of mass of the control arm if x = 0.5, y = 1/3 and z = 0. Thus, the responses resulting of a certain x′ y′ and z′ setup are highly dependent on the positioning of A B and C.

Table 17 shows a complete list of the design variables and the respective design range. Together they form the complete design space. The initial values of the attachment points, called the nominal design, was provided with the model by Altair. The initial values of the bushing stiffnesses are arbitrarily set as approximately the mean value of their ranges. ”p” denotes attachment point, ”bsh” is buching, ”t_r” is translational radial stiffness, ”t_a” is translational axial stiffness, ”r_r” is rotational radial stiffness and ”r_a” is rotational axial stiffness.

DV Nr	DV Name	Lower Value	Initial Value	Upper Value
1	p_CtrlArmBodyFront_x	-100	0	100
2	p_CtrlArmBodyFront_y	-100	0	100
3	p_CtrlArmBodyFront_z	-100	0	100
4	p_CtrlArmBodyRear_x	-100	0	100
5	p_CtrlArmBodyRear_y	-100	0	100
6	p_CtrlArmBodyRear_z	-100	0	100
7	p_CtrlArmKnuckle_x	-100	0	100
8	p_CtrlArmKnuckle_y	-56.3	0	100
9	p_CtrlArmKnuckle_z	-30	0	100
10	p_ToeLinkKnuckle_x	-100	0	100
11	p_ToeLinkKnuckle_y	-89.5	0	100
12	p_ToeLinkKnuckle_z	-100	0	100
13	p_ToeLinkBody_x	-100	0	100
14	p_ToeLinkBody_y	-100	0	100
15	p_ToeLinkBody_z	-100	0	100
16	p_StrutBody_x	-100	0	100
17	p_StrutBody_y	-50	0	100
18	p_StrutBody_z	-100	0	100
19	p_SpringCtrlArm_x	0	0	1
20	p_SpringCtrlArm_y	0.2	0.6	0.8
21	p_SpringCtrlArm_z	-40	0	40
22	bsh_CtrlArmBodyFront_t_r	100	13000	20000
23	bsh_CtrlArmBodyFront_t_a	1000	5500	10000
24	bsh_CtrlArmBodyFront_r_r	100	15500	30000
25	bsh_CtrlArmBodyFront_r_a	1000	5500	10000
26	bsh_CtrlArmBodyRear_t_r	1000	13000	25000
27	bsh_CtrlArmBodyRear_t_a	1000	5500	10000
28	bsh_CtrlArmBodyRear_r_r	100	15500	30000
29	bsh_CtrlArmBodyRear_r_a	1000	5500	10000
30	bsh_ToeLinkBody_t_r	1000	13000	25000
31	bsh_ToeLinkBody_t_a	100	5500	10000
32	bsh_ToeLinkBody_r_r	1000	15500	30000
33	bsh_ToeLinkBody_r_a	1000	5500	10000
34	bsh_StrutBody_t_r	1000	13000	25000
35	bsh_StrutBody_t_a	100	5500	10000
36	bsh_StrutBody_r_r	1000	15500	30000
37	bsh_StrutBody_r_a	1000	5500	10000

Table 17: Design space for the design variables.

The stiffness of the spring and the damping of the damper could have been used as additional design variables. But, since each load case is applied at a low rate, they are practically a set of static loads where damping have no effect. The stiffness of the spring is very small compared to the stiffnesses of the bushings, and would only have a very small effect on the results.

3.2.2 Simulation Responses

The responses from the multibody dynamics (MBD) simulation, Section 3.1.3, are analysed using the methods described in Section 3.1.4 and 3.1.5. A list of the computed values is shown in table 18. In order to avoid confusion these responses will here after be called the HyperStudy (HS) responses and the responses from the MBD simulation will be called the MBD responses.

HS responses 1-14, denoted with D_N as type, are the normalized weighted absolute mean deviations. HS responses 15-28, denoted with DLOAD as type, are the true response values at the design load. HS response 29, denoted with STD as type, is the standard deviation of the max forces measured during the reaction force distribution analysis. HS responses 30-31 are the mean value of the D_N values of the responses belonging to the Ride and Handling objectives. HS response 32 is the normalized value of HS response 29 divided by the value of HS response 29 measured in a simulation with the nominal setup. There are no limits to the NVH objective, this approach instead compare improvements in the NVH objective to the nominal model. HS responses 33-41, denoted with LIMITS as type, is the summarized number of responses in respective category with design load response target factors lesser than 1,2 and 3. Effectively they give the number of responses in respective category which fulfills $1\times$, $2\times$, and $3\times$ the range of the limits.

Response Nr	Response Name	Type
1	Wheelbase Change	D_N
2	Track Width Change (TP)	D_N
3	Roll Steer	D_N
4	Roll Camber	D_N
5	Lateral Force Compliance (WC)	D_N
6	Lateral Force Compliance (TP)	D_N
7	Lateral Force Steer	D_N
8	Lateral Force Camber	D_N
9	Longitudinal Force Compliance (WC)	D_N
10	Longitudinal Force Steer	D_N
11	Longitudinal Force Camber	D_N
12	Overturning Moment Steer	D_N
13	Overturning Moment Camber	D_N
14	Aligning Torque Steer	D_N
15	Wheelbase Change	DLOAD
16	Track Width Change (TP)	DLOAD
17	Roll Steer	DLOAD
18	Roll Camber	DLOAD
19	Lateral Force Compliance (WC)	DLOAD
20	Lateral Force Compliance (TP)	DLOAD
21	Lateral Force Steer	DLOAD
22	Lateral Force Camber	DLOAD
23	Longitudinal Force Compliance (WC)	DLOAD
24	Longitudinal Force Steer	DLOAD
25	Longitudinal Force Camber	DLOAD
26	Overturning Moment Steer	DLOAD
27	Overturning Moment Camber	DLOAD
28	Aligning Torque Steer	DLOAD
29	NVH	STD
30	WEIGHT Ride	WEIGHT
31	WEIGHT Handling	WEIGHT
32	WEIGHT NVH	WEIGHT
33	1L Ride+Handling	LIMITS
34	2L Ride+Handling	LIMITS
35	3L Ride+Handling	LIMITS
36	1L Ride	LIMITS
37	2L Ride	LIMITS
38	3L Ride	LIMITS
39	1L Handling	LIMITS
40	2L Handling	LIMITS
41	3L Handling	LIMITS

Table 18: HyperStudy responses.

3.2.3 Design of Experiments

Similar studies of multi-objective optimizations of vehicle suspensions, presented in Section 1.7, shows that the initial approach to this kind of problem formulation should be a sensitivity analysis. Hence, the need to perform a design of experiment (DOE) study arise. However, these studies interpret and use the information from the sensitivity analysis differently. In most studies, the most influential design variables (DVs) are found and used in the following steps. The data from the DOE is also used to find an appropriate response surface model (RSM) in order to describe the system in a mathematical way. These RSMs are used in the optimizations of the suspensions.

In this thesis a somewhat different approach to the interpretation of the DOE information will be utilized. First of, a RSM will not be used since the simulation time of the multibody dynamics model is very short, in general one simulation takes about five seconds. By taking advantage of multi-core processors, multiple simulations can be run simultaneously. This means that a large number of simulations can be performed over a reasonable time period. 1000 simulations per hour has been estimated to be the average performance of the computers used in this thesis.

When it comes to determine which DVs that have a greater influence on the suspension, the conventional approach, the interpretation of the magnitude of the main & interactions effects in comparison to each other will be utilized. Those design variables that are deemed influential with the conventional approach will then be selected and used in one of the optimizations in order to test this approach. All other optimizations use all of the design variables, since the removal of design variables would introduce limitations to the suspension and potentially limit the performance. However, another way to interpret the main & interaction effects is also suggested. The suggested approach will also make it easier to interpret the amount of effect data that is available in this problem due to the large number of design variables.

The main purpose of our DOE is to perform a concept screening and gain an understanding of the suspension system. The potential performance, which shows if it is possible to reach the target limits, as well as which responses that will be troublesome to optimize, are found. The results will also show which responses are troublesome to optimize. For instance if the suspension has difficulties to reach the target values for one response, that response will be limiting the results of the optimization later on. It might be that a response is insensitive, in the sense, that the response takes values in a limited range, regardless of how the design variables are setup. If that is the case, that response will not be a major driving force in the optimization, since the sensitive responses will have a greater effect on the objective values. In the end the information from the DOE will be interpreted to give an answer to what to expect of the suspension model in terms of potential performance. This will be valuable information if more than one model would be investigated and compared. At an early stage in the design process, one could find the potential performance of the suspension concepts and there after make a more accurate decision to which one of suspension models to

continue with.

The DOE study will be performed in the software `HyperStudy`, where a connection to the MBD model in `MotionView` is established. As presented in Section 2.1.2, a modern DOE method is suitable for computer experiments, which tend to generate sample points in the interior of the design space. Hence, to obtain the best uniformity of the sample points, the modern DOE method Hammersley, which belongs to the quasi-Monte Carlo methods, will be used to generate the sample points. Since the simulations are not that time consuming, 5000 sample points will be generated and then evaluated.

3.2.3.1 Design Variables

The design variables and their design space presented in Table 17 will be used in the Design of Experiments.

3.2.3.2 Design of Experiment Responses

The HS responses 15-28 that evaluates the MBD responses at design load will be used as responses for the Design of Experiments. These are the only responses of interest since the other HS responses have been modified and are therefore not suited for evaluation in terms of main and interactions effects. The modified responses have been rated, normalized and weighted, these procedures may influence the effect calculations and their interpretation.

3.2.4 System Optimization

The main objective of the system optimization is to find a setup for the suspension that fulfill the design load response limits for all responses. This is a very difficult task, as all types of suspension systems have advantages and disadvantages, and it might be impossible to fulfill all of the set requirements at the same time as some of them are contradictory. A problem thus occur if all requirements cannot be fulfilled, and some responses are of greater importance than others. This problem is taken on by splitting the main objective into multiple objectives of equal importance. The responses which are used in the system optimization are divided into the ride, handling, and NVH objectives. Table 14 shows the responses and the objectives they belong to. The ride responses, which provide good comfort, are directly contradictory to the handling responses, which improve the driving performance. Some of these responses are also contradictory to the NVH response, which improve comfort and possibly reduce weight of the suspension components as forces are evened out. An optimization set up using these objectives will generate multiple solutions which all are balanced between ride, handling, and NVH performance, in a pareto surface.

3.2.4.1 Design Variables

The design variables presented in Table 17 are used in the system optimization.

3.2.4.1.1 Design Space Reduction Method (DSRM)

At an early stage in the attempts to perform the system optimization it became obvious that it is rather difficult to reach the target values. This problem was tackled by conducting several optimizations with different setups and interpreting the results.

One first observation was made on how the convergence of the optimizations where influenced by how strictly the constraints were set. Using looser constraints that were easily fulfilled yielded better results than using stricter constraints which was never fulfilled.

A second observation was that it did not help to let to optimization continue with more iterations than the by `HyperStudy` recommended number, since the optimization algorithms converge and little or no improvement in the results show after the recommended number.

A third observation was that by reducing the design space, to the ranges of design variable values where the slackened constrains where fulfilled in an primary optimization, it was possible to fulfill the stricter constraints in a secondary optimization. The results improved significantly as well.

These observations are applied in the suggested Design Space Reduction Method (DSRM) approach. The DSRM is an, to the optimization algorithm, external method which handles the design space. The general idea of the DSRM is to perform an initial optimization with slackened constraints at 3×limits. The iterations which fulfill the constraints are extracted. The design variable values of these iterations has been normally distributed in their design ranges as the optimization algorithm has attempted to find the optimal solution. Three standard deviations (99.73%) of the design ranges where the constraints are fulfilled are saved. After making sure these new design ranges does not violate the original design space, or that design ranges where stricter constraints are fulfilled is not cut out, the new design space is assembled. A new optimization is run using the new design space, where 3×limits is fulfilled, with the constraints tightened to 2×limits. This iterative scheme is repeated until a satisfactory solution is found. Figure 40 shows the DSRM flowchart.

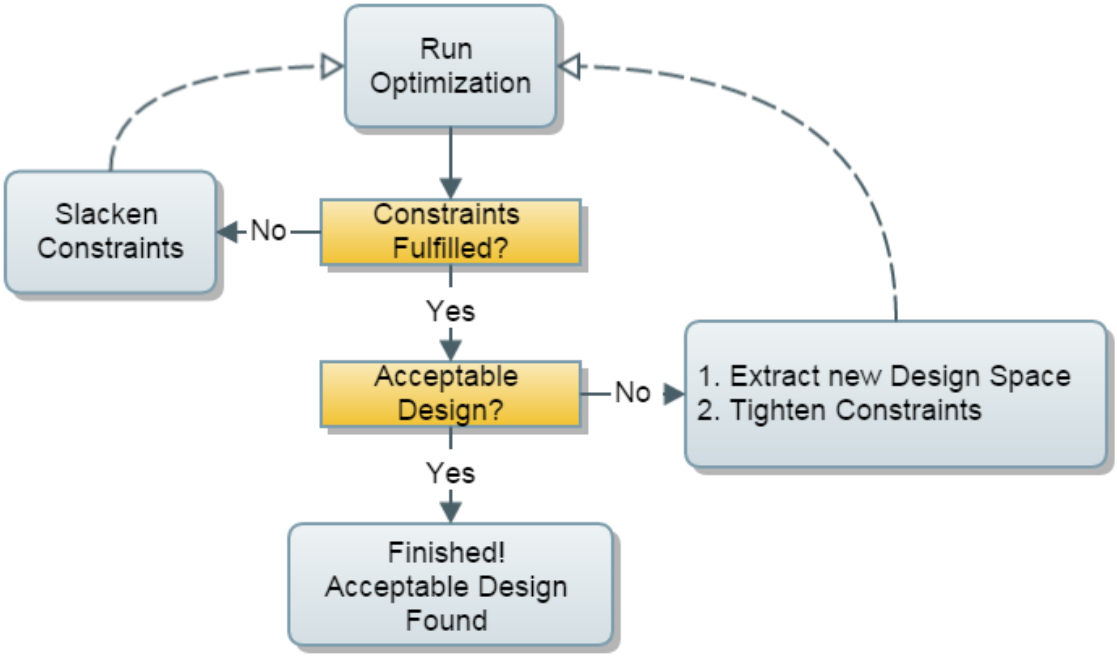

Figure 40: DSRM flowchart.

3.2.4.2 Optimization Responses

The responses used as constraints and objectives are active in the optimization setup.

3.2.4.3 Constraints

The desired response is a linear response which satisfies its target values at the design load. The design responses is therefore used as the constraints. HS responses 33, 34, and 35 gives the number of responses which satisfies the target values, dependent on how strictly the constraint is set in the current optimization. One of these responses is used as constraint in the optimizations.

3.2.4.4 Objectives

Non-linear responses may satisfy the constrains, but is still undesired. The `Weighted Absolute Mean Deviation` method presented in Section 3.1.4.1 punishes non-linear responses as well as it rewards responses for fulfilling the constraints. HS responses 30 and 31 are used for the Ride and Handling objectives. They are the mean of the normalized weighted absolute mean deviation values of the responses belonging to respective objective. As the NVH response does not have any set target values, it is compared to the NVH response of the nominal run instead. HS response 32 is used for the NVH objective.

3.2.4.5 Optimization Methods

`HyperStudy` provides two optimization methods which support multi-objective optimization. Both are evaluated. A brief description of each is given below.

3.2.4.5.1 Global Response Surface Method (GRSM)

The Global Response Surface Method (GRSM) performs a number of initial iterations globally in the design space. These are used to build a response surface. During each following step, a number of iterations are generated based on the response surface, and additional iterations is performed globally in the design space in order to ensure a good balance between the both. The response surface is updated with these new samples and new designs are generated until a satisfactory solution is found.

The GRSM method is a good choice if the model analysis is time consuming, as well if there is a large number of design variables [7].

Figure 41 shows the GRSM flowchart.

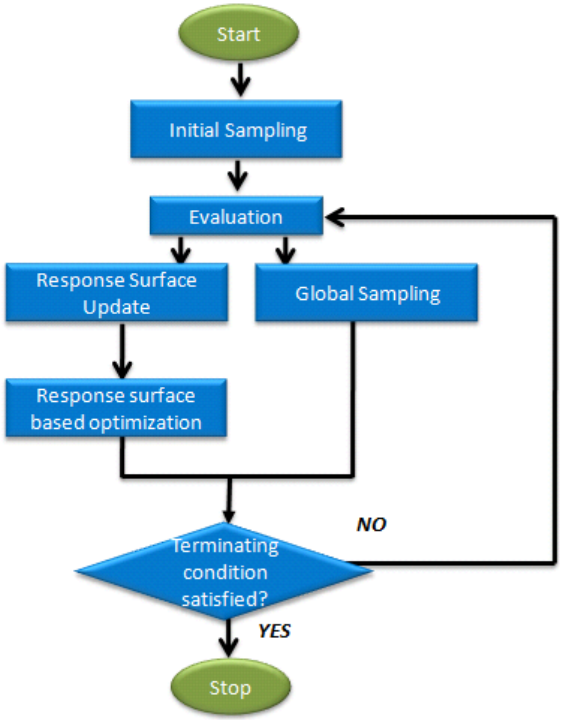

Figure 41: Global Response Surface Method (GRSM) flowchart [7].

3.2.4.5.2 Multi-Objective Genetic Algorithm (MOGA)

The Multi-Objective Genetic Algorithm (MOGA) is modeled after the evolutionary process theory. The MOGA creates an initial population of designs. These are ranked with respect to their constraint violation and objective function values. The elite population in this ranking is then reproduced through the application of genetic operators such as crossover and mutation. The children of this process become members of the next generation. This process is repeated for many generations until the evolution of the population converges to the optimal solution.

The MOGA is recomended if the model analysis time is cheap and a thorough search of the design space is needed [7].

Figure 42 shows the MOGA flowchart.

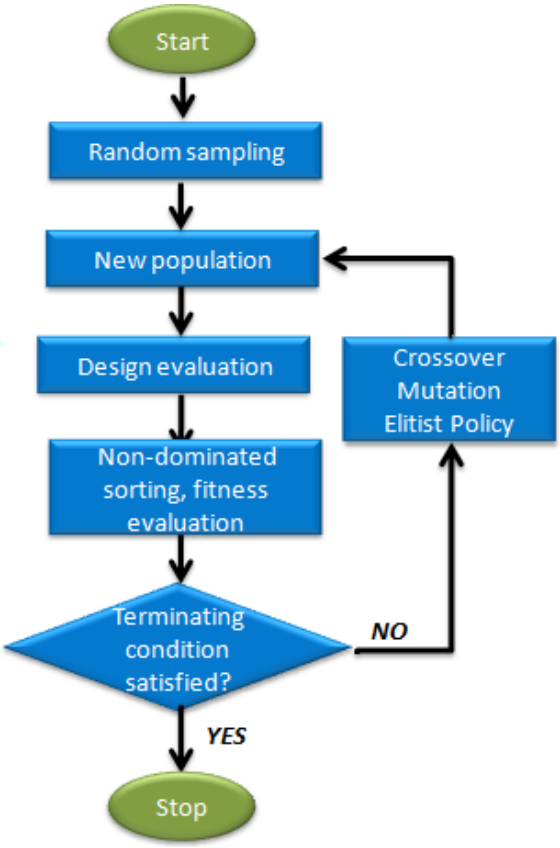

Figure 42: Multi-Objective Genetic Algorithm (MOGA) flowchart [7].

3.3 Investigations

The optimizations that was run in order to verify the setup and validate DSRM method described in Section 3.2.4.1.1 are presented below in Table 19. The different denotations will be discussed below.

Nr.	Objectives	Constraint	DVs	DS	Algorithm	Settings
1	3×Weighted	3L	All	Max	MOGA	Standard
1.1	3×Weighted	2L	All	Reduced(1)	MOGA	Standard
1.2	3×Weighted	1L	All	Reduced(1.1)	MOGA	Standard
1.3	3×Weighted	2L	All	Reduced(1.1)	MOGA	Standard
2	3×Weighted	2L	All	Max	MOGA	Standard
3	15×Invidiual	3L	All	Max	MOGA	Standard
4	3×Weighted	2L	All	Max	GRSM	Standard
5	3×Weighted	3L	Limited	Max	MOGA	Standard
6	3×Weighted	2L	All	Max	MOGA	Longrun
7	3×Weighted	-	All	Max	MOGA	Standard
8	3×Weighted	3L	All	Max Low Bsh	MOGA	Standard
8.1	3×Weighted	2L	All	Reduced(8)	MOGA	Standard
8.2	3×Weighted	1L	All	Reduced(8.1)	MOGA	Standard
8.3	3×Weighted	1L	All	Reduced(8.2)	MOGA	Standard

Table 19: Optimization setups.

Objectives

It is possible to setup the objectives in two ways, either with the weighted sum approach or as individual evaluations. The first approach will give a weight value for each objective type, Ride, Handling, and NVH, whilst the latter will evaluate each rating value individually. The first approach is denoted as ”3×Weighted” whilst the latter is denoted as ”15×Individual”.

Constraints

The constraints are set according to the method discussed in Section 3.2.4.3 and the difference between the setups is the target limits and how strictly they are set. The target limits that was defined in Table 14 will be denoted 1L. Consequently ”2L” and ”3L” corresponds to two respectively three times the limit ranges defined in the Table 14. The denotation ”-” is used when no constraints was used.

Design Variables

Regarding the design variables two different setups has been evaluated, namely, one where all the design variables have been used and a second where the design variables with most influence has been used. The first setup is denoted ”All” whilst the latter ”Limited”.

Design Space

Regarding the design space setup, the standard setup is the one denoted ”Max” and corresponds to the design space defined in Table 17. The setup denoted ”Max Low Bsh” is similar to the ”Max” design space, except that the lowest allowed bushing value is set to 100 for all bushings. Those denoted ”Reduced(X)” have a new design space, that is based on the previous optimization X, in the sense that the range has been narrowed down in the vicinity of the mean value for each design variable, for more details see Section 3.2.4.1.1.

Algorithm

The optimization algorithms used are presented in Section 3.2.4.5.

Settings

Settings is the available settings for the different algorithms. The setup denoted ”Standard” use the standard settings for the algorithms, and the one denoted ”Longrun” forced the algorithm to evaluate three times the number of evaluations of the standard setup.

A detailed description of the setups is given since the different optimizations will be used to investigate how the setups influence the results. In the end, these investigations will show which setup that is preferable for this kind of problem formulation. Table 20 shows a list of the investigated optimization setups and which optimizations these are compared to. In Table 20 the investigations 1-4 are used to show how the constraint, objectives, optimization algorithm, and design variables influence the results, while investigation 5-6 is used to validate the DSRM approach, and how the results with the DSRM can be improved with an extended design space.

Nr	Investigation	Optimizations Compared
1	Influence of Constraints	1,2,7
2	Influence of Objectives	1,3
3	Influence of Optimization Algorithm	2,4
4	Influence of Design Variables	1,5
5	Validity of the DSRM	1-1.2,6
6	DSRM with Extended Design Space	1-1.2,8-8.2

Table 20: Investigations.

3.4 Structural Optimization

A structural optimization was performed in order to prove that it can be integrated into the early design process of a suspension system. The result of a structural optimization on the chosen suspension solution should be used as a concept for an optimal part. A designer would use the concept to create a optimized design which satisfies economical and manufacturing constraints.

The nominal model was used for testing the structural optimization in the design process. The control arm was chosen as the part to be optimized. Topology optimization was selected as optimization method.

Two optimizations was performed using two different materials, a steel material and an aluminum material, to investigate the differences in the generated optimal designs.

3.4.1 Topology Design Space

The design variables used in the control arm in the nominal model is given in Table 17. A local coordinate system, defined by the control arm plane discussed in Section 3.2.1, with origin in the control arm to knuckle attachment point and the axis X′, Y′, and Z′, was setup and the positions of the control arm attachment points in this coordinate system was calculated, Table 21.

Attachment Point	X′	Y′	Z′
Control Arm to Knuckle	0	0	0
Control Arm to Body Front	-274.7	442.1	0
Control Arm to Body Rear	42.2	442.1	0
Control Arm to Spring	16.9	176.8	14.0
Spring Seat	16.9	176.8	0

Table 21: Attachment points.

Figure 43 shows the design space (transparent brown) setup around the attachment points (grey) using the concept design tool `Inspire`.

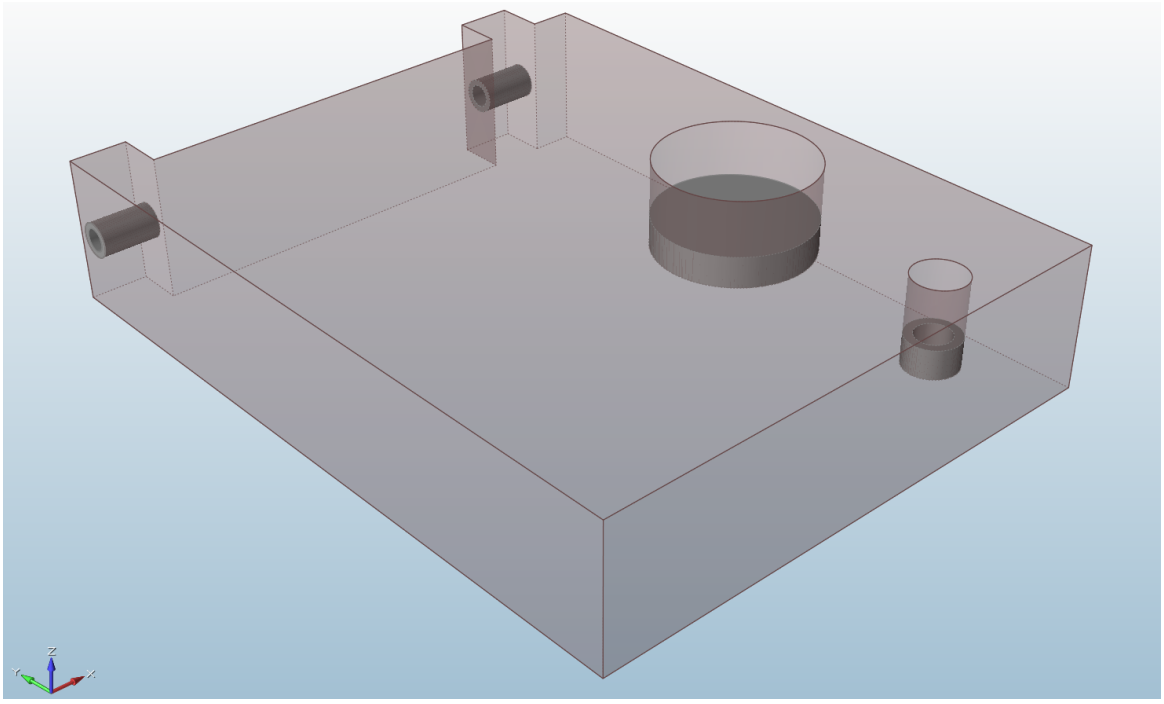

Figure 43: Topology design space.

The design space covers approximately the maximum dimensions in the local X′Y′ plane. It is in 100 mm thick in the local Z′ direction. The horizontal cylinders at the rear of the design space is the geometry of the control arm to body attachment bushings. The big solid cylinder in the middle is the spring seat. The vertical cylinder at the front is the ball joint connecting the control arm to the knuckle. These geometries are the non-design space. Holes has been cut in the design space to avoid intersection with the spring and knuckle geometry.

The topology design space was exported to the finite element pre-and post-processor `HyperMesh`.

3.4.2 Finite Element Setup

The design space imported to `HyperMesh` was divided into design and non-design components.

3.4.2.1 Elements

The components was filled with first order 3D tetrahedral elements, with an element size of 2.5 mm. In total 2 704 304 elements was created using 498 342 nodes. The geometries of the non-design components was connected to their attachment points, where the loads and constraints are applied, using 1D rigid elements.

Figure 44 shows the tetrahedral meshed design space and non-design components.

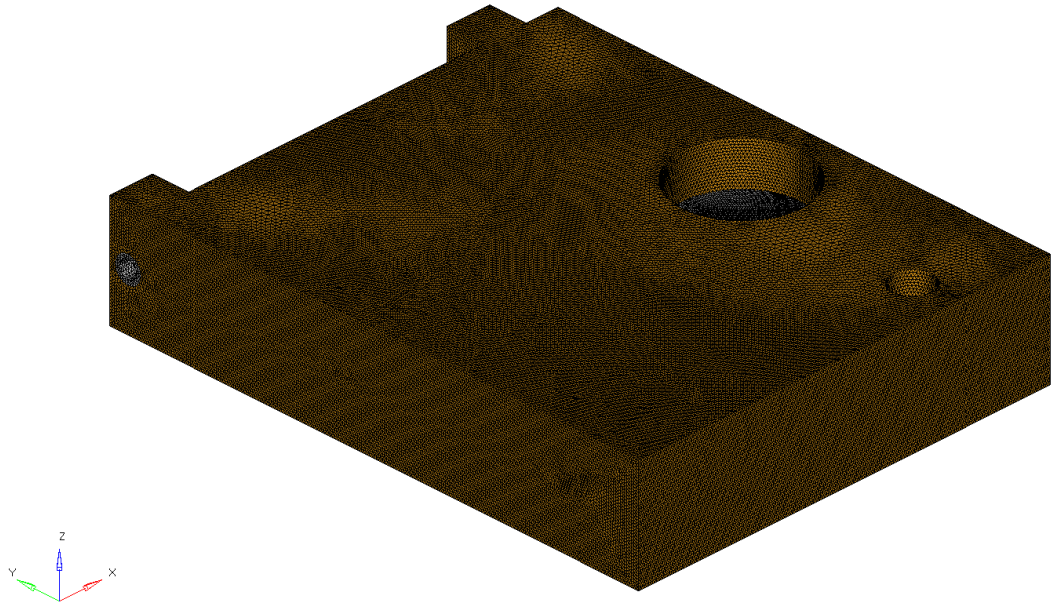

Figure 44: Meshed design space and non-design components.

3.4.2.2 Materials

The data for the materials used in the two optimizations are presented in Table 22. All components where assigned the aluminum material in the first optimization, and the steel material in the second. The allowable stress is set with a safety factor to the yield strength.

Mechanical Property	Symbol	Aluminum AA 354.0-T6	Steel GS-20Mn5	Unit
Young's Modulus	E	73.10	210.00	GPa
Shear Modulus	G	72.60	80.77	GPa
Poisson's Ratio	ν	0.32	0.30	
Density	ρ	2.71	7.85	Mg/m^3
Yield Strength	$R_{p\,0.2}$	250.00	360.00	MPa
Tensile Strength	R_m	305.00	575.00	MPa
Allowable Stress	$\sigma_{\max}$	203.33	383.33	MPa
Safety Factor	n	1.5	1.5	

Table 22: Materials.

3.4.2.3 Loads Cases

3.4.2.3.1 Stress Constraints

The Max Force Analysis, Section 3.1.2.4, provides the forces which the control arm

needs to sustain with stress levels below the allowed stress $\sigma_{\max}$ for the materials. The extracted forces are applied in their respective load cases: Max Load X (±1.2 G Longitudinal Force (WC)), Max Load Y (±1.2 G Lateral Force (WC)), and Max Load Z (±3.5 G Vertical Force (WC)). For each loads step these forces are the sum of all forces experienced by the control arm. The model needs to be constrained in all degrees of freedom, otherwise the result would only be rigid displacement. The loads are almost balanced around the control arm to spring attachment point, where the forces are small in comparison. The forces at this attachment point are replaced by a single point constraint in all degrees of freedom. The reaction forces at this point due to the applied constraints are equal to the forces that where removed.

The Max Load load cases are summarized in Table 23, and are visualized in Figure 45.

Ctrl Arm Attachment Point	FX′ [N]	FY′ [N]	FZ′ [N]	MX′ [Nmm]	MY′ [Nmm]	MZ′ [Nmm]
Max Load X						
Body Front	$-8.35 \cdot 10^{3}$	$2.21 \cdot 10^{4}$	$-4.12 \cdot 10^{1}$	$1.34 \cdot 10^{1}$	$-5.45 \cdot 10^{-1}$	$-1.96 \cdot 10^{2}$
Body Rear	$-8.20 \cdot 10^{3}$	$-3.00 \cdot 10^{4}$	$8.34 \cdot 10^{1}$	$1.34 \cdot 10^{1}$	$-5.45 \cdot 10^{-1}$	$-1.96 \cdot 10^{2}$
Knuckle	$1.65 \cdot 10^{4}$	$7.91 \cdot 10^{3}$	$-3.36 \cdot 10^{0}$			
Max Load Y						
Body Front	$8.05 \cdot 10^{1}$	$-6.82 \cdot 10^{2}$	$2.92 \cdot 10^{0}$	$-7.47 \cdot 10^{-1}$	$2.71 \cdot 10^{-3}$	$-1.40 \cdot 10^{1}$
Body Rear	$1.06 \cdot 10^{1}$	$-4.30 \cdot 10^{3}$	$2.49 \cdot 10^{0}$	$-7.47 \cdot 10^{-1}$	$2.71 \cdot 10^{-3}$	$-1.40 \cdot 10^{1}$
Knuckle	$-1.98 \cdot 10^{1}$	$4.98 \cdot 10^{3}$	$5.32 \cdot 10^{0}$			
Max Load Z						
Body Front	$8.31 \cdot 10^{2}$	$-1.88 \cdot 10^{3}$	$9.73 \cdot 10^{0}$	$1.94 \cdot 10^{1}$	$5.99 \cdot 10^{-2}$	$2.67 \cdot 10^{1}$
Body Rear	$8.35 \cdot 10^{2}$	$5.19 \cdot 10^{3}$	$-3.18 \cdot 10^{0}$	$1.94 \cdot 10^{1}$	$5.99 \cdot 10^{-2}$	$2.67 \cdot 10^{1}$
Knuckle	$-1.67 \cdot 10^{3}$	$-3.30 \cdot 10^{3}$	$2.97 \cdot 10^{1}$			

Table 23: Max Loads.

3.4.2.3.2 Compliance Constraints

The compliance constraints, as provided by Altair, are: The X′ compliance of the control arm is to be less than 10% of the control arm to body translational axial bushing compliance. The Y′ compliance of the control arm is to be less than 10% of the control arm to body translational radial bushing compliance. The Z′ compliance of the control arm is to be less than 30% of the control arm to body translational radial bushing compliance.

The compliance constraints in the X′ and Y′ directions are applied at the control arm to knuckle attachment point in the Knuckle Compliance X′ and Knuckle Compliance Y′ load cases. As the control arm to body bushings have the translational axial stiffnesses of 5500 N/mm, a 55 N force is applied in the X′ direction in the control arm to

knuckle attachment point in the Knuckle Compliance X′ load case, and a displacement constraint in the same point is set to 1 μm. The translational radial stiffnesses in the control arm to body bushings is 13 000 N/mm. In the Knuckle Compliance Y′ load case a 130 N force is applied in the Y′ in the control arm to knuckle attachment point, and a displacement constraint in the same point is set to 1 μm. In these load cases the attachment points from the control arm to the vehicle body are constrained in all degrees of freedom. The control arm to spring attachment point is constrained in the Z′ direction. Thus, this point is allowed rotate freely, and move in the X′Y′ plane.

The compliance constraint in the Z′ direction is applied in the control arm to spring attachment point, to which the spring seat is rigidly connected. The bushing stiffnesses in the Z′ direction are the translational radial stiffnesses, at 13 000 N/mm. In the Spring Seat Compliance Z′ load case a 39 N force is applied in control arm to spring attachment point in the Z′ direction, and a displacement constraint in the same point is set to 1 μm. The control arm to body attachment points are constrained in all degrees of freedom and the control arm to knuckle attachment point is constrained in the translational degrees of freedom, as it is a ball joint.

The Compliance constraint load cases are visualized in Figure 45.

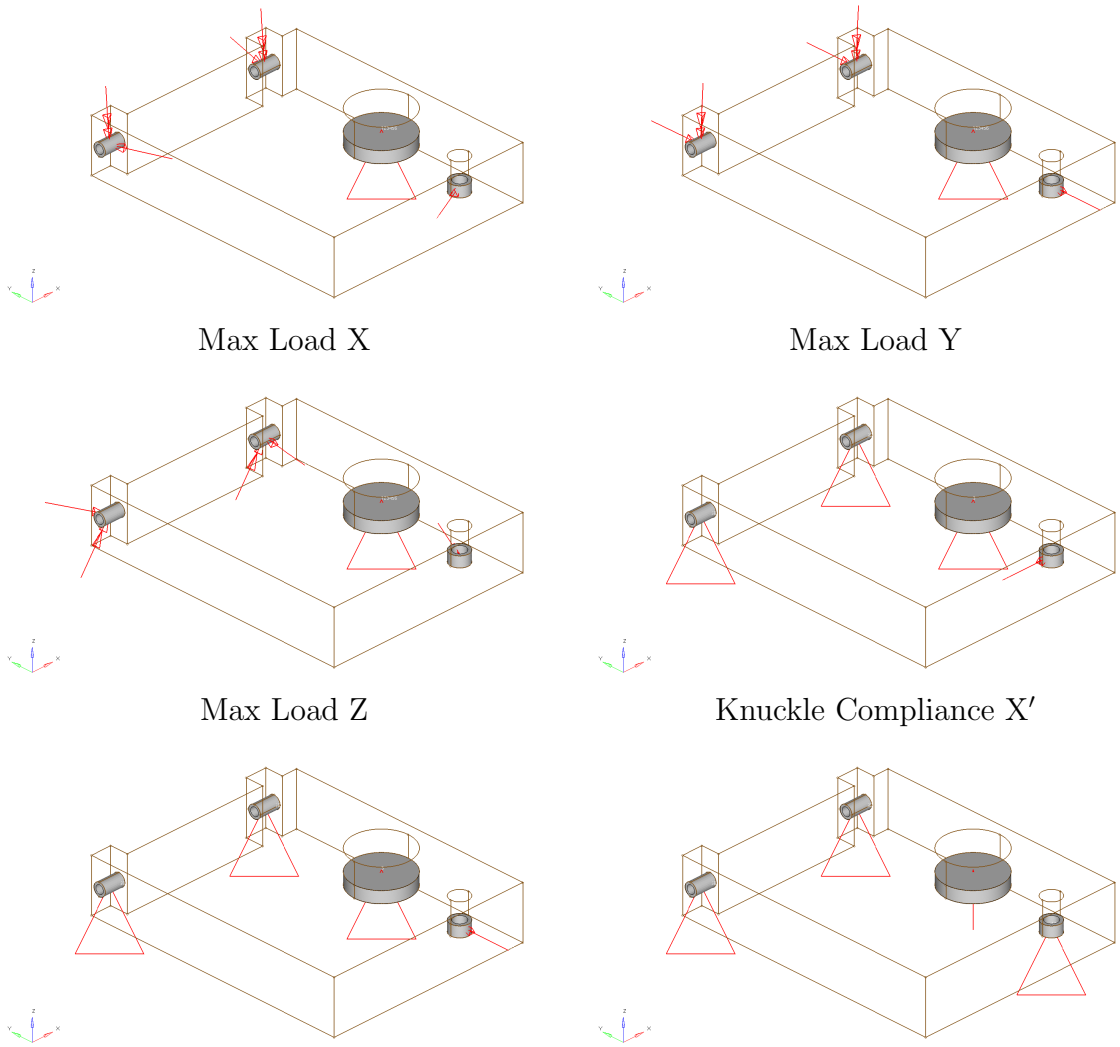

Figure 45: Topology optimization load cases.

3.4.2.4 Objective

Minimize mass.

3.4.2.5 Design Variables

The design variables used in a topology optimization is the element densities. The algorithm performs a finite element analyses and evaluates the stress and compliance constraints. It then adjusts the element densities towards an optimal solution, where the compliance constraints are fulfilled, the stress is evenly distributed in the elements, and the mass is the lowest possible. This optimal solution would be intermediate densities in most elements. But, it is impossible to manufacture a component built of semi-material. The optimization algorithm therefore punishes elements with intermediate densities and forces them to either become high density elements (filled with

material) or low density elements (empty). This solves the semi material problem, but often result in a checkered or spider web construction. This is also an impractical solution for manufacturing unless 3D printing is used. This problem is solved by adding a filter if the part is to be constructed using traditional manufacturing methods. The minimum member size filter forces the material to be grouped together to at least form the desired minimum thickness. The lower limit for the minimum member size is three elements, and is therefore set to 7.5 mm.

4 Results

4.1 Design of Experiments

As discussed in Appendix A, the results from the DOE will mainly be used to get an understanding of the suspension model in terms of potential performance. It was also discussed that the main and interaction effects will be studied to find out how the different design variables influence the responses. Note that this is not an easy task since there are a lot of responses and design variables, therefore it is rather difficult to comprehend the information that can be extracted from the DOE. Initially, the main effects will be presented in a conventional way, although as will be discussed, another approach will be used to interpret the main effects due to the relative meaning of the effect values. Thereafter, a similar approach will be used to compress the interaction effect information to be able to present it in a manageable manner. Finally, the potential performance will be shown by looking at histograms of the responses, in that way one could understand how the responses behave in comparison to the defined targets. The responses that will be evaluated in the DOE are the HS responses 15-28 defined in Table 18.

The main effects from the DOE study have been extracted from `HyperStudy` and can be found in Appendix A.1, Table 33 and 34. In these tables the main effect value for each design variable on every response can be found, however it is rather difficult to comprehend the meaning of the values in these tables. As discussed in Section 2.1.4, it is possible to visualize the main effects in a plot in order to be able to interpret the effects in a more manageable way. A somewhat different plot than the one presented in Section 2.1.4 will be used to visualize the main effects using a bar plot. An example of such a bar plot is shown in Figure 46. In this plot the main effect of the design variables on a certain response is represented by bars, where the height of the bars corresponds to the effect values. Main effect bar plots have been generated for each of the responses, these plots can be found in Appendix A.

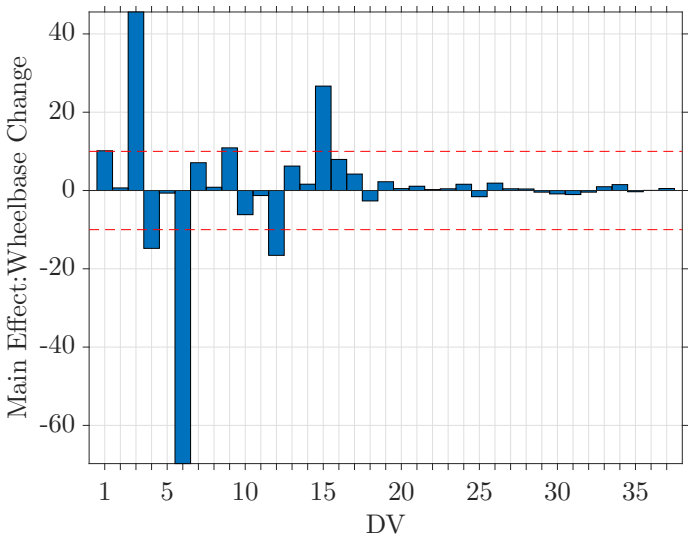

Figure 46: Main effect example.

The conventional way to interpret the effects would be: The larger the magnitude of the effect value is, the more influential that design variable is on the response. This conventional interpretation holds for this problem. However, the conventional decision of when to neglect a design variable, due to no visible effect on the responses, may not. In a conventional problem the main goal is to minimize/maximize the responses, and therefore it becomes rather obvious that a design variable that has a much greater effect is driving the problem and the response values. In that case it is viable to neglect design variables with much lower magnitudes.

If the conventional way to select the design variables with most influence is applied to the example in Figure 46, one can with certainty say that design variables 6, 3, and 15 have greater influence relative to the other design variables, and will therefore solely influence the response values. However, if the influence of the other design variables is neglectable is questionable. The main goal is not to minimize/maximize the responses, but to reach a certain response range. In the end, the goal is to tune in the responses into the target range and find the the optimal solution in the middle of the range. Consequently, there are reasons to believe that design variables which have an effect magnitude matching the magnitude of the target range could influence the tuning of the response values. Therefore, it is concluded in this thesis, the effect values should be compared to the target range, whereafter it will be possible to decide if influences of certain design variables are neglectable. In Figure 46 the red dashed line correspond to the target range, and it is noticeable that other design variables than 6, 3, and 15 have effect values that are comparable to the target range. Thus, with this new approach to find the most influential design variables, it seems that not as many design variables as before are neglectable.

This new approach is based on the fact that the main effect can be described as the average response change at low and high levels of a design variable. If this average

change is comparable to the target range, then it seems that the design variable will have noticeable effect on the response in the end. The red dashed line in the bar plot is not the easiest way to do this comparison for a lot of data.
One way to make the comparison easier, developed during this thesis, is to normalize the main effects by dividing the main effect values for each response by the target range of their response. The normalized effect values can be found in Appendix A.1 in Table 35, respectively 36. These values can be seen as a ratio of how great an effect is compared to the target range. A value greater than 1 is a clear indication that the design variable have influence on the response. An advantage with this normalization is the comparability of the ratio magnitudes for all responses.

It is rather difficult to interpret all the effects in the normalized main effects tables, so in order to get a better overview a Main Effect Matrix has been generated. The idea is to create a grid according to the effects and these are then color coded dependent on the effect ratios. The Main Effect Matrix is shown in Figure 47. Note that the red color correspond to ratios greater than 1, which are not included in the color scale.

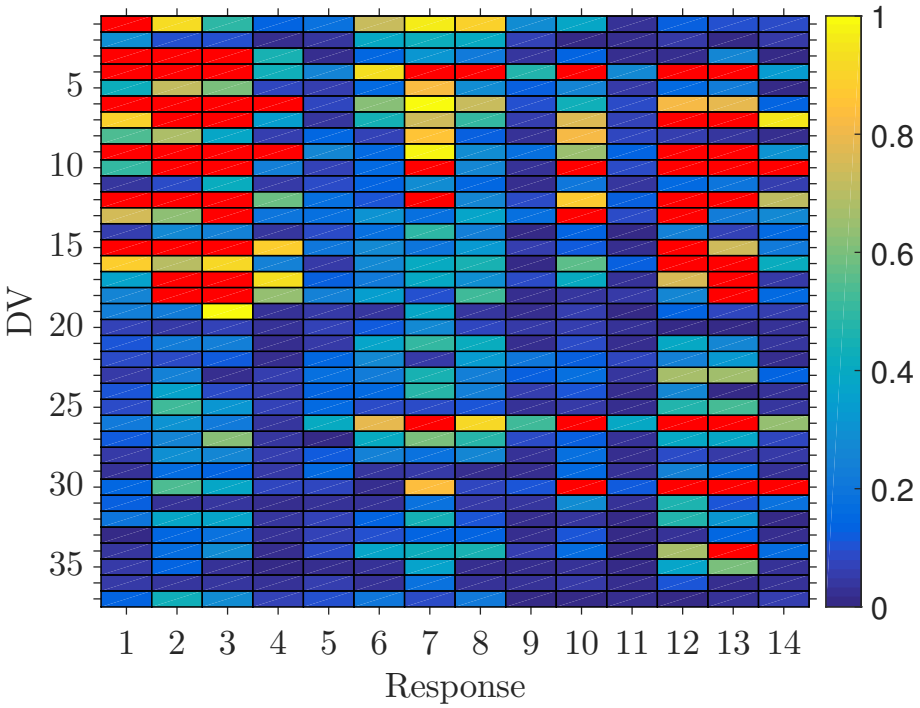

Figure 47: Main Effect Matrix.

With this new approach it becomes rather easy to see the relationships between design variables and responses. It is especially easy to distinguish the effects which are the more influential ones. However, it is still up for debate by which magnitude the ratios need to be in order to be seen as influential on the problem. In this thesis, ratios above 0.4 will be regarded as influential. It is clear that almost every design variable influence at least one response if this ratio limit is used to interpret the Main Effect Matrix. Although, the most interesting thing that can be interpreted from the Main

Effect Matrix would be how the responses 5, 9, and 11 are insensitive in the way that they are not that influenced by any design variables.

The interaction effects also need to be interpreted before any design variable can be neglected. The interpretation of the interaction effects are somewhat tedious and comprehensive since an interaction effect table can be generated for each design variable. Each interaction effect table is of the same size as the main effect table. Which means a total of 37 14×37 tables with interaction effects that should be compared to the main effects. It is rather obvious that it is not feasible to interpret this data manually by looking at the values in the tables. Therefore, a weighted ratio approach has been developed in this thesis. The main idea of this weighted ratio approach is to compress the data in the interaction tables to a single 37×37 matrix. The weighted ratio at each position in the matrix will represent the influence of the interaction between two design variables on all the responses, and should be compared to the Weighted Ratio Vector for the main effects. Basically, each column in this Weighted Ratio Matrix corresponds to an interaction table. The weighted ratio approach compress the tables into a single column vectors with the length equal to the number of design variables.

First, each interaction table is normalized in the same way as the main effect table is, and 37 figures such as Figure 47 can be generated. These normalized interaction tables have their ratios discretized and weighted in the following way:

$$\text{Weight Value} = \begin{cases} 0 & \text{if} \quad 0 < \text{ratio} < 0.4 \\ 1 & \text{if} \quad 0.4 < \text{ratio} < 0.7 \\ 2 & \text{if} \quad 0.7 < \text{ratio} < 1 \\ 3 & \text{if} \quad \text{ratio} > 1 \end{cases}$$

With this discretization a new interaction table, containing the weight values instead of ratios, is constructed. A row-wise summation of weight values is performed and a Weighted Ratio Vector is obtained. Each value in the Weighted Ratio Vector reflects the importance of the interaction effects on all responses between a pair of design variables. In total 37 weighted ratio vectors are generated. These are assembled into a 37×37 weighted ratio matrix. The steps involved in the creation of the Weighted Ratio Matrix are shown in a flowchart in Figure 48.

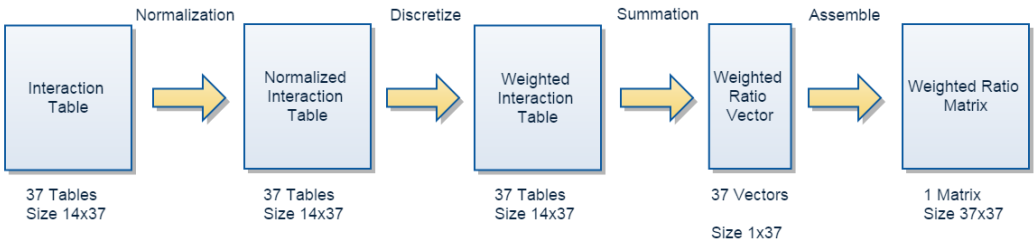

Figure 48: Weighted Ratio Approach flowchart.

Note that the Weighted Ratio Matrix by itself does not give very much information,

hence, it is necessary to create a Weighted Ratio Vector of the main effects that will be used to interpret the matrix. The Weighted Ratio Matrix and Weighted Ratio Vector can be visualized in a way similar to the visualization of the Main Effect Matrix shown in Figure 47. Their weight values are color coded for easy comparison and both are shown in Figure 49. The Weighted Ratio Matrix is symmetric since each position in the matrix is a measurement of the relative interaction effect importance between two design variables, and they are both found in both the rows and the columns. The diagonal of the matrix holds no values since a single design variable have no interaction effect with itself. The diagonal elements are therefore colored white.

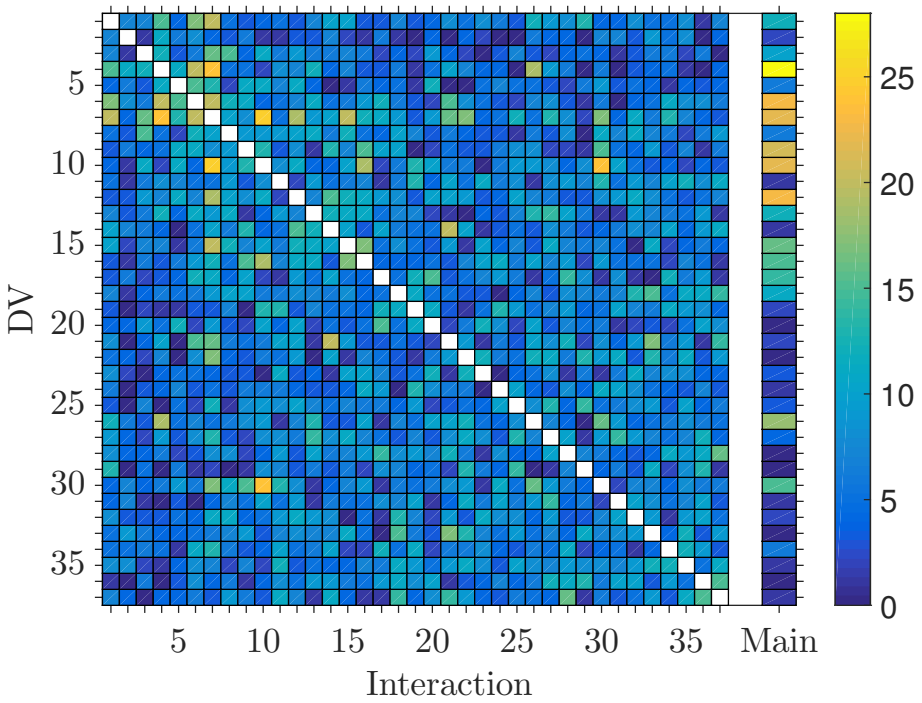

Figure 49: Weighted Ratio Matrix of the interaction effects.

The main goal with the weighted ratios this approach is to compress the effect information into a manageable format and make it comparable to the main effects. In the end, the answer one is looking for, would be if the interaction effects are as influential as the main effects. It is possible to answer this by comparing the weighted values in the matrix to the weighted values in the vector. How to interpret and compare these is relative and has to be set in perspective to the ratio effect value that was deemed as influential. In this thesis it was suggested that ratio effects above 0.4 was influential, and with the weight values used in the discretization it would mean that summed weight values above 1 would have at least one influential interaction effect. By observing the Weighted Ratio Matrix it is also clear that there are several interaction effects which obtain weighted values at magnitudes matching the main effect magnitudes. Therefore, there is reason to believe that it is not correct to neglect design variables due to the main effects alone. Most design variables show that they are of some importance in regard to interaction effects, and these should not be neglected.

With the relative measure set for this thesis it would have been reasonable to neglect a design variable due to low interaction effect if a complete row or column had the weighted value 0.

This new approach to select influential design variables suggests that none of the design variables can be neglected as each of them was deemed to have influence when both main and interaction effects was taken into consideration. If the developed approach is a feasible way to compare the effects can be discussed. No basis for this approach have been found in the literature, but it is suggested as a way to interpret the effects for this kind of problem formulation. It is an efficient way to compress the effect information to a manageable format, which is somewhat comparable. The effects have also been evaluated in the conventional way by looking at only the main effects in the bar plots. With the conventional way to evaluate the effects one could with certainty say that the design variables 1, 3, 4, 5, 6, 7, 9, 10, 12, 13, 15, 16, 17, 18, 26 and 30 have great influence in comparison to the other design variables. An investigation has been performed to see if it is viable to select only these design variables for an optimisation. The results are compared to an optimization where all design variables where kept. The results from the investigation can be found in 4.2.4.

The result from DOE has been used to generate histograms of the responses in order to investigate the potential performance of the suspension model. Some examples are shown in Figure 50. The y-axis in the histograms correspond to the probability for a design to take on a value within a bar range. The bar ranges are found on the x-axis. The red solid lines in the histogram shows the target limits, and the red dashed line shows the optimal target value. The histograms for the responses not shown here can be found in Appendix A.

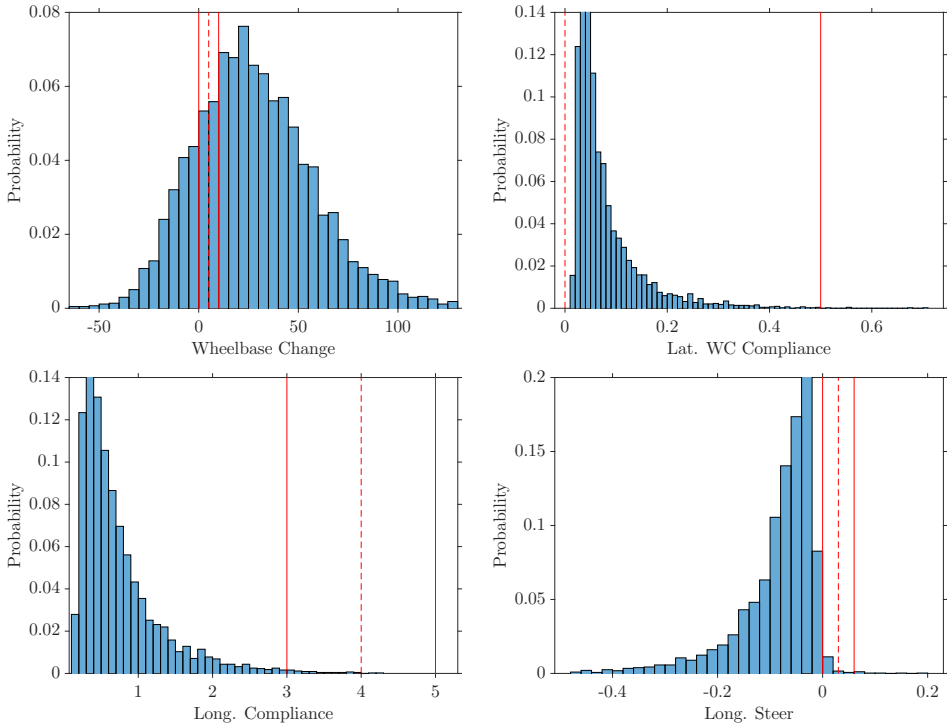

Figure 50: Histogram examples.

The histogram is a useful post-processing tool that will be used to observe the distribution of the response values in comparison to the target limits. As can be seen in the examples shown in Figure 50, the responses are distributed in a few different ways, compared to the limits, and the appearance of these give valuable information. The distributions will be evaluated by studying three key factors, namely the Sensitivity Ratio, Samples Within Limits and Mean Value Offset. The purpose for each key factor and how they should be interpreted is presented below:

Sensitivity Ratio

The Sensitivity Ratio is a measure that is used to describe how the responses are distributed in comparison to the target limits. This ratio is calculated as:

$$\text{Sensitivity Ratio} = \frac{\text{Distribution Range}}{\text{Target Range}}$$

It is a measure of how the response values are varying. Values below 1 indicates that the responses are distributed within a target range whilst above 1 indicates that the responses are distributed in a range wider then the target range. Therefore, this ratio should in general be interpreted as the lower the better, if the distribution is positioned close to the limits.

Samples within limits

Samples within limits, refers to the number of samples points which are within limits in the DOE, and is presented in percentage of the number of sample points. This will be a relative measure of the potential to be within the limits, a higher value indicates that it is easier to reach the limits.

Mean Value Offset

The Mean Value Offset is used to measure how the response distributions are positioned in comparison to the target limits. Some responses have a tendency to have the mean of their distribution far away from the target limits, and in general, the further away, the more difficult it will be to reach the limits. The Mean value Offset is calculated by rating the mean value with the rating method `Design Load Response Target Factor`, hence these rated values are a factor of the limits that describes where the mean of the distribution is positioned in relation to the optimal value. The closer the rated value is to zero, the better, since the mean of the distribution is closer to the optimal value.

The three key factors have been calculated for the responses and are shown in Table 24.

Nr	Response Name	Sensitivity Ratio	Samples within limits	Mean Value offset
1	Wheelbase Change	19.3	10.9%	2.3
2	Vertical Wheel Travel	38.3	5.6%	2.1
3	Roll Steer	47.3	7.3%	-1.9
4	Roll Camber	5.2	43.9%	-0.3
5	Lateral WC Compliance	1.4	99.9%	0.2
6	Lateral TP Compliance	1	100%	0.1
7	Lateral TP Steer	6.9	6.2%	-1.2
8	Lateral TP Camber	1.2	99.7%	-0.3
9	Longitudinal Compliance	2.1	0.8%	-1.6
10	Longitudinal Steer	11.3	1.4%	-1.9
11	Longitudinal Camber	1.3	94.7%	0.2
12	Overturning Moment Steer	27.7	12.6%	-3
13	Overturning Moment Camber	14.7	12.5%	3.1
14	Aligning Torque Steer	4.3	81.3%	-0.2

Table 24: Histogram key factors.

By observing the histograms and the key factors it is possible to draw some conclusions about the potential performance of the suspension. For instance, responses 5, 6, 8 and 11 will more or less be within the limits regardless of the design choices. In other words, these responses are insensitive and will not be driving the optimization, due to the fact that they have already reached the targets. The Sensitivity Ratio for these responses confirm the insensitivity because they have values around one, which means the response values are distributed within the target ranges. The Mean Value Offset indicates that the distribution ranges are positioned around the optimal values. The Main Effects Matrix shown in Figure 47 shows how these responses lack design variables of great importance, which also confirm the insensitivity.

Another response that show signs of insensitivity is response 9, but in contrast to previous responses, this response have difficulties to be within the limits. The combination of insensitivity and a large Mean Value Offset is the reason for the difficulties. This response is distributed far away from the optimal value and the range is not large enough to cover the target range, hence the difficulties. Therefore, it will be more or less impossible to get this response within the limits in the optimization unless the sensitivity can be altered.

When it comes to the responses 4 and 14, they will rather easy reach target limits because the Mean Value Offset are in the vicinity of zero and the Sensitivity Ratios are quite low. This means that the responses are distributed in the vicinity of the optimal value but the distribution ranges are somewhat larger then the target ranges, and therefore are not all the designs within the limits. These responses can be viewed as semi-sensitive. This is confirmed by the Main Effects Matrix in Figure 47. Note how these responses have a few design variables of great importance, which probably are responsible for the variance of the response values.

Regarding the responses 1, 2, 3, 12, and 13, these responses should be viewed as sensitive. Since the Sensitivity Ratios are quite high and the Main Effect Matrix shown in Figure 47 reveals that there are a large number of design variables which influence these responses. Note how the Mean Value Offsets are rather large for these responses, which indicates that the mean values of the distributions are far away from the limits. Although, the sensitivity remedy the Mean Value Offset, since it allow the responses to take on values in a wider range. The combination of high sensitivity and large Mean Value Offset yield responses which can be within the limits, but in general they are not. During the optimization the design variables which influence these responses need to be tuned in, to reduce the response distribution ranges.

The last responses, 7 and 10, have a Sensitivity Ratio and Mean Value Offset similar to previously mentioned responses. Although, these two responses have a somewhat left skewed distribution, which means the responses tends to take on values to the left of the distribution mean. The skewness is seen in the histograms. The negative Mean Value Offsets indicates that the distribution mean is positioned at the left side of the optimal value. The combination of distribution skewness and the Mean Value Offset makes it difficult for these responses to be within the limits. Hence, a lower probability to be within the limits than the other sensitive responses.

4.2 System Optimization

As mentioned in Section 3.3, the setup of the optimization was to be investigated in order to find out how the setup influence the optimization results. Evolution plots of the limits and weights values have been generated to compare the different optimizations in each investigation. The evolution plots show how the different responses change over time in the optimizations, in other words, the x-axis correspond to the evolution number and the y-axis to the response of interest. The difficult task is to interpret these plots in a meaningful way.

The limits should be interpreted as, that the higher value, the more target values are fulfilled. The highest value is 14, which corresponds to the maximum number of fulfilled Ride and Handling responses. Three different limits plots are presented, namely one, two and three times the limits. In the end, it is just the one limit plot that is of interest since that limit corresponds to the targets values defined for the suspension model. The other two limit plots can still be used to determine if the optimization algorithm is converging towards the target values.

Three different weight evolution plots will be presented, namely one for each objective, Ride, Handling and NVH. The lower value of the weighted objectives, the better the design is regarding to the linearity of the responses and how close the responses are to the target values. However, a low weight value does not necessarily mean that all the target values are fulfilled, since the weighted sum approach is used to bundle the responses belonging to the respective objectives Ride and Handling. It might be that some responses reach the targets values perfectly, while others are outside the limits. Such a combination could still yield a low weight value. Therefore, it is necessary to evaluate both the limits and weights for each individual design in order to know if it is an acceptable design. Regarding the weight for NVH, a value below 0.5 means that the design has improved compared to the initial design. Note that a design that reaches the target values is preferred to one that has a lower weight value, but can not fulfill the target values.

4.2.1 Investigation 1: Constraints

The three optimizations denoted 1, 2, and 7 in Table 25, are compared to show the influence of the constraints. The first optimization had a 3L constraint, the second a 2L constraint and the last had no constraints. The other setup options for the optimizations are identical, hence, the optimizations are comparable when it comes to the constraints influence on optimizations. The limit evolution plots used in this investigation are shown in 51, and the weight evolution plots in Figure Figure 52. The plots to the left are with no constraints, in the middle with 3L constraints and to the right with 2L constraints. It is possible to say that the lowest weight values are obtained if no constraints are used in the setup. However, with no constraints none of the limits are fulfilled. If one looks more closely at the constraint plots it is evident that it is only optimization 1 which consistently reach the 3L limit. Optimization 2 succeed to reach the 3L limit a few times, but not as often as optimization 1. It is clear that lower weight values are obtained in optimization 1, compared to optimization 2. Furthermore, it seems like the distribution of the limit and weight values are narrowed down to a tighter range if a more strict limit is used in the constraint formulation. In other words, the variance is reduced when stricter limits are used in the constraint formulation. In conclusion it seems preferable to set a more loose limit as a constraint since the 3L limits are then fulfilled and the weight values seems to converge better.

Nr.	Objectives	Constraint	DVs	DS	Algorithm	Settings
1	3×Weighted	3L	All	Max	MOGA	Standard
2	3×Weighted	2L	All	Max	MOGA	Standard
7	3×Weighted	-	All	Max	MOGA	Standard

Table 25: Optimization setups: Investigation 1.

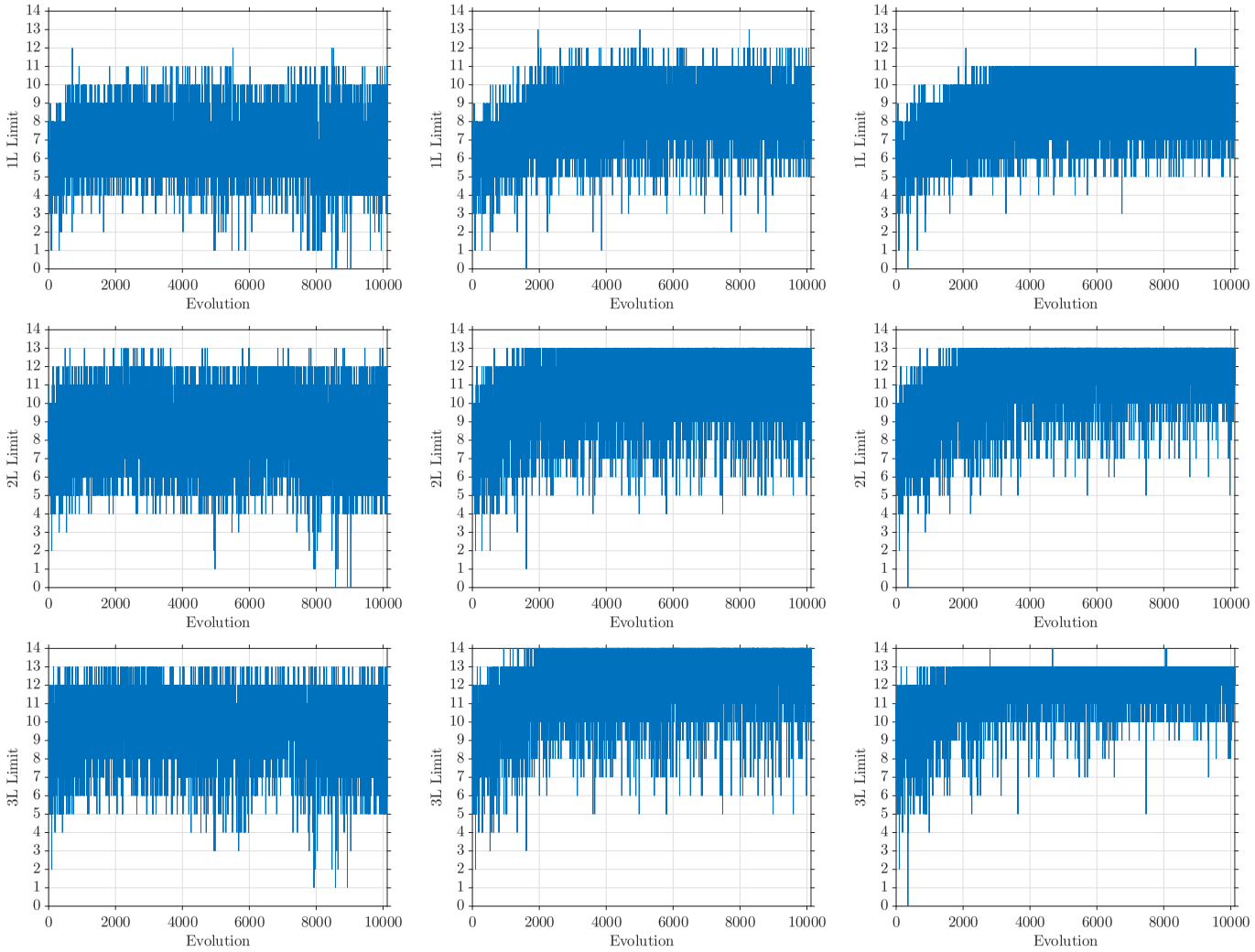

Figure 51: Limits evolution: Optimization 7 (left), 1 (middle) and 2 (right).

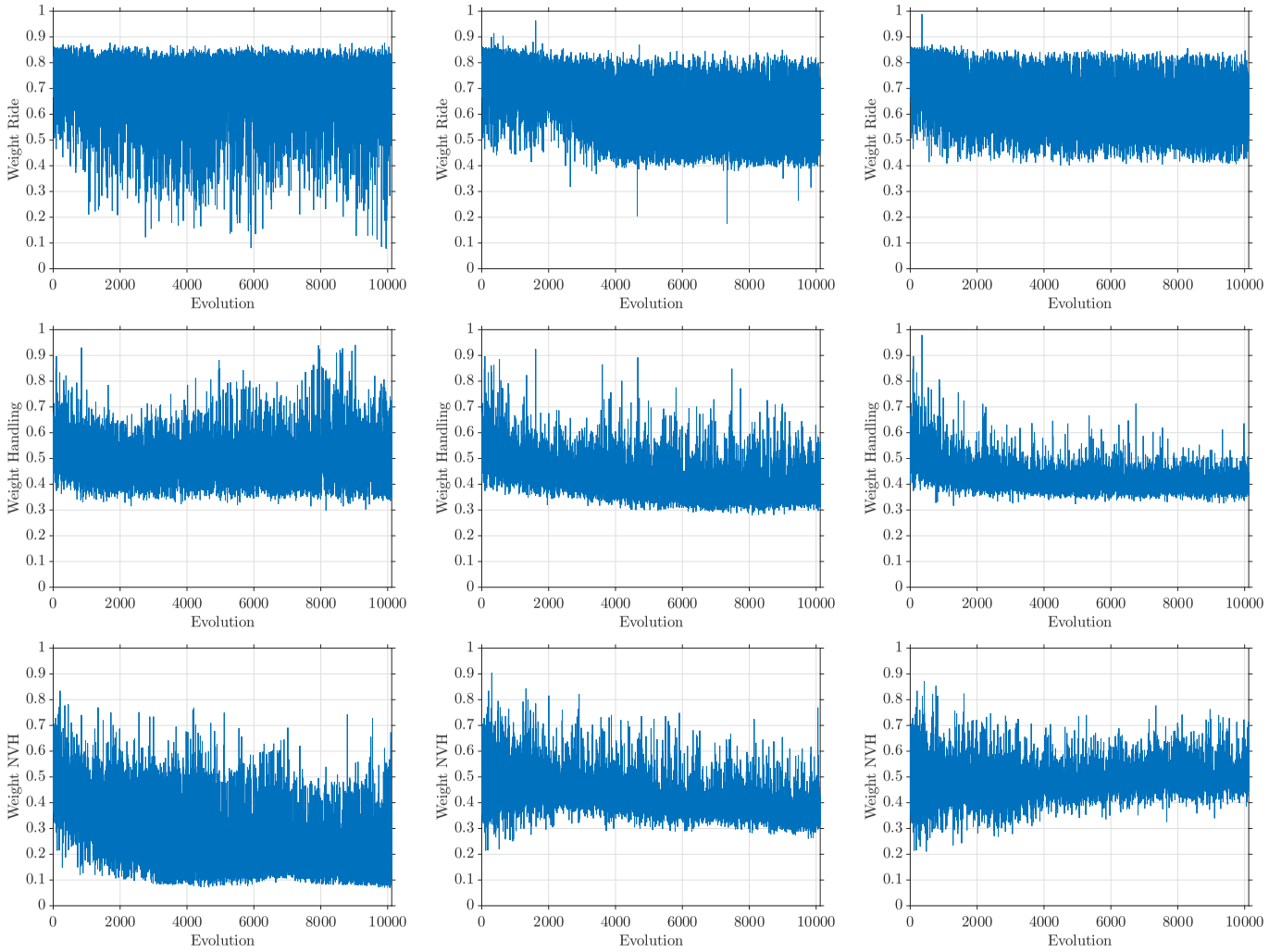

Figure 52: Weights evolution: Optimization 7 (left), 1 (middle) and 2 (right).

4.2.2 Investigation 2: Objectives

The influence of the objective formulation is investigated by comparing optimizations 1 and 3 in Table 26. These two optimizations have an identical setup, except for the objective formulation, where the first had the 3×Weighted setup whilst the latter had a 15×Individual setup. The weight and limit evolution plots for these optimizations are shown in Figure 53 and 54, where the plots to the left shows optimization 1, and those to the right optimization 3. The appearances of the limit evolution plots are very similar for both optimizations, which succeed to fulfill the 3L limits with ease. It seems like the objective formulation does not effect the optimization ability to reach the limits. Regarding the weight evolutions plots however, optimization 1 seems to be better on converging at lower weight values. In conclusion, it appears viable to utilize the weighted sum approach on the Ride and Handling objectives. Thus, the optimization algorithm only have three objectives to take into consideration while optimizing. Even if this summation of responses should lead to some loss of information, the algorithm seems to converge faster and to lower values. Another aspect is the bundling of the responses. The Ride and Handling objectives are typically contradictory. It might be easier for the algorithm to balance the contradictory responses if they are sorted into separate opposing groups.

Nr.	Objectives	Constraint	DVs	DS	Algorithm	Settings
1	3×Weighted	3L	All	Max	MOGA	Standard
3	15×Invidiual	3L	All	Max	MOGA	Standard

Table 26: Optimization setups: Investigation 2.

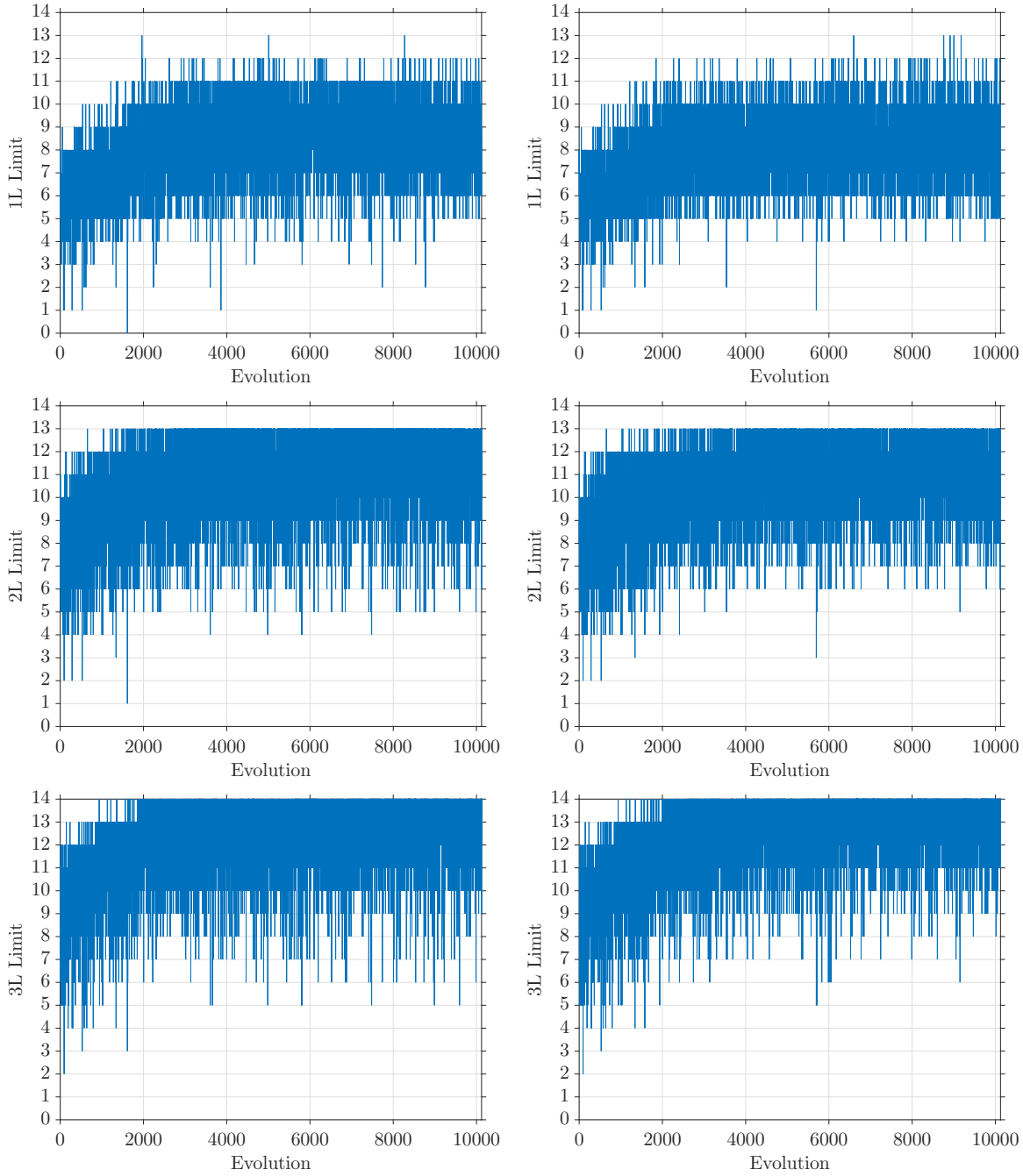

Figure 53: Limits evolution: Optimization 1 (left) and 3 (right).

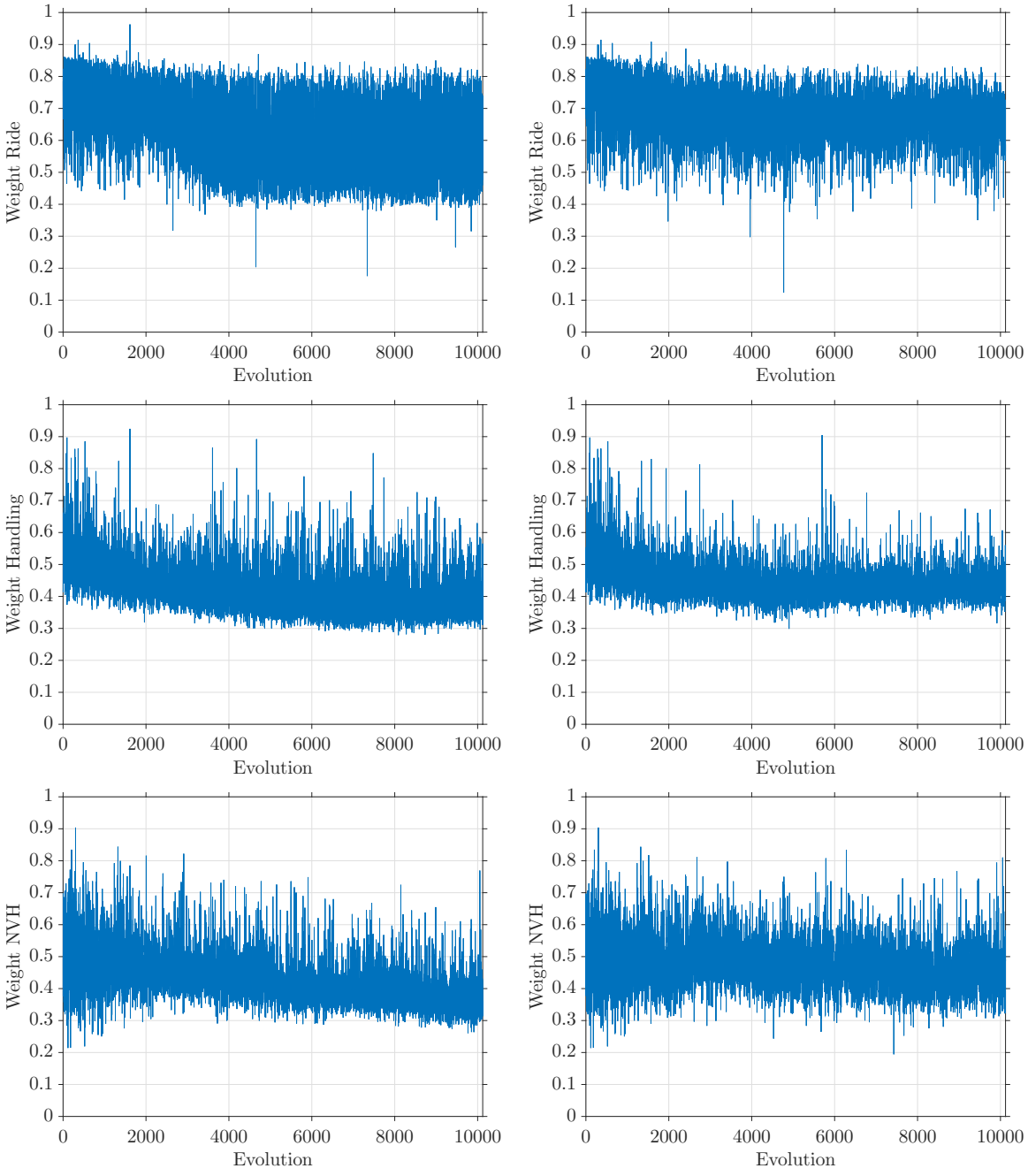

Figure 54: Weights evolution: Optimization 1 (left) and 3 (right).

4.2.3 Investigation 3: Optimization Algorithm

Optimizations 2 and 4 in Table 27 are compared in order to be able to decide which optimization algorithm is the most suitable for this problem formulation. These two optimizations have identical setups except for the selected optimization algorithms. The limit and weight evolution plots for these optimizations are shown in Figure 55, respectively Figure 56. It is evident, by looking at the limit plots, that the MOGA algorithm is much better at converging and reaching the limits. Moreover, the MOGA algorithm has a lower variance of the limits values compared to the GRSM algorithm, the latter also seems to have difficulties in converging towards a solution. The GRSM algorithm is based on a RSM model, and searches the RSM model to find optimal solutions to evaluate in the next iteration, but the RSM model appears to not show conformity with the real MBD model. The algorithm is evaluating some rather bad designs, but theoretically it should have found better designs to evaluate over time. Although, if one looks at the weight plots it is possible to say that the GRSM algorithm obtain weight values in a wider range compared to the MOGA algorithm.

With increasing number of iterations it is clear that the MOGA algorithm obtain decreasing weight values. However, the GRSM succeed in finding some designs with lower weight values but there is no consistency in the improvement over time. Low weight values is not that decisive unless the limits are reached. In conclusion, it appears that an evolutionary algorithm like MOGA is preferable for this kind of problem formulation since the algorithm show a more stable converging capability.

Nr.	Objectives	Constraint	DVs	DS	Algorithm	Settings
2	3×Weighted	2L	All	Max	MOGA	Standard
4	3×Weighted	2L	All	Max	GRSM	Standard

Table 27: Optimization setups: Investigation 3.

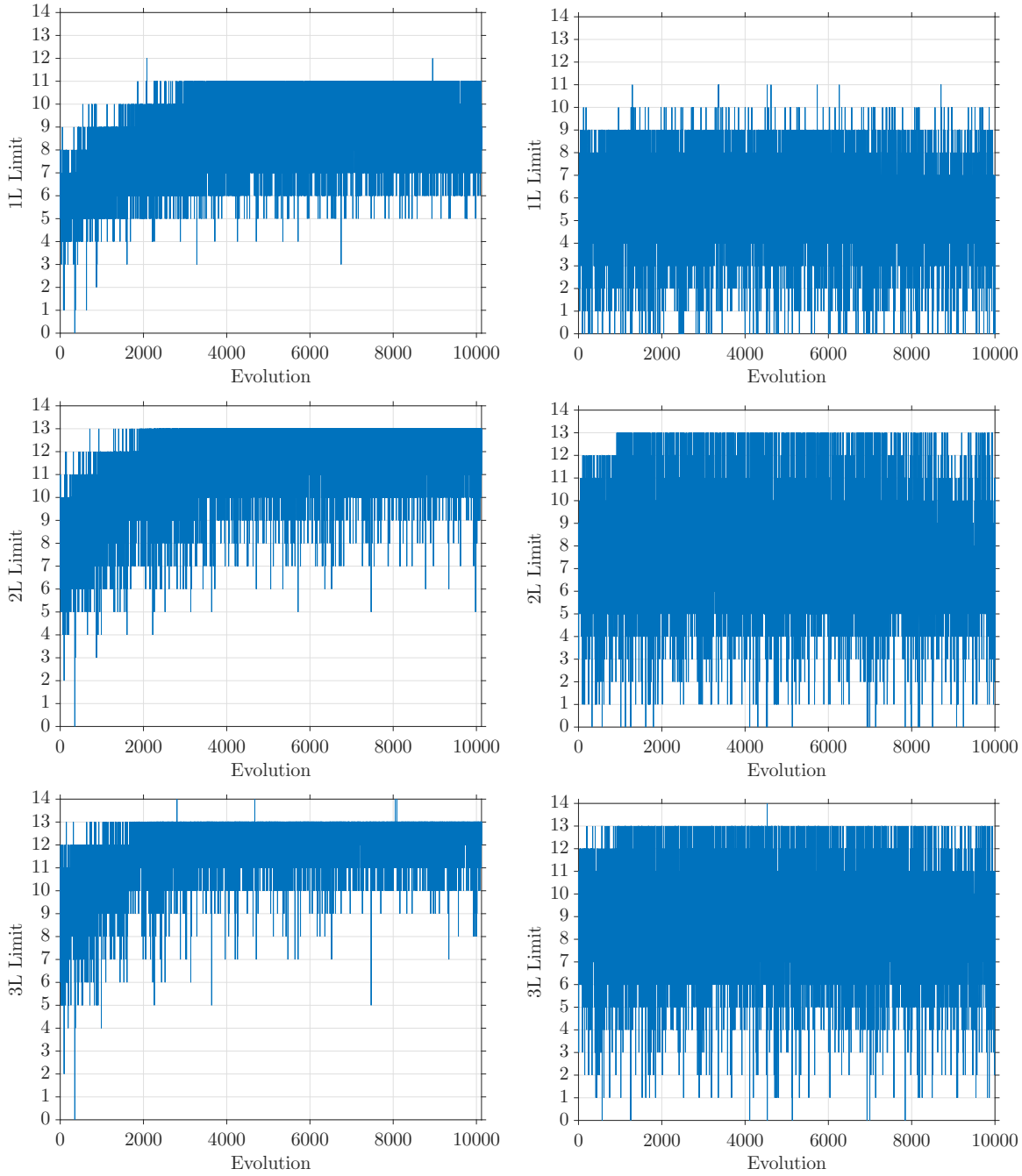

Figure 55: Limits evolution: Optimization 2(left) and 4(right).

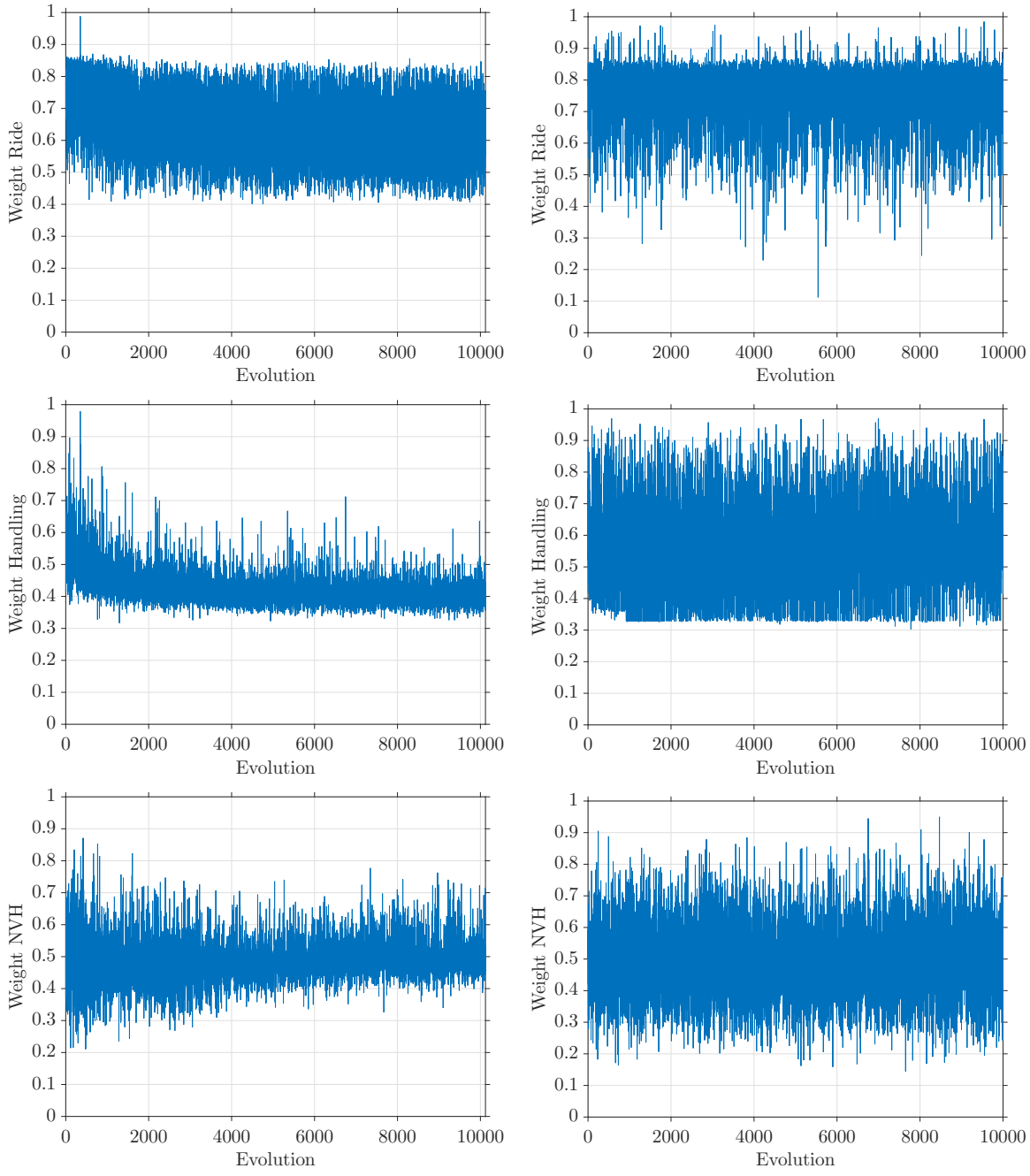

Figure 56: Weights evolution: Optimization 2 (left) and 4 (right).

4.2.4 Investigation 4: Remove Design Variables

Optimizations 1 and 5 in Table 28 are compared in order to investigate how the optimization results are influenced when the least important design variables are removed. The setup of these optimizations are identical, except that optimizations 5 have fewer design variables. A list of the design variables that have been removed can be found in Section 4.1. Note that the selection of design variables is based on the main effect values, and the interactions have not been taken into consideration. Hence, the results can give an answer to if it is viable to neglect the interaction effect in the selection of the most influential design variables. In other words, are the main effects influence much greater then the interaction effects?

The limit and weight evolutions plots for these optimizations are shown Figure 57, respectively Figure 58. Note that the number of evolutions differ between the two optimizations, since the number of evaluation depends on the number of design variables used. Clearly, the removal of design variables will limit the possibility for the optimization algorithm to find solutions witch satisfy the limits. This is seen in the limit plots. It is only optimization 1, with all the design variables, that succeed in fulfilling the 3L limits. Overall, optimization 5 is somewhat worse at fulfilling the different limits. Furthermore, if the weight plots are studied, one can clearly see that optimization 1 is converging to lower weight values compared to optimization 5. It is a quite noticeable difference between the optimizations weight values for the objectives Ride and NVH. This is not that surprising since most of the design variables that was removed was bushing stiffnesses. These design variables mostly influence Ride and NVH objectives. One can conclude that the removal of design variables with low main effects, without taking the interaction effects into consideration, will influence the optimization results in an unfavorable way.

Nr.	Objectives	Constraint	DVs	DS	Algorithm	Settings
1	3×Weighted	3L	All	Max	MOGA	Standard
5	3×Weighted	3L	Limited	Max	MOGA	Standard

Table 28: Optimization setups: Investigation 4.

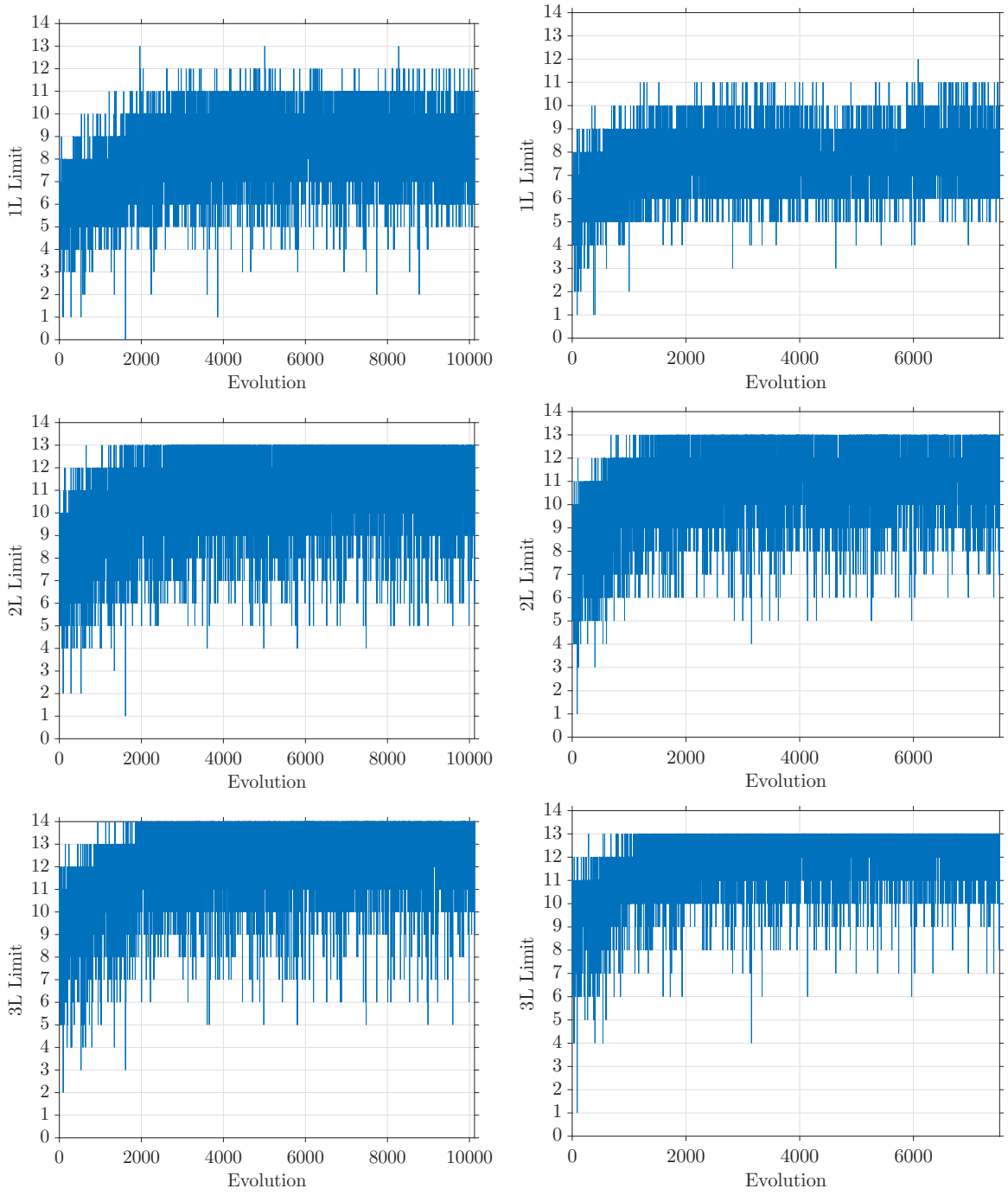

Figure 57: Limits evolution: Optimization 1(left) and 5(right).

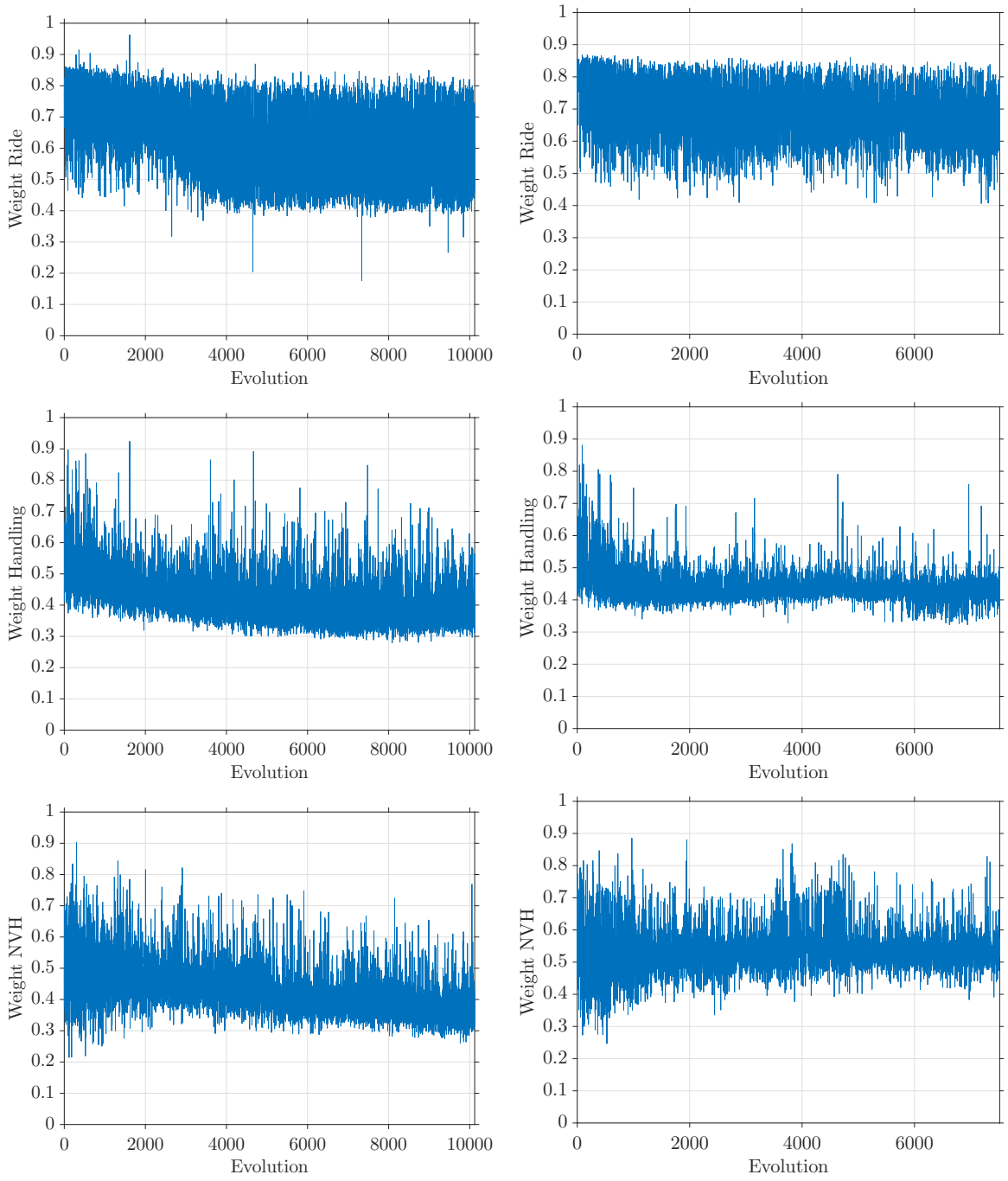

Figure 58: Weights evolution: Optimization 1 (left) and 5 (right).

4.2.5 Investigation 5: DSRM

To decide if the DSRM is a viable approach for the system optimization, the results from the last iterative optimization in the DSRM will be compared to an optimization that has been allowed to do at least the same number of evaluations as the DSRM in total. The optimizations in question are denoted optimization 1.3 and 6 in Table 29, and note that these optimization do not have identical setups in terms of the limits used in the constraint formulations, and the design spaces used. Although, it will not matter when the results are compared, since the question which is to be answered in this investigation is which of the approaches that is best at converging towards the 1L limits. The limit and weight evolution plots are shown in Figure 59, respectively Figure 60. By looking at the limit plots it is evident that the last optimization in the DSRM scheme surpass the optimization with many evaluations in terms of limits fulfilled. By utilizing the DSRM scheme both 3L and 2L limits are fulfilled. The DSRM scheme is almost successful in fulfilling the target, which is 1L, whilst the other optimization does not fulfill any of the limits. Regarding the weight plots, the DSRM scheme has converged to lower weight values for all objectives compared to optimization 6. These result show that the optimization algorithm has problems to find design that fulfill the 1L limits even if the optimization is allowed to continue for a longer time. The suggested DSRM approach seems viable as the results show. This approach helps the optimization algorithm to find designs that fulfill both 3L and 2L limits.

To show of the external DSRM scheme helps the the optimization algorithm to find better solutions a scatter pareto plot has been generated for the optimizations in Table 29. The scatter pareto plot contains the 100 optimal designs in terms of the objectives Ride, Handling and NVH and is shown in Figure 61. As can be seen in the pareto plot optimization 6 has the highest weight values, but the interesting thing is how the weight values for the DSRM optimizations decrease for each optimization and create different fronts. Although, the scatter pareto plots can only visualize two dimensions so in order to study the NVH objective also, a bubble pareto plot has also been generated. The bubble pareto plot is shown in Figure 62 and contains the 300 optimal designs in regard of the objectives. Note that the reference optimization 6 and the last optimization (1.3) in the DSRM iteration scheme are the optimizations shown in the bubble plot. The bubble plot also indicates that the DSRM scheme surpass the approach of letting a optimization do a lot more evaluations.

Nr.	Objectives	Constraint	DVs	DS	Algorithm	Settings
1	3×Weighted	3L	All	Max	MOGA	Standard
1.1	3×Weighted	2L	All	Reduced(1)	MOGA	Standard
1.2	3×Weighted	1L	All	Reduced(1.1)	MOGA	Standard
1.3	3×Weighted	2L	All	Reduced(1.1)	MOGA	Standard
6	3×Weighted	2L	All	Max	MOGA	Longrun

Table 29: Optimization setups: Investigation 5.

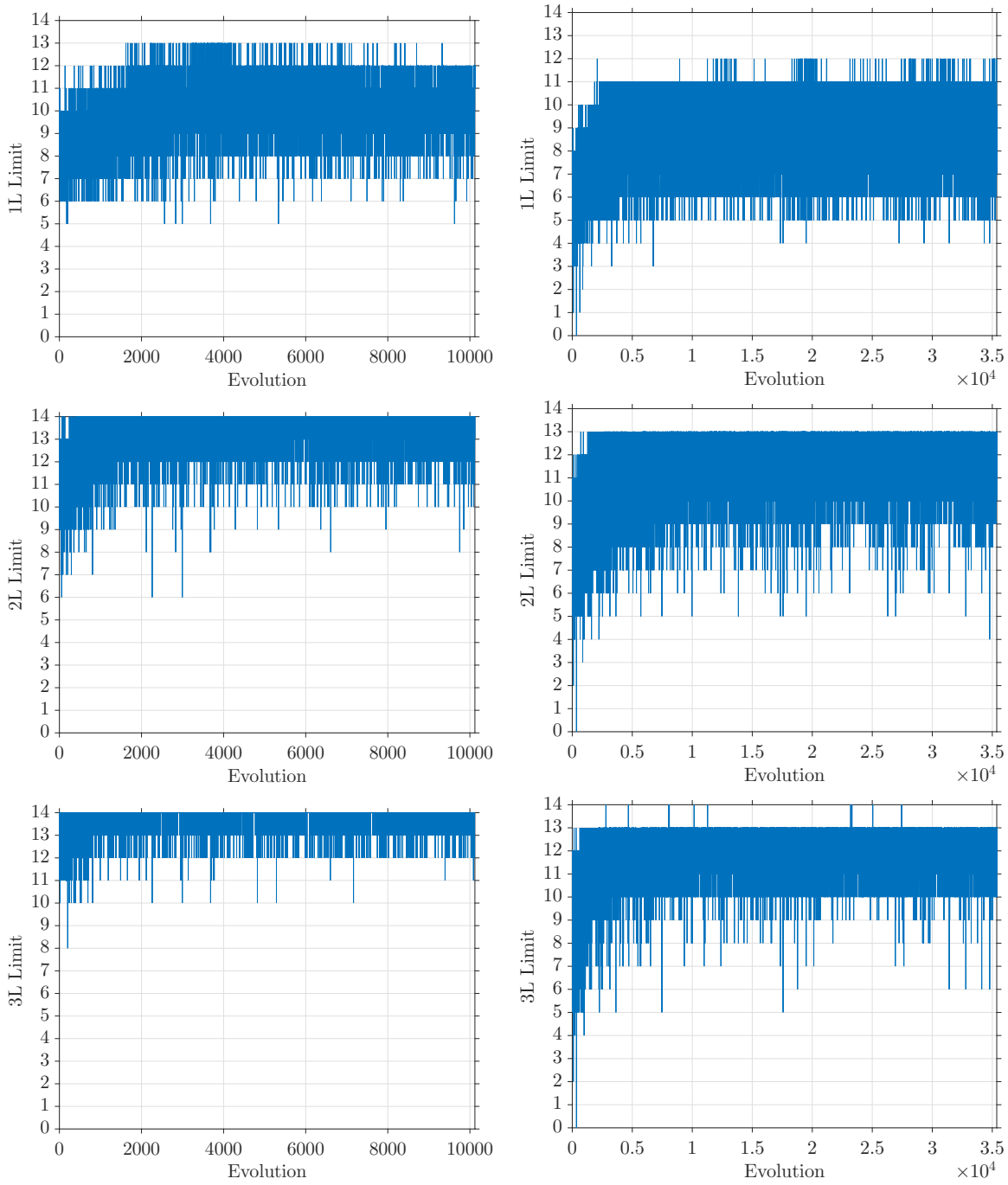

Figure 59: Limits evolution: Optimization 1.3(left) and 6(right).

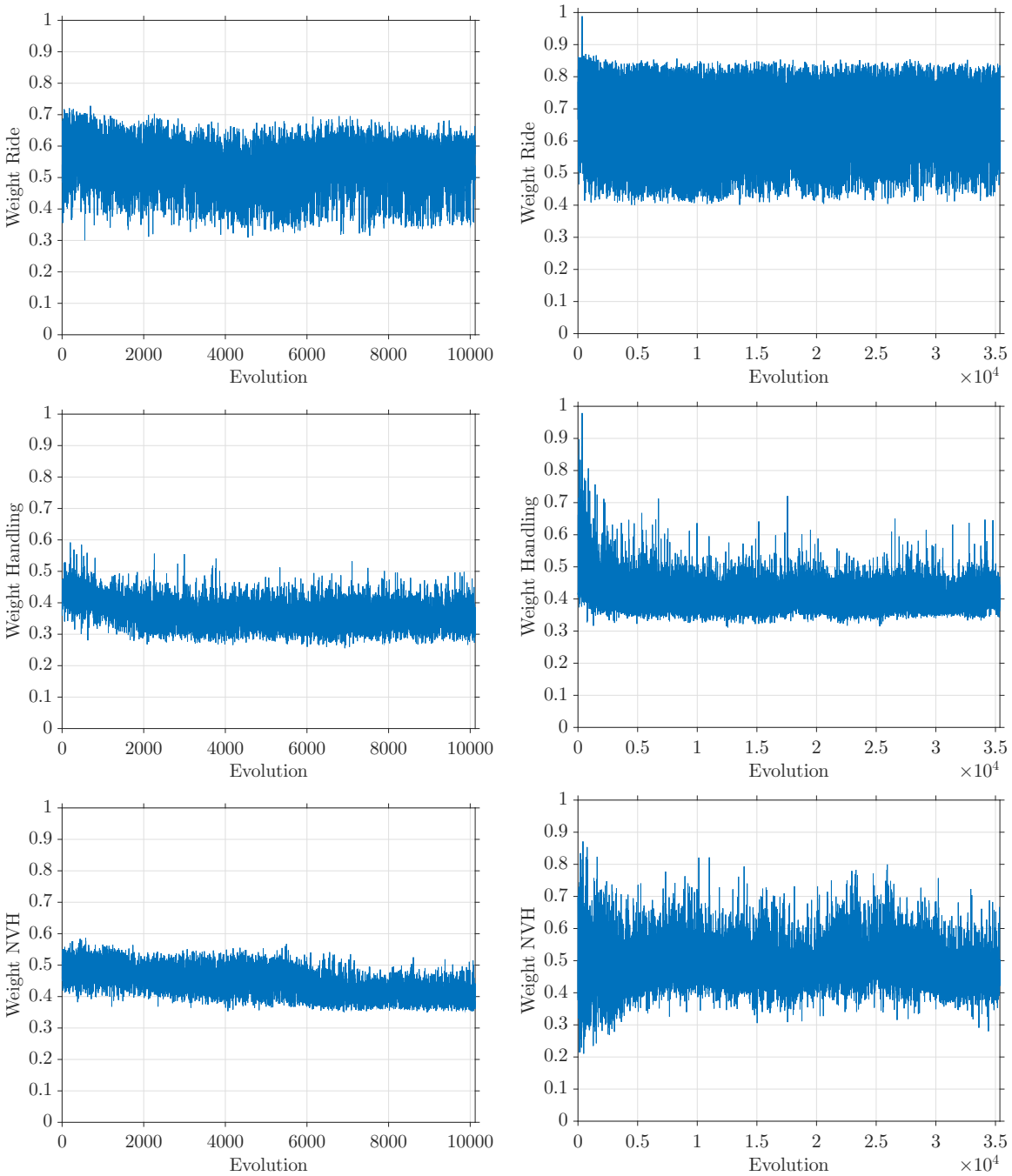

Figure 60: Weights evolution: Optimization 1.3 (left) and 6 (right).

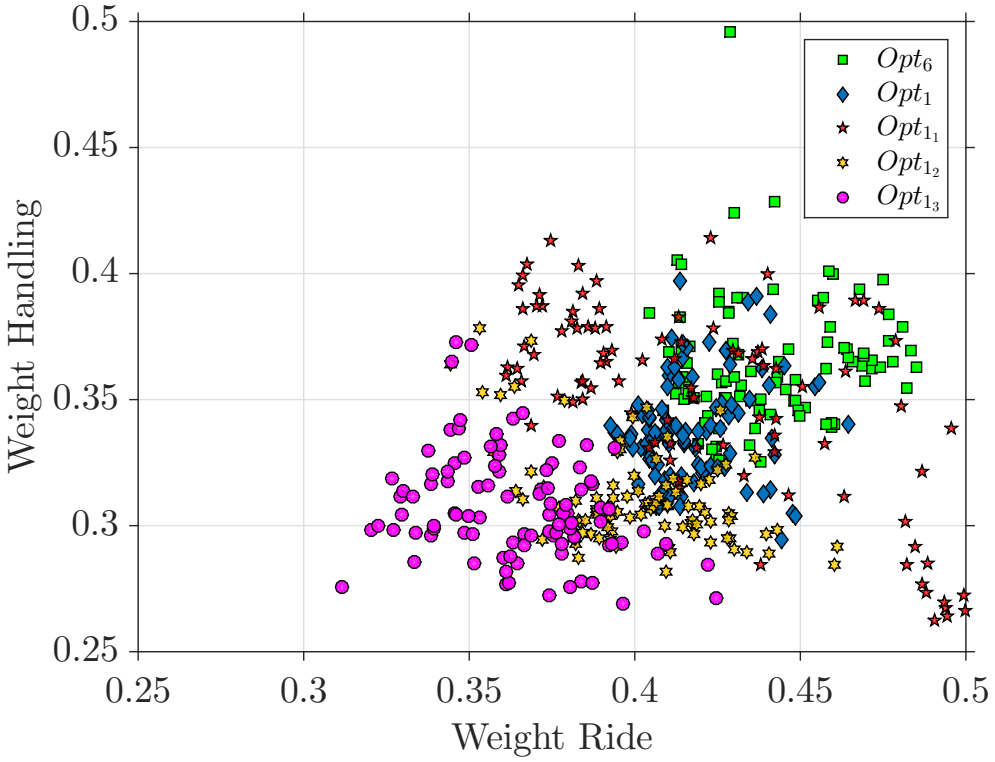

Figure 61: Scatter Pareto: Investigation 5, 100 best runs in regard to Ride, Handling and NVH.

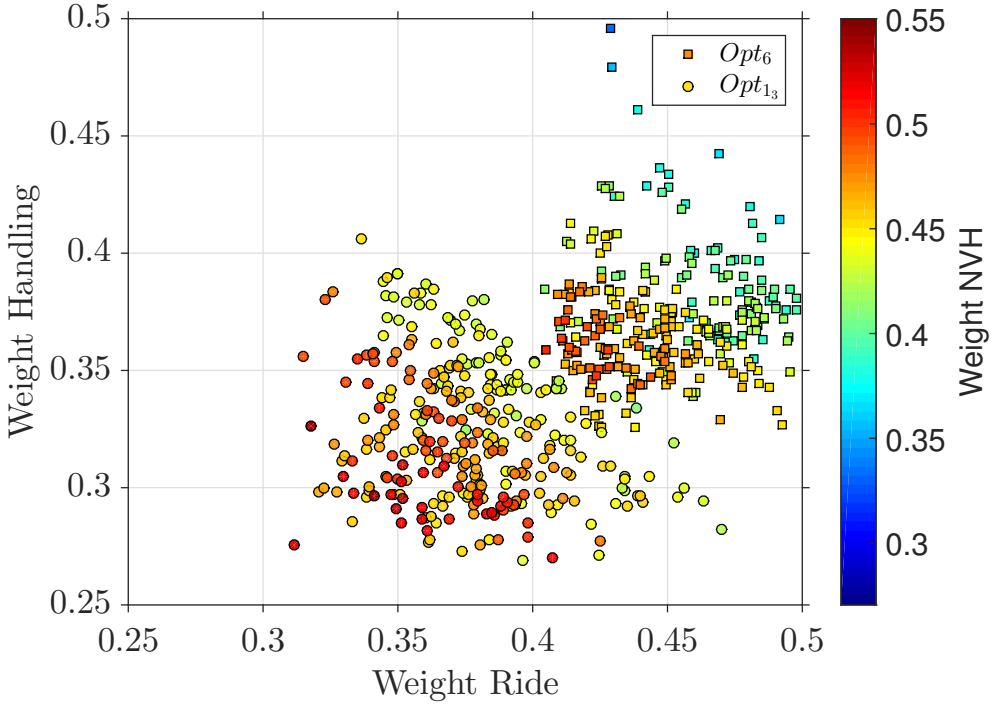

Figure 62: Bubble Pareto: Investigation 5, 300 best runs in regard to Ride, Handling and NVH.

4.2.6 Investigation 6: Initial Design Space

To find out how the initial design space influence the results obtained with the DSRM approach, the last optimization in two different DSRM schemes will be compared in limit and weight evolution plots. The optimizations in question are optimization 1.3 and 8.3 in Table 30, where both optimizations are the third optimization iteration of the DSRM approach. However, optimization 1.3 has used the 2L limits in the constraint formulation while optimization 8.3 has used the 1L limits. Optimization 1.3 has used the 2L limits since a previous optimization with 1L limit did not perform in a satisfying manner, as the DSRM scheme suggests, the constraints should then be slackened. The limit and weight evolution plots for these optimizations are shown in Figure 63 and Figure 64. It is clear, if the limit plot is studied, that the initial design space extension allow optimization 8.3 to reach the 1L limits, while optimization 1.3 with the ordinary design space does not. Furthermore, the weight plots show that the weight objectives Ride and NVH decrease further if the initial design space is extended, since optimization 8.3 obtain lower weight values than optimization 1.3. Apparently these objectives improve if the bushings are allowed take on values in a lower range. If such low bushing values are feasible in reality for this suspension model it would be possible to satisfy the defined target limits. Note that there is no clear change in the weight values for the objective Handling with lower bushing values. This was to be expected as the bushings are foremost connected to the Ride and NVH objectives.

As in previous investigation, a scatter and bubble pareto plot has been generated in order to study how the different optimization in the DSRM schemes perform. In this investigation however, it is more interesting to compare the same optimization iteration between the two DSRM schemes in the scatter pareto plots. For instance the optimization 1.3 should be compared to 8.3 and the scatter pareto plot is shown in Figure 65. By doing this it is clear that the DSRM scheme were lower bushing values are allowed, obtain lower weight values of the Ride objective. The last optimization in the two DSRM schemes has been included in the bubble pareto plot to be able to compare how they perform in regards to the NVH objective. The bubble pareto plot is shown in Figure 66 and it is evident that the NVH objective perform better in the DSRM scheme that is allowed to take lower bushing values.

Nr.	Objectives	Constraint	DVs	DS	Algorithm	Settings
1	3×Weighted	3L	All	Max	MOGA	Standard
1.1	3×Weighted	2L	All	Reduced(1)	MOGA	Standard
1.2	3×Weighted	1L	All	Reduced(1.1)	MOGA	Standard
1.3	3×Weighted	2L	All	Reduced(1.1)	MOGA	Standard
8	3×Weighted	3L	All	Max Low Bsh	MOGA	Standard
8.1	3×Weighted	2L	All	Reduced(8)	MOGA	Standard
8.2	3×Weighted	1L	All	Reduced(8.1)	MOGA	Standard
8.3	3×Weighted	1L	All	Reduced(8.2)	MOGA	Standard

Table 30: Optimization setups: Investigation 6.

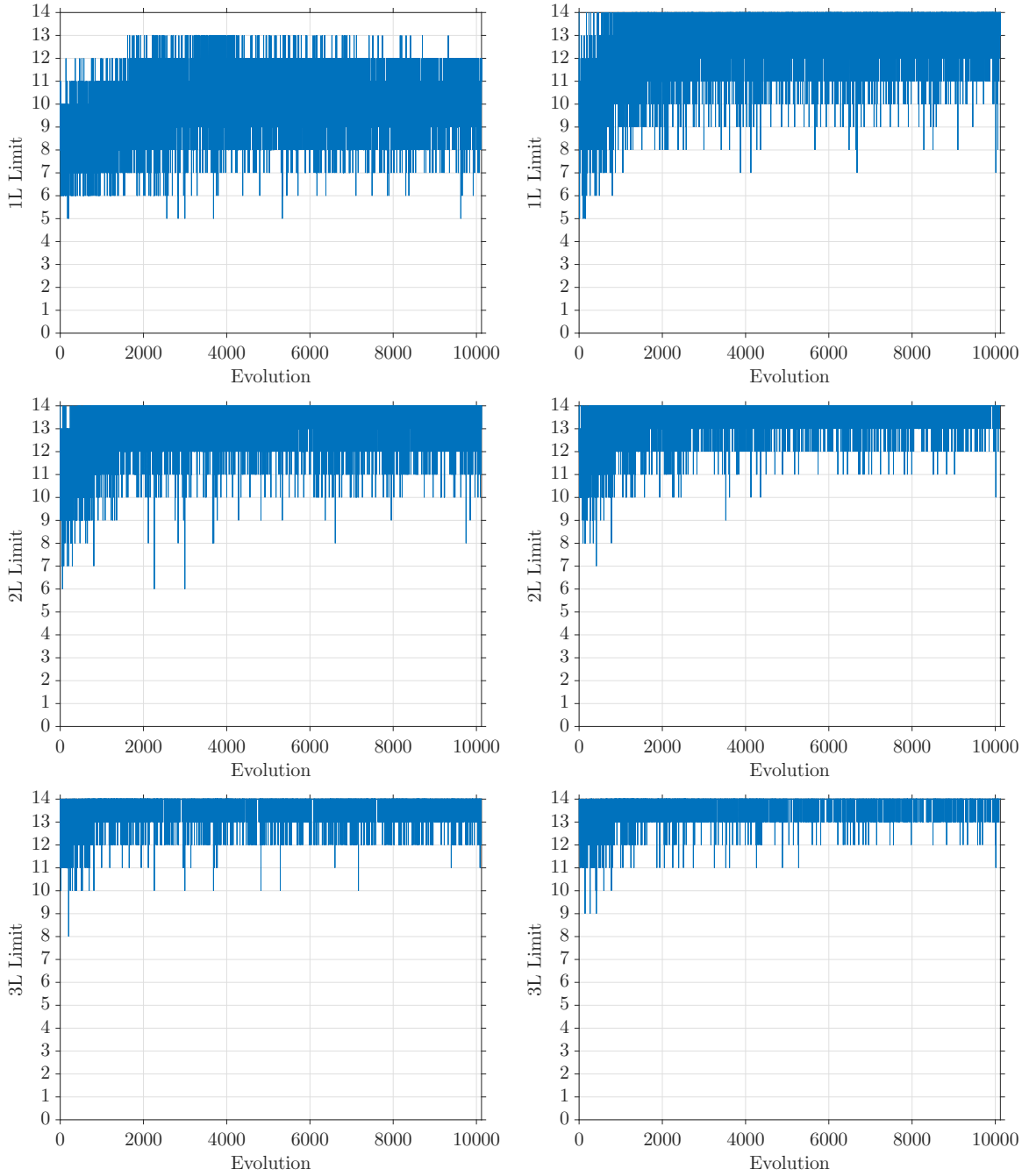

Figure 63: Limits evolution: Optimization 1.3 (left) and 8.3 (right).

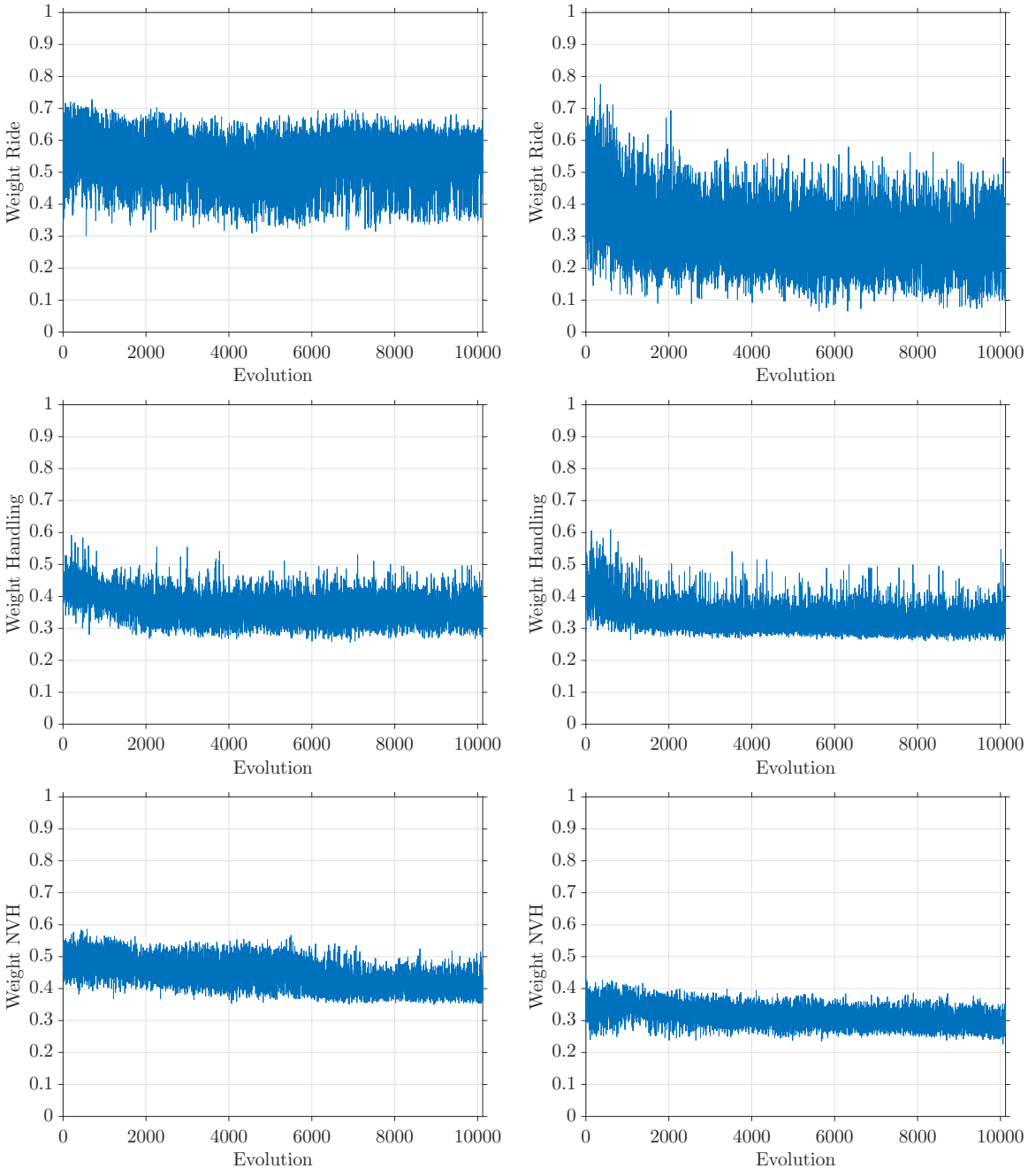

Figure 64: Weights Evolution: Optimization 1.3 (left) and 8.3 (right).

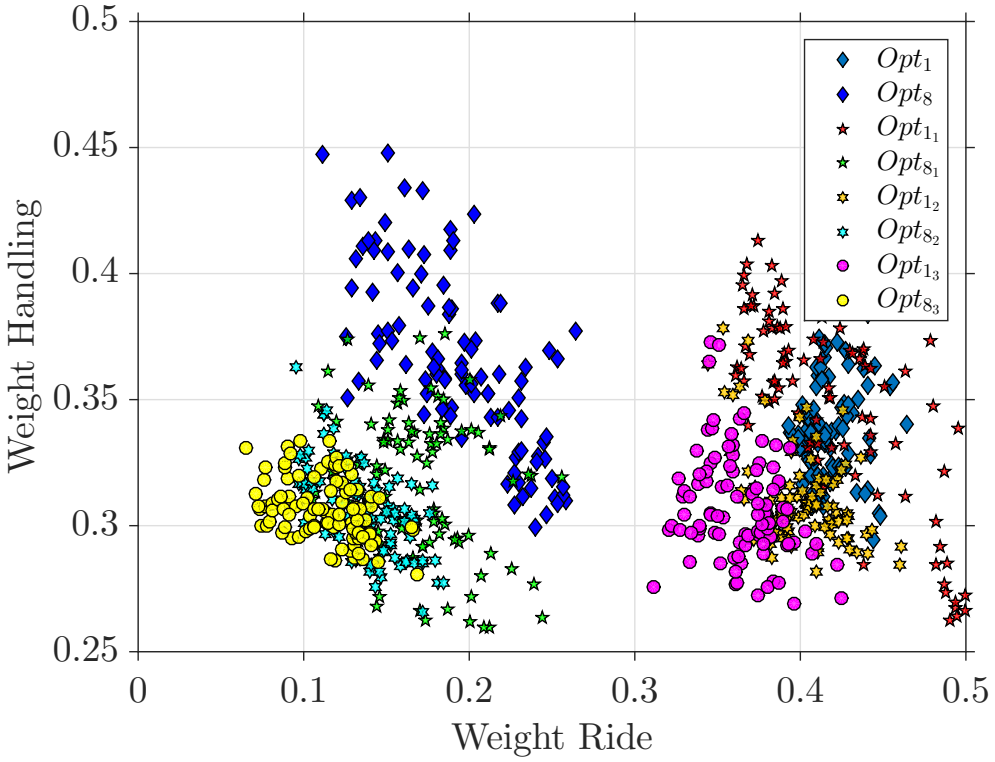

Figure 65: Scatter Pareto: Investigation 6, 100 best runs in regard to Ride, Handling and NVH.

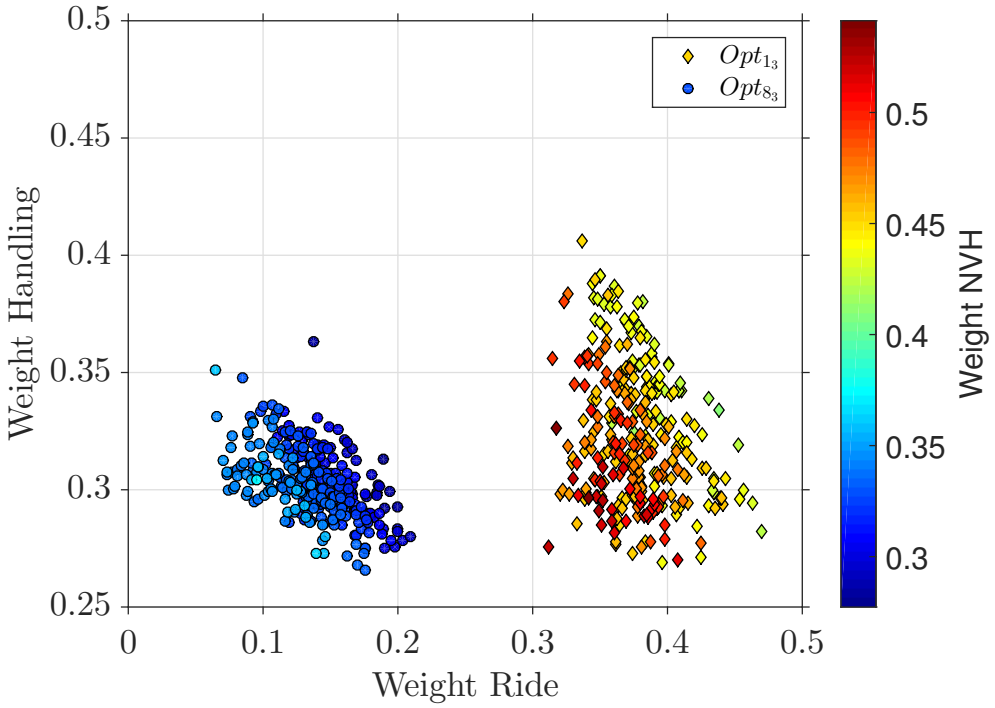

Figure 66: Bubble Pareto: Investigation 6, 300 best runs in regard to Ride, Handling and NVH.

4.2.7 Optimal Designs

To understand how much better the optimal designs have become after an optimization, the optimal designs from the last iterations in the DSRM optimizations will be compared to the nominal design. First a Barplot over the design load values have been generated and is shown in Figure 67. Another Barplot that shows the individual Deviation weight values can be found in Figure 68. It is obvious that the two optimal designs has improved greatly in comparison to the nominal design.

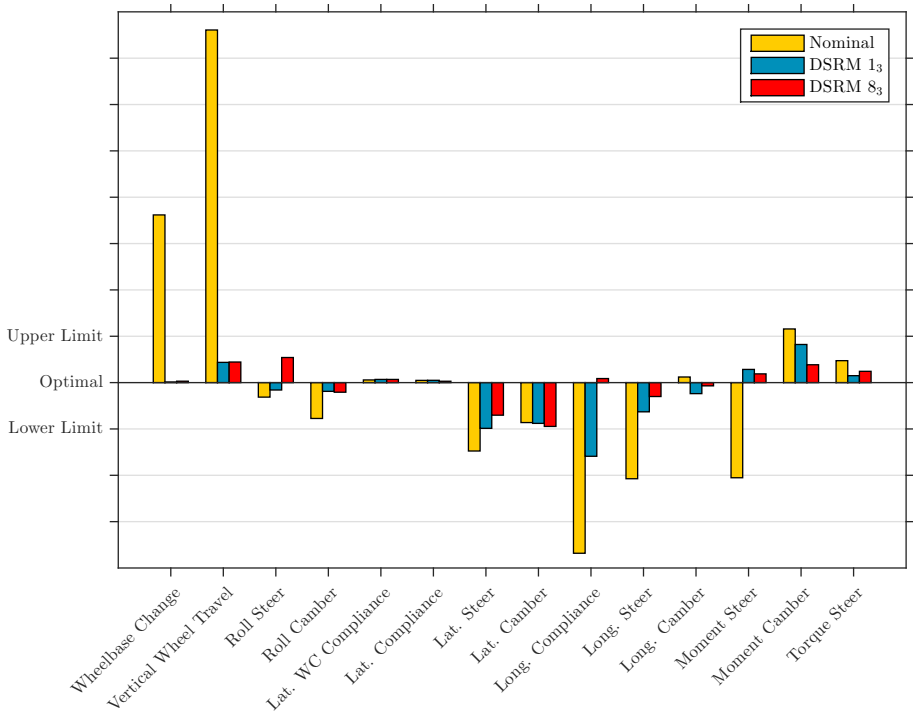

Figure 67: Barplot of design load response values of the optimal designs.

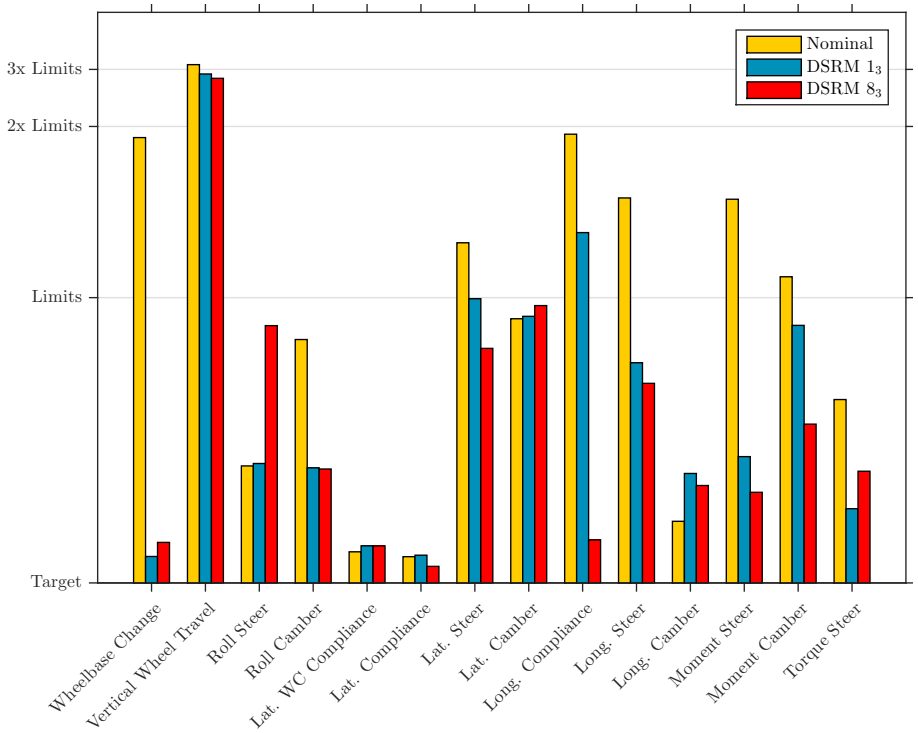

Figure 68: Barplot of the Weighted Absolute Mean Deviation values of the optimal designs.

4.3 Structural Optimization

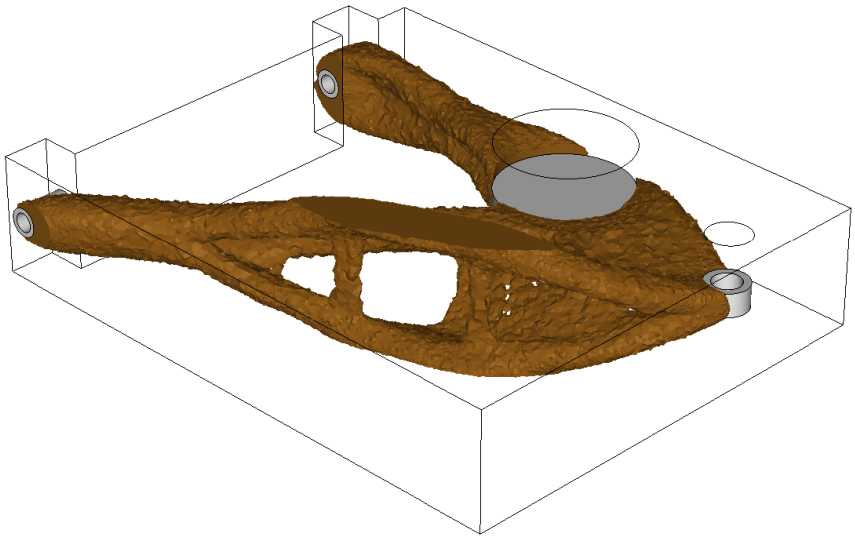

Aluminum

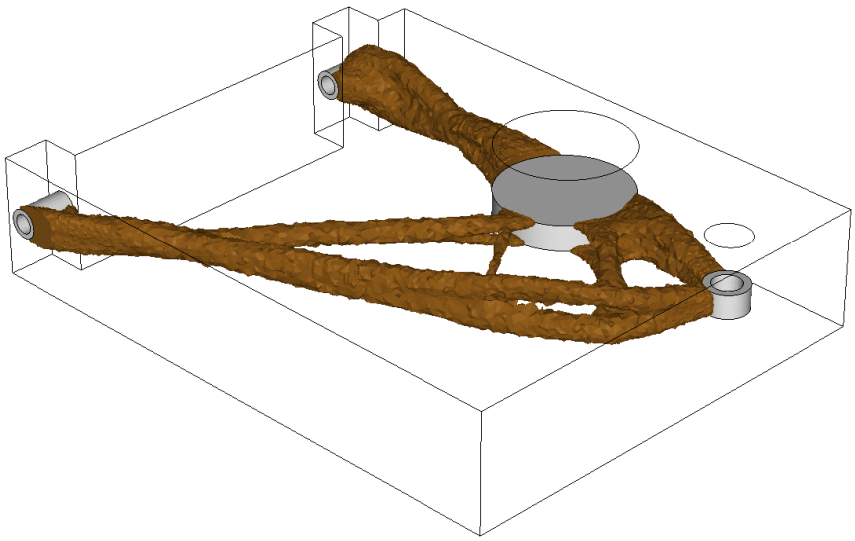

Steel

Figure 69: Topology optimization: Elements with density $\geq 20\%$.

The non-design components are assigned the same material as the design space. Thus, to make the weight comparison fair, only the design space is taken into consideration when comparing the two results. The weight of the design space in the aluminum

control arm is 4.362 kg, and in the steel control arm 5.083 kg. The aluminum arm is 0.721 kg (14.18%) lighter, even though it is much bulkier. A lot of material is placed at the boundary of the design space, suggesting that optimization would have expanded the control arm even further if it could.

Flexbodies was generated from the results shown in Figure 69 above using the Component Mode Synthesis (CMS) method. The finite element models was reduced to single super elements with only the interface degrees of freedom and 10 normal modes. The super elements are approximations of the original finite element models, but are suitable for use in multibody dynamics simulations as the mass matrices are captured correctly. When inserted into the multibody model the super elements are called flexbodies. Figure 70 shows the nominal multibody model with the rigid control arm bodies exchanged for the flexbodies.

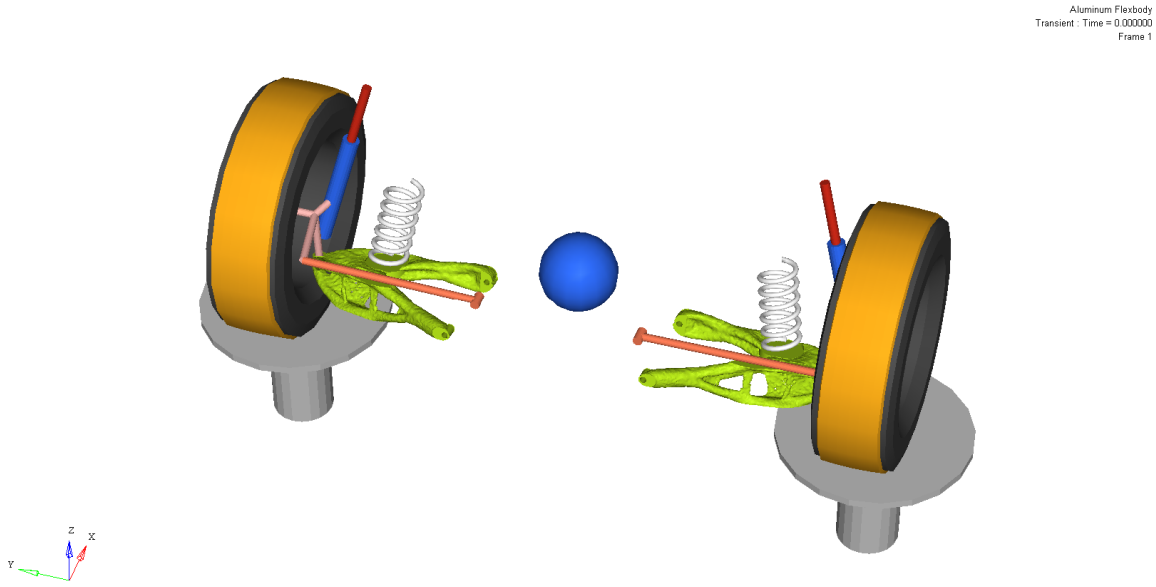

Aluminum Control Arm Flexbody

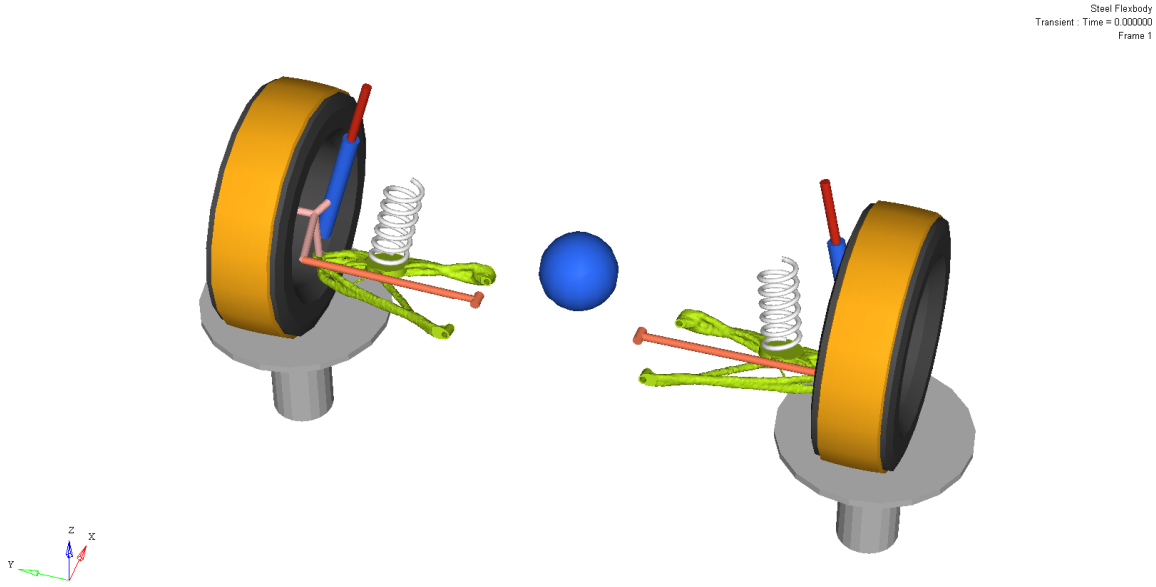

Steel Control Arm Flexbody

Figure 70: Topology optimization: Control Arm flexbodies.

Simulations where run to investigate how the model was effected when the flexbodies was introduced. Table 32 shows how the responses changed, and Table 32 shows how the magnitude of the forces and moments changed.

Response	Rigid	Aluminum Flexbody	Steel Flexbody	Unit
Wheelbase Change	23.0910	23.0590 (−0.14%)	23.0300 (−0.26%)	$^{mm}/_{100mm}$
Track Width Change (CP)	15.2170	15.2200 (+0.02%)	15.2240 (+0.05%)	$^{mm}/_{100mm}$
Roll Steer	-0.0188	-0.0186 (−1.04%)	-0.0185 (−1.76%)	$^{deg}/_{deg}$
Roll Camber	0.5565	0.5566 (0%)	0.5565 (0%)	$^{deg}/_{deg}$
Lateral Force Compliance (WC)	0.0288	0.0303 (+5.09%)	0.0306 (+6.01%)	$^{mm}/_{kN}$
Lateral Force Compliance (CP)	0.1204	0.1281 (+6.34%)	0.1291 (+7.17%)	$^{mm}/_{kN}$
Lateral Force Steer	-0.0190	-0.0201 (+5.51%)	-0.0203 (+6.68%)	$^{deg}/_{kN}$
Lateral Force Camber	0.0138	0.0146 (+5.64%)	0.0146 (+6.27%)	$^{deg}/_{kN}$
Longitudinal Force Compliance (WC)	0.3178	0.3458 (+8.81%)	0.3771 (+18.69%)	$^{mm}/_{kN}$
Longitudinal Force Steer	-0.0322	-0.0329 (+5.51%)	-0.0342 (+6.68%)	$^{deg}/_{kN}$
Longitudinal Force Camber	0.0121	0.0122 (+0.64%)	0.0126 (+4.10%)	$^{deg}/_{kN}$
Overturning Moment Steer	-0.0411	-0.0429 (+4.46%)	-0.0432 (+5.27%)	$^{deg}/_{kNm}$
Overturning Moment Camber	0.0347	0.0361 (+3.98%)	0.0362 (+4.36%)	$^{deg}/_{kNm}$
Aligning Torque Steer	-0.1579	-0.1606 (+1.69%)	-0.1615 (+2.26%)	$^{deg}/_{kNm}$

Table 31: Effect on responses by introduction of a flexible Control Arm body.

The average response change when the control arm was replaced with the aluminum flexbody was +3.32%, and when it was replaced with the steel flexbody it was +4.68%.

Rigid

Attachment Point	Max Load X		Max Load Y		Max Load Z	
	F [N]	τ [Nmm]	F [N]	τ [Nmm]	F [N]	τ [Nmm]
Body Front	23604	196	682	14	2054	33
Body Rear	31082	196	4297	14	5254	33
Knuckle	18329		4980		3701	
Spring	30		1		25	

Aluminum Flexbody

Attachment Point	Max Load X		Max Load Y		Max Load Z	
	F [N]	τ [Nmm]	F [N]	τ [Nmm]	F [N]	τ [Nmm]
Body Front	24908 (+5.52%)	207 (+5.61%)	700 (+2.64%)	18 (+28.57%)	2178 (+6.04%)	35 (+6.06%)
Body Rear	30450 (−2.03%)	338 (+72.45%)	4297 (0%)	18 (+28.75%)	5218 (−0.69%)	44 (+33.33%)
Knuckle	18312 (−0.09%)		4979 (−0.02%)		3702 (+0.03%)	
Spring	32 (+6.67%)		1 (0%)		25 (0%)	

Steel Flexbody

Attachment Point	Max Load X		Max Load Y		Max Load Z	
	F [N]	τ [Nmm]	F [N]	τ [Nmm]	F [N]	τ [Nmm]
Body Front	25164 (+6.61%)	415 (+111.73%)	690 (+1.17%)	19 (+35.71%)	2207 (+7.45%)	55 (+66.67%)
Body Rear	30359 (−2.33%)	507 (+158.67%)	4296 (−0.02%)	26 (+85.71%)	5211 (−0.82%)	63 (+90.91%)
Knuckle	18295 (−0.19%)		4979 (−0.02%)		3702 (+0.03%)	
Spring	32 (+6.67%)		1 (0%)		25 (0%)	

Table 32: Effect on force and moment magnitudes by introduction of a flexible Control Arm body.

The relative changes in force magnitudes, +1.51% average for the Aluminum control arm, and +1.69% average for the steel control arm, are comparable to the changes in the responses. But, the magnitudes of the moments are greatly effected by the introduction of the flexbodies, +29.13% average for the Aluminum control arm, and +91.57% average for the steel control arm.

The average error on the response values that is introduced in the model by using rigid bodies is less than 5%. However, if higher precision is required, one should consider replacing the rigid bodies with beam elements with stiffnesses derived from

the compliance constraints. These beam elements would increase the simulation time slightly, but the differences between the responses in the system optimization and the responses generated when the beams are replaced by flexbodies would be less.

5 Methodology

One of the main objectives with this thesis is to establish a CAE methodology that could be incorporated into the development process of a vehicle suspension system. To be able to establish such a methodology the different steps involved in the design process have been thoroughly investigated for the Strut & Coil suspension model. If the established methodology will hold for other suspension models can therefore be discussed. From the beginning of the thesis it was quite obvious that two phases were involved, namely a DOE and a Multi-objective Optimization, but how to setup the problem and interpret the results were somewhat diffuse at the time. Although, with time and the investigations performed an understanding on how to address these phases were developed and resulted in a methodology.

First and foremost it was concluded that that the design process consist of more than these two phases and that each phase in general has several stages. To visualize how the phases are connected a flowchart of the design process has been generated and is shown in Figure 71. In this figure the different boxes correspond to the phases involved in the design process. The boxes that are inside the dashed blue line are the phases that are within the scope of this thesis, which means that the initial phase is outside the scope of this thesis. Nonetheless, this phase is one of the most important ones since it will be defining the results in the following phases. Although, this overall view of the design process lack the details of which stages that is involved in every phase and their purpose. A thorough description of the different phases with their respective stages will be presented below.

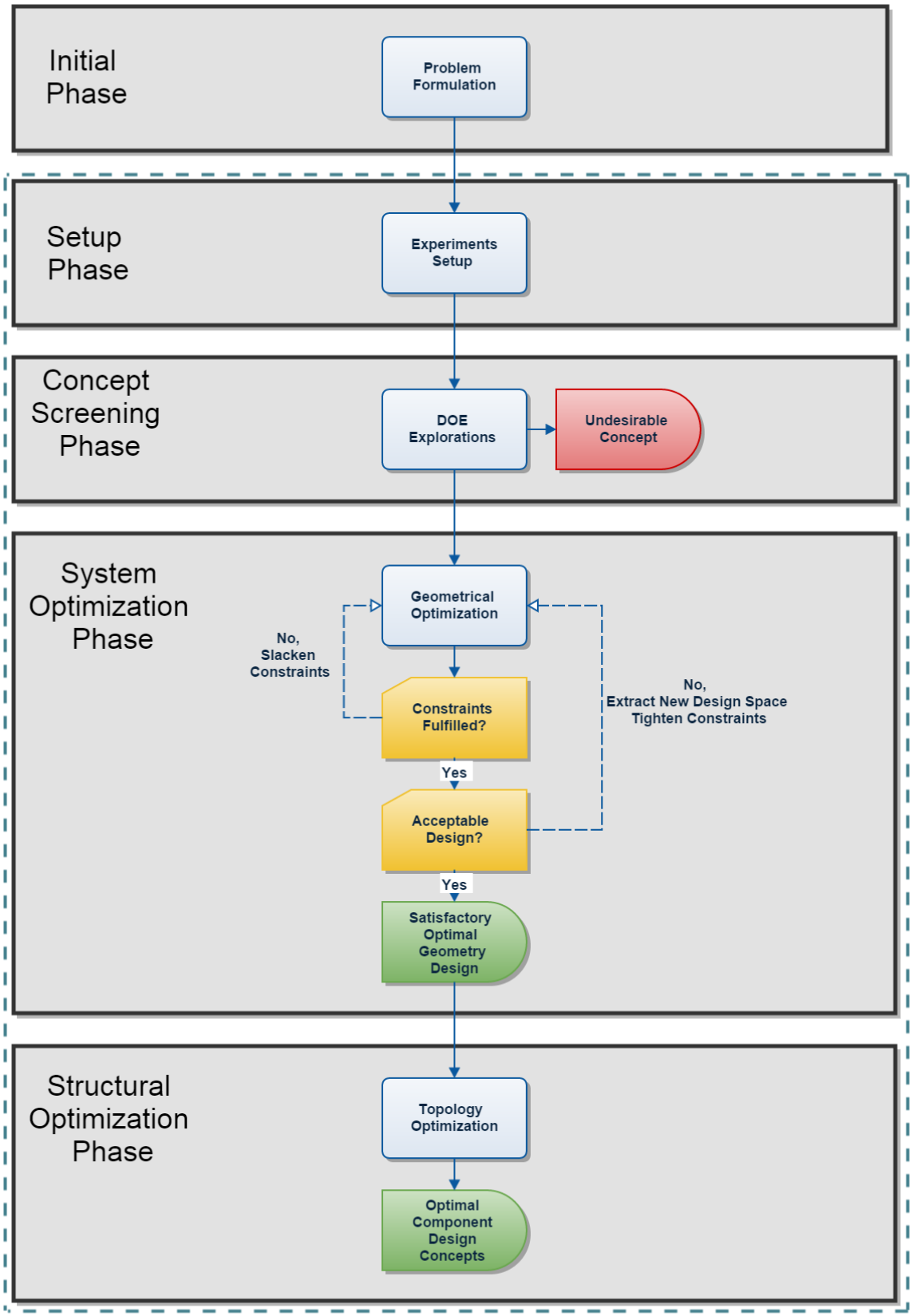

Figure 71: CAE methodology flowchart.

5.1 Initial Phase

The initial phases consist of several stages that will more or less define the problem formulation for the design process. Since these stages are outside the scope of this thesis they will not be discussed in greater detail but are presented due to the fact that they are required in order begin the design process. First of all, a specification of the targets and the limits needs to be established. This specification is preferably established by benchmarking and measuring existing vehicles. With an established specification, the load cases and corresponding responses for the design process are automatically defined. Note that it is favorable to specify exactly how different responses should be calculated, since this information is helpful in the modeling of the MBD models. Secondly, one needs to decide which conceptual suspension designs to bring forth into the design process. Finally, MBD models have to be created for the chosen conceptual designs. These MBD models should be created in a similar manner, in other words the same assumptions and limitations should be applied to all models. For instance if the linkage is modeled as rigids in one model, it should not be flexible in other models. In the end these models should have the defined load cases and the corresponding outputs needed for the calculation of the responses. It is essential that a validation of the MBD models is performed before these are used in the design process. If the MBD models contain errors or are missing vital load cases/outputs, there is no use in beginning the design process. These problems will effect the setup and results of the later phases and it will results in a longer lead time of the design process due to remodeling and revisiting of phases. A flowchart, shown in Figure 72, has been generated to clarify how the stages are connected for the initial phase.

Figure 72: Initial phase flowchart.

5.2 Setup Phase

The main goal with the setup phase is to formulate the problem in a experimental software, like `HyperStudy`, and establish a connection to the MBD models. However, before one can address the problem formulation in the experimental software, the output data from the MBD simulations needs to be analysed and processed into response values. The two stages involved in this phase will therefore be denoted Response Script respectively Experimental Software and will be presented below.

5.2.1 Response Script

First of all, the necessity and contents of this script is highly dependent on the MBD responses to be evaluated. If the MBD responses are such that they are supposed to reach a target range it is a necessity. In general, MBD responses connected to

suspension models show this behavior and therefore these need to be rated. In this thesis the MBD responses have been calculated using the MBD outputs, and thereafter rated within the software `HyperMath`. Section 3.1.3 respectively 3.1.4 describe how the MBD responses are calculated and then rated. Anyhow, these rated values are not ready to be used since they still need to be normalized and weighted into the separate objectives. Section 3.1.5 describes how the normalization and weighting have been performed in this thesis. The necessary calculation procedures in the Response Script stage have been visualized in a flowchart, shown in Figure 73.

Figure 73: Response Script flowchart.

In conclusion these are the necessary calculation steps needed, although the way to perform the calculations is up for debate. However, the output from the Response Script should be the responses that are to be evaluated in the experimental software as objectives and constraints. Hence, at this stage it is important to decide how to calculate these response values as they have great influence on how a design is deemed as good or poor in the forthcoming phases.

5.2.2 Experimental Software

The main goal of this stage is to formulate the problem within the experimental software. This process is more or less straightforward, but nonetheless an important one since the choices made in the process will effect the results later on. A flowchart, shown in Figure 74, visualizes the steps involved in this process.

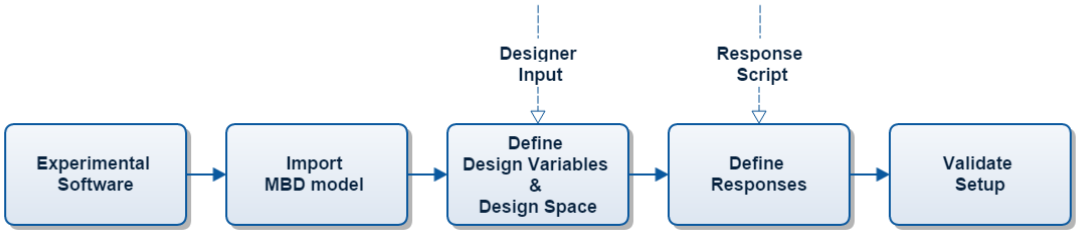

Figure 74: Experimental Software flowchart.

Initially, a link between the MBD model and experimental software needs to be established. Thereafter, the design variables and the corresponding design space needs to be defined. In general the design variables that are of interest for suspension models are the attachment points and bushing stiffnesses. If other typical parameters, such as the damping in the damper, in the suspension model should be included as

design variables depends on if the defined load cases are dynamic or not. Regarding the design space for the chosen design variables, it is preferably set in conjunction with a designer. This is preferable since the design space will greatly influence the optimal design in forthcoming optimizations, hence if a non-feasible design space is set, then some phases may need to be revisited to obtain feasible designs. Regarding the responses that are to be evaluated, they have been calculated using the Response Script and therefore just needs to be imported. Speaking from experience it is utterly important to validate the set up in the experimental software, especially the Response Script, since it will greatly effect the forthcoming results.

5.3 Concept Screening Phase

The main objective with the Concept Screening Phase is to get to know the suspension model and its potential performance. By performing the screening at a relative early stage in the design process it will be possible to determine if a certain suspension model has the characteristics one is looking for. The stages involved in the Screening Phase are visualized in a flowchart shown in Figure 75.

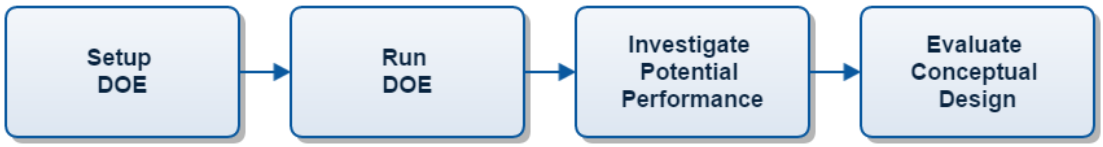

Figure 75: Concept Screening flowchart.

The screening process starts with the setup of a DOE. The choices available at this stage are more or less which DOE method to use and the number of iterations that should be evaluated. It is recommended to use a modern DOE method, since the simulations are deterministic computer experiments, for more details on the selection of DOE methods see Section 2. Typical modern methods would be the Hammersley or the Latin Hypercube. The potential performance can be investigated after the experiments are completed, and with this knowledge it is possible to perform an evaluation of the conceptual design. The last two stages will be discussed more in detail below. Note the recommendation to not use the DOE for generation of a RSM, which could be used in the System Optimization Phase, since the simulations are not much more expensive to perform.

5.3.1 Investigate Potential Performance

The investigation of the potential performance is all about how to post-process and interpret the results. First off, the most challenging part with the post-processing is the amount of data available, and in general it is difficult to comprehend and visualize it in a compact format. In this thesis two different post-processing tools have been presented in the investigation of the potential performance, namely the

main&interaction effects and histograms of the responses. These two tools give valuable information about influential design variables and the behavior of the different responses. Note that a somewhat different interpretation of the main&interaction effect is suggested. See Section 4.1 for more details on how they are used to investigate the potential performance.

5.3.2 Evaluate Conceptual Design

If several conceptual designs are to be investigated this stage will be used to evaluate the differences between the suspension models in terms of potential performance. With the potential performance investigation one should have information about which responses that are easily within limits and those which are not. Those suspension models that show promising characteristics should be kept in the design loop while those that do not can be left out. Although, the decision on which suspension model to bring into the System Optimization phase should not entirely be determined by the potential performance. There might be other factors that could be crucial in the decision making, like manufacturing and mounting costs.

5.4 System Optimization Phase

Those suspension models that seemed to have a potential is brought into the System Optimization phase where the goal is to find an optimal geometry design. The optimal design refers to the best performance within the three objectives Ride, Handling, and NVH. In this thesis it is the lowest weight values for the objectives, and as many responses within the 1L limits as possible. For the setup that have been used in this thesis one could say in conclusion that it is preferable to use slackened limits as constraints, an evolutionary optimization algorithm, and a weighted approach for the objectives. Although, to obtain more optimal designs the recommendation is to use the DSRM approach in the System Optimization phase. A more detailed description of the DSRM approach is found in Section 3.2.4.1.1. Another observation in this thesis was that the design space definition effects the results, if the design space is limited for some design variables it may prevent some responses to fulfill the target limits. Before an optimal design is chosen for the next phase it is important to verify that the design is feasible. This verification is recommended to be done in conjunction with a designer.

5.5 Structural Optimization Phase

In this phase the optimal suspension system is to be realized into a manufacturable design. A topology optimization is recommended as the initial approach. The result should be used as concept for models in further optimizations, taking manufacturing constraints and economical constraints into account. The errors that result from the assumptions taken, such as rigid bodies, can be found by converting the finished suspension parts into a flexbodies and inserting them into the MBD model. A simulation

using flexbodies will yield results closer to the real world version of the suspension model. For more details on the Structural Optimization Phase, see Section 4.3.

6 Conclusion

The results in this thesis clearly point out that it is viable to introduce a CAE methodology in the design process of a vehicle suspension system. The optimal designs that are obtained from the optimization have certainly improved in Ride, Handling and NVH performance in comparison with the nominal design. Moreover, it is also possible to use these optimal designs in a topology optimization to obtain component designs which then can be used at an early stage in a complete vehicle design process. By utilizing the CAE methodology in the design process one could certainly reduce the lead time for the design process and it is possible to obtain designs that meet the specifications in terms of target values. The suggested CAE methodology seems to be an efficient way to address the design process in comparison with a trial and error approach. One of the main advantages would be that engineers without any prior knowledge of vehicle suspension design could with some guidance incorporate the CAE methodology and obtain component designs with optimized performance. Another advantage would be the easiness to evaluate several suspension design concepts. As long the setup has been completed for one design it is more or less straightforward procedure for the others.

The CAE methodology that has been suggested is based on observations from one vehicle suspension model, namely the Strut & Coil suspension system, and therefore there are some uncertainties if this methodology is applicable on other suspension systems. The suggested methodology has been developed to be as general as possible, and the suggested phases and stages are those that were deemed necessary for this type of problem formulation. Although, if other suspension models are to be evaluated there might be other things to take into consideration during the setup, resulting in new stages. There is especially one phase that would have been really interesting to evaluate for several suspensions models, and that is the concept screening phase. The formulation of the investigation of potential performance stage is the most uncertain part since it have not been possible to compare the potential performance between different models. It would be interesting to investigate if it is possible to predict which suspension model would perform the best in the System Optimization phase simply by investigating the potential performances.

In the System Optimization phase there are also uncertainties, especially if the suggested DSRM approach is viable for other suspension models. At least for the Strut & Coil suspension the approach helped the optimization algorithm to find more optimal designs. Some observations were made during the System Optimization phase. The first observation was that the optimization algorithm generates quite many non-feasible designs. These designs are concluded to be non-feasible since the MBD simulations ends prematurely, or the obtained response values are much larger in magnitude compared to the majority of the designs. It might be possible to improve the converging capabilities of the optimization algorithm if one could prevent these non-feasible designs from being generated. The second observation made was that the optimization algorithm more or less finds one optimal design. The algorithm selects the design vari-

able values in such a way that they converge towards a specific combination of values. The algorithm seem to have found a global minimum, but the question arise if there are other local minimums which have performances comparable to the global minimum. On the subject of optimization, it would have been interesting to investigate how different evolutionary algorithms performs in this type of problem formulation.

From the investigation of similar studies it is quite clear that one important step have been left out in this thesis, namely Robust Design. Robust Design has not been taken into consideration since it was not the main goal from the beginning. Although, it has been given some thought and some different ways to approach Robust Design have been discussed during the thesis. One way would have been to do Robust Designing for the optimal designs from the System Optimization, in other words introduce a variance for the design variables and then check how robust the optimal designs are. In that way robustness could have been another criteria in the evaluation of the optimal design. A second way to approach this would have been to introduce the variance for the design variables in the System Optimization, which would have given designs with a measure of robustness. The drawback with this approach would be that much more evaluations would have been necessary in the optimization. Robust Design was not investigated further due to lack of time.

The MBD model used in this theses was modeled using rigid bodies. Thereby a controllable error was introduced into the model. It was assumed that the compliance in the suspension components would be very small compared to the bushing compliances, and the results would only be marginally effected. However, when the control arm rigid was replaced by flexbodies, to check how the response values where effected in a more correct setup, the introduced error was found to be at an average of 3-5%, with up to 18.69% difference for a single response. This difference is significant. We suggest that the rigid bodies are exchanged for bar elements if the extra simulation costs are affordable. The results differences between bar elements and flexbodies should be less than the difference experienced between rigid bodies and flexbodies.

In this thesis a linear approach was taken in the methodology due to lack of time. An iterative approach between the System Optimization phase and the Structural Optimization phase should be investigated.

References

[1] O.Mirzadeh A.Eskandari and Sh.Azadi. *Optimization of a McPherson Suspension System Using the Design of Experiments Method*. SAE Technical Paper 2006-01-1953. 2006. DOI: 10.4271/2006-01-1953.

[2] D. O. Kang et al. "Robust Design Optimization Of Suspension System By Using Target Cascading Method". In: *International Journal of Automotive Technology* Vol. 13 (2011-09-23). DOI: 10.1007/s12239-012-0010-y.

[3] Steven F. Wojtkiewicz Anthony A. Giunta and Michael S. Eldred. *Overview of Modern Design of Experiments Methods for Computational Simulations*. Technical Paper AIAA-2003-0649. Sandia National Laboratories, 2003.

[4] Xianfu Cheng and Yuqun Lin. "Multiobjective Robust Design of the Double Wishbone Suspension System Based on Particle Swarm Optimization". In: *The Scientific World Journal* (2014-02-11). DOI: 10.1155/2014/354857.

[5] Kaitai Fang. *Design and modeling for computer experiments*. Boca Raton, FL: Chapman & Hall/CRC, 2006.

[6] Julian Happian-Smith. *An Introduction to Modern Vehicle Design*. Warrendale, PA: SAE International, 2002.

[7] Altair Engineering Inc. *HyperWorks Manual 13.0*. 2014.

[8] Inna Krykova. "Evaluating of Path-Dependent Securities with Low Discrepancy Methods". Master's Thesis. Worcester Polytechnic Institute, 2003.

[9] Kai-Tai Fang & Dennis K. J. Lin. *Uniform Experimental Designs and their Applications in Industry*. In: C R Rao R Khattree. *Handbook of Statistics: Vol 22 Statistics in Industry*. Elsevier Science Ltd, 2003, pp. 131–166.

[10] Christopher J Longhurst. *The Suspension Bible*. URL: http://www.carbibles.com/suspension_bible.html.

[11] Douglas C. Montgomery. *Design and Analysis of Experiments*. Hoboken, NJ: John Wiley & Sons, 2005.

[12] Harald Niederreiter. *Random number generation and quasi-Monte Carlo methods*. Philadelphia, Pa: Society for Industrial and Applied Mathematics, 1992.

[13] Joonhong Park Yong-Sub Yi and Kyung-Jin Hong. *Design Optimization of Suspension Kinematic and Compliance Characteristics*. SAE Technical Paper 2014-01-0394. 2014. DOI: 10.4271/2014-01-0394.

Appendix A Design of Experiments

A.1 Main Effects

DV \ Responses	1	2	3	4	5	6	7
p_CtrlArmBodyFront_x	14.212	3.701	0.059	-0.064	0.089	1.813	-0.078
p_CtrlArmBodyFront_y	2.886	-0.364	-0.011	0.003	0.017	0.979	-0.033
p_CtrlArmBodyFront_z	46.785	13.703	0.195	-0.224	0.007	0.341	-0.025
p_CtrlArmBodyRear_x	-21.602	17.114	0.369	-0.217	-0.125	-2.341	0.144
p_CtrlArmBodyRear_y	-4.223	2.878	0.072	-0.035	-0.024	-0.373	0.066
p_CtrlArmBodyRear_z	-76.431	62.406	1.361	-0.806	-0.037	-1.543	0.08
p_CtrlArmKnuckle_x	9.004	-12.959	-0.263	0.171	0.016	1.112	0.059
p_CtrlArmKnuckle_y	5.444	-2.719	-0.046	0.024	0.068	0.154	-0.068
p_CtrlArmKnuckle_z	15.82	-37.814	-0.74	0.504	0.132	0.386	-0.079
p_ToeLinkKnuckle_x	-5.003	5.101	0.283	-0.113	0.029	0.375	-0.091
p_ToeLinkKnuckle_y	-0.267	0.306	0.049	-0.019	0.04	-0.319	-0.023
p_ToeLinkKnuckle_z	-20.368	7.114	1.265	-0.288	-0.084	-0.261	0.098
p_ToeLinkBody_x	7.532	-2.503	-0.473	0.096	-0.084	-0.759	-0.014
p_ToeLinkBody_y	0.537	-1.064	-0.029	0.016	0.038	-0.422	-0.039
p_ToeLinkBody_z	31.382	-14.058	-1.8	0.445	0.101	0.669	-0.016
p_StrutBody_x	8.893	-2.807	0.111	0.119	-0.018	0.675	-0.032
p_StrutBody_y	3.637	13.369	-0.235	-0.47	0.06	-0.532	0.032
p_StrutBody_z	-2.513	-9.281	0.227	0.322	-0.122	-0.847	0.007
p_SpringCtrlArm_x	2.301	-0.882	-0.12	0.012	-0.018	-0.078	0.031
p_SpringCtrlArm_y	-0.604	0.163	0.007	0.012	-0.029	0.277	-0.021
p_SpringCtrlArm_z	1.011	-0.874	0.027	0.003	-0.019	0.914	-0.04
bsh_CtrlArmBodyFront_t_r	0.767	0.318	0.013	-0.003	-0.068	-0.68	0.003
bsh_CtrlArmBodyFront_t_a	0.434	0.948	-0.002	-0.025	-0.085	-0.554	0.036
bsh_CtrlArmBodyFront_r_r	1.028	-1.426	-0.01	0.023	-0.066	0.385	-0.039
bsh_CtrlArmBodyFront_r_a	-0.787	2.092	0.037	-0.028	-0.077	0.203	0.006
bsh_CtrlArmBodyRear_t_r	2.114	-1.183	-0.025	0.015	-0.198	-1.969	0.166
bsh_CtrlArmBodyRear_t_a	1.126	-0.981	-0.075	0.016	0.001	-1.007	0.048
bsh_CtrlArmBodyRear_r_r	0.371	-1.179	-0.031	0.026	0.056	-0.611	0.014
bsh_CtrlArmBodyRear_r_a	-0.173	-0.644	0.016	0.022	0.076	0.072	0.003
bsh_ToeLinkBody_t_r	1.367	-2.147	-0.045	0.035	-0.033	-0.03	0.068
bsh_ToeLinkBody_t_a	-1.203	0.091	0.004	-0.006	0.008	-0.056	0.015
bsh_ToeLinkBody_r_r	1.856	-1.538	-0.045	0.017	-0.029	0.315	-0.035
bsh_ToeLinkBody_r_a	0.015	-0.55	0.021	0.01	-0.028	0.233	-0.011
bsh_StrutBody_t_r	0.324	-0.642	0.033	0.005	0.038	-0.916	0.034
bsh_StrutBody_t_a	0.406	-0.501	-0.002	0.001	0.007	0.043	0.029
bsh_StrutBody_r_r	0.357	0.138	-0.004	-0.008	0.027	-0.039	-0.014
bsh_StrutBody_r_a	-1.289	1.708	0.034	-0.031	0.044	0.495	0.006

Table 33: Main Effects.

DV \ Responses	8	9	10	11	12	13	14
p_CtrlArmBodyFront_x	0.18	0.563	-0.023	0.004	-0.005	-0.003	-0.046
p_CtrlArmBodyFront_y	0.08	0.118	0	-0.003	-0.001	0	-0.025
p_CtrlArmBodyFront_z	0.042	0.051	-0.008	0.003	0	-0.008	0.002
p_CtrlArmBodyRear_x	-0.217	-0.944	0.098	-0.054	0.088	-0.05	0.201
p_CtrlArmBodyRear_y	-0.057	0.236	-0.015	0.007	0.006	-0.007	0.003
p_CtrlArmBodyRear_z	-0.146	-0.17	0.026	-0.015	0.033	-0.024	0.08
p_CtrlArmKnuckle_x	0.1	0.096	0.046	-0.011	0.254	-0.099	0.576
p_CtrlArmKnuckle_y	0.023	0.035	-0.049	0.014	-0.002	-0.001	0.006
p_CtrlArmKnuckle_z	0.057	0.332	-0.039	0.025	-0.115	0.09	-0.18
p_ToeLinkKnuckle_x	0.051	0.047	-0.067	0.017	-0.183	0.058	-0.795
p_ToeLinkKnuckle_y	-0.027	0.011	-0.012	0.005	-0.006	0.006	-0.032
p_ToeLinkKnuckle_z	-0.051	-0.154	0.053	-0.024	0.18	-0.066	0.428
p_ToeLinkBody_x	-0.075	0.338	-0.084	0.016	-0.042	0.006	-0.165
p_ToeLinkBody_y	-0.047	0.006	0.008	0.001	0.01	0.002	0.089
p_ToeLinkBody_z	0.065	-0.093	0.007	0.001	-0.044	0.022	-0.124
p_StrutBody_x	0.091	0.004	0.034	0.025	-0.122	0.096	0.246
p_StrutBody_y	-0.057	0.163	-0.024	-0.003	0.03	-0.037	0.023
p_StrutBody_z	-0.104	0.016	-0.002	-0.007	0.01	-0.053	-0.089
p_SpringCtrlArm_x	-0.007	0.023	-0.003	-0	0.005	-0.002	0.03
p_SpringCtrlArm_y	0.014	0.078	-0.003	0.004	0	-0	0.01
p_SpringCtrlArm_z	0.082	0.016	-0.005	0.002	-0.016	0.008	-0.019
bsh_CtrlArmBodyFront_t_r	-0.065	-0.408	-0.007	0.014	0.01	-0.01	-0.005
bsh_CtrlArmBodyFront_t_a	-0.046	-0.238	0.01	-0.007	0.027	-0.02	0.076
bsh_CtrlArmBodyFront_r_r	0.045	-0.091	0.006	-0.003	0.01	0	0.011
bsh_CtrlArmBodyFront_r_a	0.019	0.04	-0.002	-0.002	0.019	-0.016	-0.017
bsh_CtrlArmBodyRear_t_r	-0.185	-1.05	0.141	-0.078	0.178	-0.108	0.383
bsh_CtrlArmBodyRear_t_a	-0.096	-0.168	0.007	-0.004	0.016	-0.011	0.042
bsh_CtrlArmBodyRear_r_r	-0.053	-0.039	0.01	-0.001	0.003	-0.001	0.025
bsh_CtrlArmBodyRear_r_a	-0.002	0.023	-0.009	0.004	-0.01	0.005	-0.012
bsh_ToeLinkBody_t_r	-0.014	-0.208	0.085	-0.022	0.148	-0.05	0.647
bsh_ToeLinkBody_t_a	-0.007	0.065	-0.017	0.003	-0.018	0.003	-0.108
bsh_ToeLinkBody_r_r	0.021	0.019	-0.002	-0	0.019	-0.009	-0.002
bsh_ToeLinkBody_r_a	0.027	0.014	-0.006	-0	-0.001	-0.004	0.005
bsh_StrutBody_t_r	-0.091	-0.094	0.01	0.001	-0.027	-0.072	0.094
bsh_StrutBody_t_a	-0.001	0.025	-0.001	-0	0.015	0.018	-0.01
bsh_StrutBody_r_r	-0.003	-0.043	-0.002	-0.002	-0.004	-0	-0.014
bsh_StrutBody_r_a	0.043	0.003	0	-0.002	-0	0.001	-0.03

Table 34: Main Effects.

A.2 Normalized Main Effects

DV \ Responses	1	2	3	4	5	6	7
p_CtrlArmBodyFront_x	1.42	0.93	0.49	-0.13	0.18	0.73	-0.97
p_CtrlArmBodyFront_y	0.29	-0.09	-0.09	0.01	0.03	0.39	-0.42
p_CtrlArmBodyFront_z	4.68	3.43	1.63	-0.45	0.01	0.14	-0.31
p_CtrlArmBodyRear_x	-2.16	4.28	3.07	-0.43	-0.25	-0.94	1.8
p_CtrlArmBodyRear_y	-0.42	0.72	0.6	-0.07	-0.05	-0.15	0.83
p_CtrlArmBodyRear_z	-7.64	15.6	11.34	-1.61	-0.07	-0.62	1
p_CtrlArmKnuckle_x	0.9	-3.24	-2.19	0.34	0.03	0.44	0.74
p_CtrlArmKnuckle_y	0.54	-0.68	-0.38	0.05	0.14	0.06	-0.86
p_CtrlArmKnuckle_z	1.58	-9.45	-6.16	1.01	0.26	0.15	-0.99
p_ToeLinkKnuckle_x	-0.5	1.28	2.36	-0.23	0.06	0.15	-1.14
p_ToeLinkKnuckle_y	-0.03	0.08	0.41	-0.04	0.08	-0.13	-0.28
p_ToeLinkKnuckle_z	-2.04	1.78	10.54	-0.58	-0.17	-0.1	1.23
p_ToeLinkBody_x	0.75	-0.63	-3.94	0.19	-0.17	-0.3	-0.17
p_ToeLinkBody_y	0.05	-0.27	-0.24	0.03	0.08	-0.17	-0.49
p_ToeLinkBody_z	3.14	-3.51	-15	0.89	0.2	0.27	-0.19
p_StrutBody_x	0.89	-0.7	0.92	0.24	-0.04	0.27	-0.4
p_StrutBody_y	0.36	3.34	-1.96	-0.94	0.12	-0.21	0.39
p_StrutBody_z	-0.25	-2.32	1.89	0.64	-0.24	-0.34	0.09
p_SpringCtrlArm_x	0.23	-0.22	-1	0.02	-0.04	-0.03	0.38
p_SpringCtrlArm_y	-0.06	0.04	0.06	0.02	-0.06	0.11	-0.27
p_SpringCtrlArm_z	0.1	-0.22	0.23	0.01	-0.04	0.37	-0.5
bsh_CtrlArmBodyFront_t_r	0.08	0.08	0.11	-0.01	-0.14	-0.27	0.04
bsh_CtrlArmBodyFront_t_a	0.04	0.24	-0.01	-0.05	-0.17	-0.22	0.45
bsh_CtrlArmBodyFront_r_r	0.1	-0.36	-0.08	0.05	-0.13	0.15	-0.48
bsh_CtrlArmBodyFront_r_a	-0.08	0.52	0.31	-0.06	-0.15	0.08	0.08
bsh_CtrlArmBodyRear_t_r	0.21	-0.3	-0.21	0.03	-0.4	-0.79	2.07
bsh_CtrlArmBodyRear_t_a	0.11	-0.25	-0.62	0.03	0	-0.4	0.6
bsh_CtrlArmBodyRear_r_r	0.04	-0.29	-0.26	0.05	0.11	-0.24	0.18
bsh_CtrlArmBodyRear_r_a	-0.02	-0.16	0.13	0.04	0.15	0.03	0.04
bsh_ToeLinkBody_t_r	0.14	-0.54	-0.38	0.07	-0.07	-0.01	0.84
bsh_ToeLinkBody_t_a	-0.12	0.02	0.03	-0.01	0.02	-0.02	0.18
bsh_ToeLinkBody_r_r	0.19	-0.38	-0.37	0.03	-0.06	0.13	-0.44
bsh_ToeLinkBody_r_a	0	-0.14	0.18	0.02	-0.06	0.09	-0.13
bsh_StrutBody_t_r	0.03	-0.16	0.28	0.01	0.08	-0.37	0.42
bsh_StrutBody_t_a	0.04	-0.13	-0.02	0	0.01	0.02	0.36
bsh_StrutBody_r_r	0.04	0.03	-0.03	-0.02	0.05	-0.02	-0.18
bsh_StrutBody_r_a	-0.13	0.43	0.28	-0.06	0.09	0.2	0.08

Table 35: Normalized Main Effects.

DV \ Responses	8	9	10	11	12	13	14
p_CtrlArmBodyFront_x	0.9	0.28	-0.38	0.02	-0.12	-0.09	-0.08
p_CtrlArmBodyFront_y	0.4	0.06	0	-0.01	-0.04	0	-0.04
p_CtrlArmBodyFront_z	0.21	0.03	-0.13	0.01	0.01	-0.26	0
p_CtrlArmBodyRear_x	-1.08	-0.47	1.64	-0.27	2.2	-1.66	0.33
p_CtrlArmBodyRear_y	-0.28	0.12	-0.25	0.04	0.15	-0.22	0
p_CtrlArmBodyRear_z	-0.73	-0.09	0.43	-0.08	0.82	-0.79	0.13
p_CtrlArmKnuckle_x	0.5	0.05	0.77	-0.06	6.35	-3.3	0.96
p_CtrlArmKnuckle_y	0.12	0.02	-0.82	0.07	-0.05	-0.03	0.01
p_CtrlArmKnuckle_z	0.28	0.17	-0.65	0.13	-2.88	3	-0.3
p_ToeLinkKnuckle_x	0.26	0.02	-1.11	0.08	-4.57	1.95	-1.32
p_ToeLinkKnuckle_y	-0.14	0.01	-0.2	0.03	-0.15	0.19	-0.05
p_ToeLinkKnuckle_z	-0.26	-0.08	0.88	-0.12	4.5	-2.22	0.71
p_ToeLinkBody_x	-0.37	0.17	-1.4	0.08	-1.06	0.22	-0.27
p_ToeLinkBody_y	-0.23	0	0.13	0	0.24	0.06	0.15
p_ToeLinkBody_z	0.32	-0.05	0.11	0.01	-1.11	0.74	-0.21
p_StrutBody_x	0.45	0	0.56	0.12	-3.05	3.2	0.41
p_StrutBody_y	-0.29	0.08	-0.4	-0.02	0.76	-1.24	0.04
p_StrutBody_z	-0.52	0.01	-0.03	-0.04	0.26	-1.75	-0.15
p_SpringCtrlArm_x	-0.03	0.01	-0.05	-0	0.13	-0.07	0.05
p_SpringCtrlArm_y	0.07	0.04	-0.05	0.02	0	-0	0.02
p_SpringCtrlArm_z	0.41	0.01	-0.08	0.01	-0.39	0.26	-0.03
bsh_CtrlArmBodyFront_t_r	-0.33	-0.2	-0.12	0.07	0.24	-0.32	-0.01
bsh_CtrlArmBodyFront_t_a	-0.23	-0.12	0.17	-0.03	0.67	-0.66	0.13
bsh_CtrlArmBodyFront_r_r	0.23	-0.05	0.1	-0.01	0.26	0	0.02
bsh_CtrlArmBodyFront_r_a	0.1	0.02	-0.04	-0.01	0.47	-0.53	-0.03
bsh_CtrlArmBodyRear_t_r	-0.92	-0.52	2.36	-0.39	4.44	-3.59	0.64
bsh_CtrlArmBodyRear_t_a	-0.48	-0.08	0.12	-0.02	0.39	-0.38	0.07
bsh_CtrlArmBodyRear_r_r	-0.26	-0.02	0.17	-0.01	0.08	-0.04	0.04
bsh_CtrlArmBodyRear_r_a	-0.01	0.01	-0.15	0.02	-0.24	0.17	-0.02
bsh_ToeLinkBody_t_r	-0.07	-0.1	1.41	-0.11	3.71	-1.65	1.08
bsh_ToeLinkBody_t_a	-0.04	0.03	-0.28	0.02	-0.46	0.1	-0.18
bsh_ToeLinkBody_r_r	0.1	0.01	-0.03	-0	0.47	-0.31	-0
bsh_ToeLinkBody_r_a	0.13	0.01	-0.1	-0	-0.02	-0.14	0.01
bsh_StrutBody_t_r	-0.45	-0.05	0.16	0	-0.67	-2.38	0.16
bsh_StrutBody_t_a	-0.01	0.01	-0.02	-0	0.37	0.6	-0.02
bsh_StrutBody_r_r	-0.02	-0.02	-0.04	-0.01	-0.1	-0.01	-0.02
bsh_StrutBody_r_a	0.21	0	0	-0.01	-0	0.02	-0.05

Table 36: Normalized Main Effects.

A.2.1 Wheelbase Change

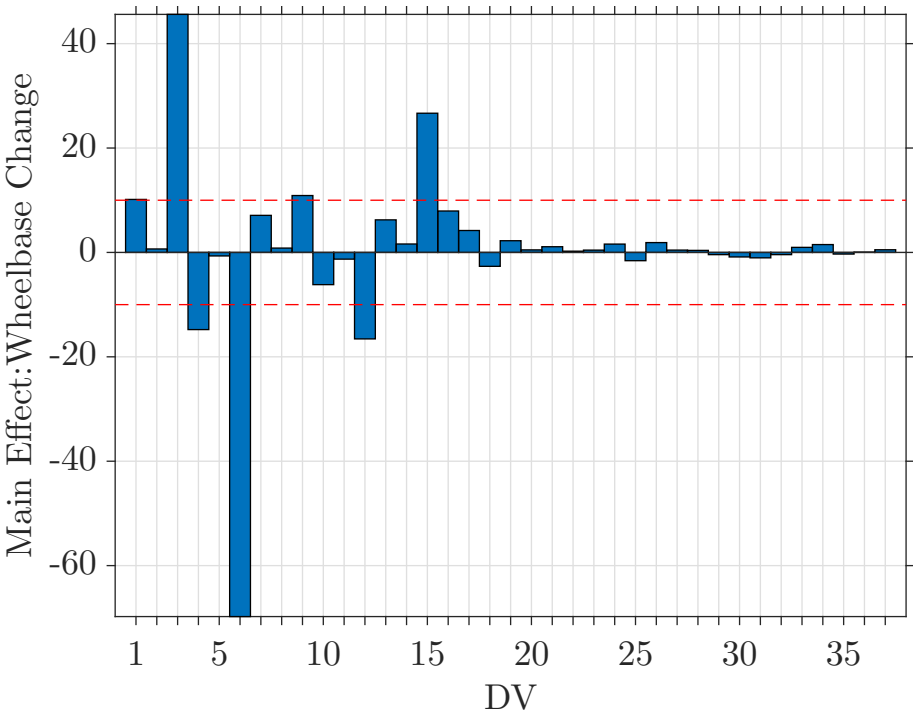

Figure 76: Main Effect: Wheelbase Change.

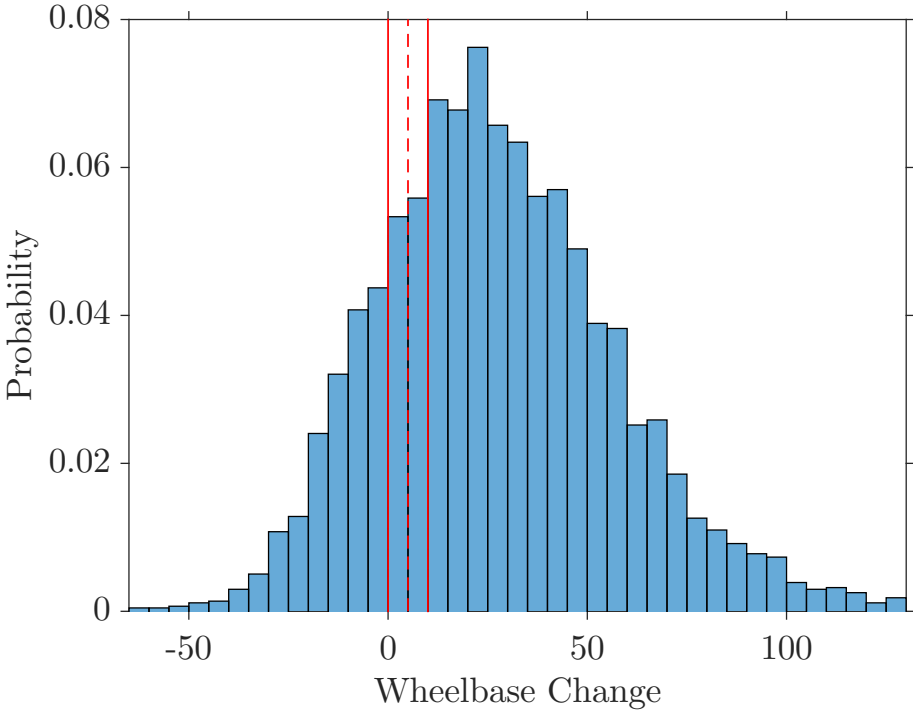

Figure 77: Histogram: Wheelbase Change.

A.2.2 Vertical Wheel Travel

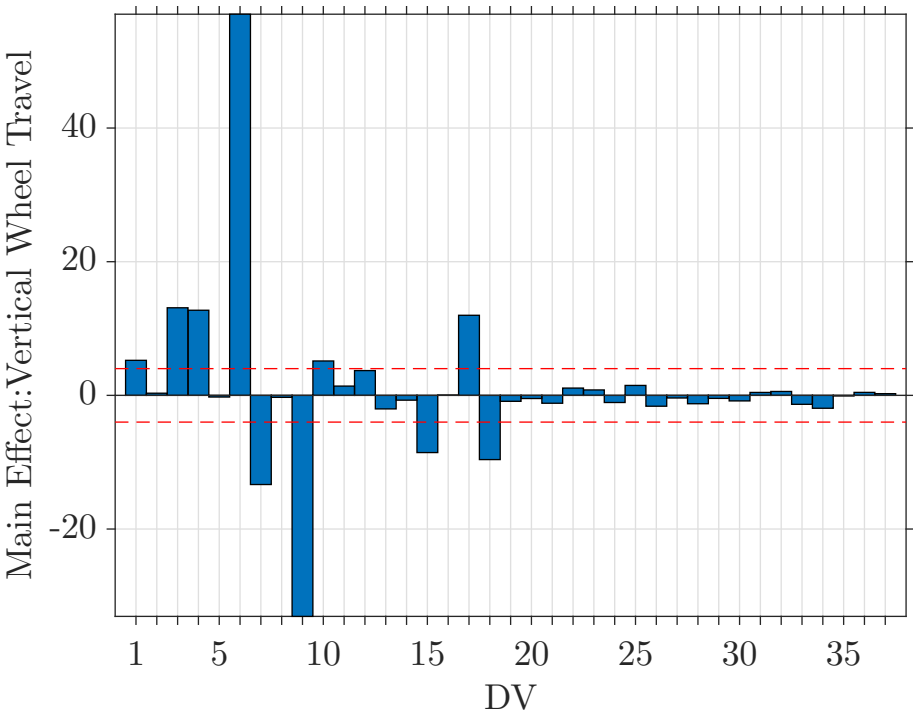

Figure 78: Main Effect: Vertical Wheel Travel.

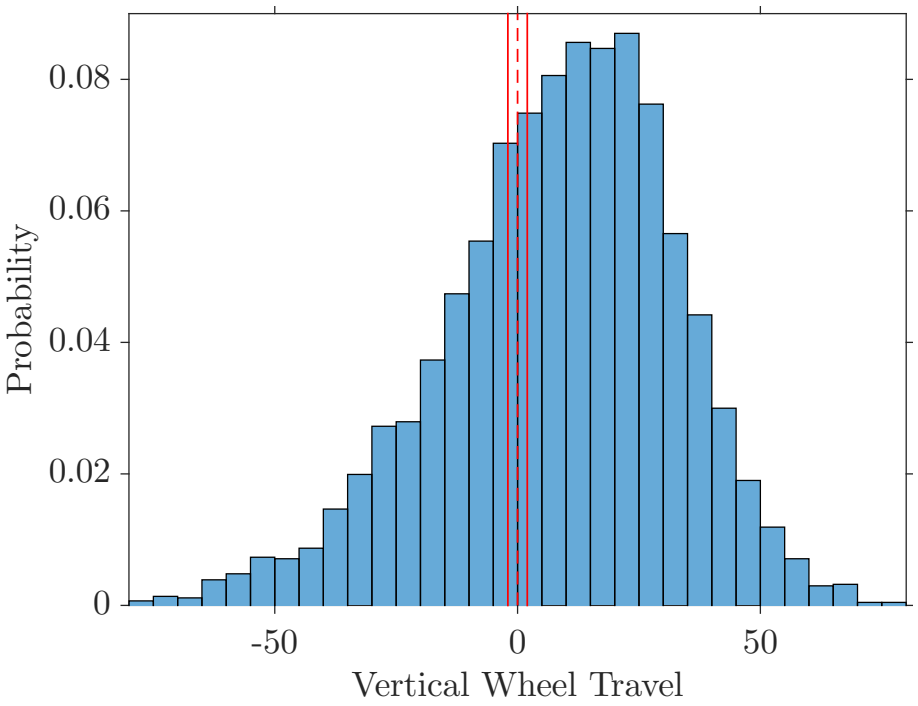

Figure 79: Histogram: Vertical Wheel Travel.

A.2.3 Roll Steer

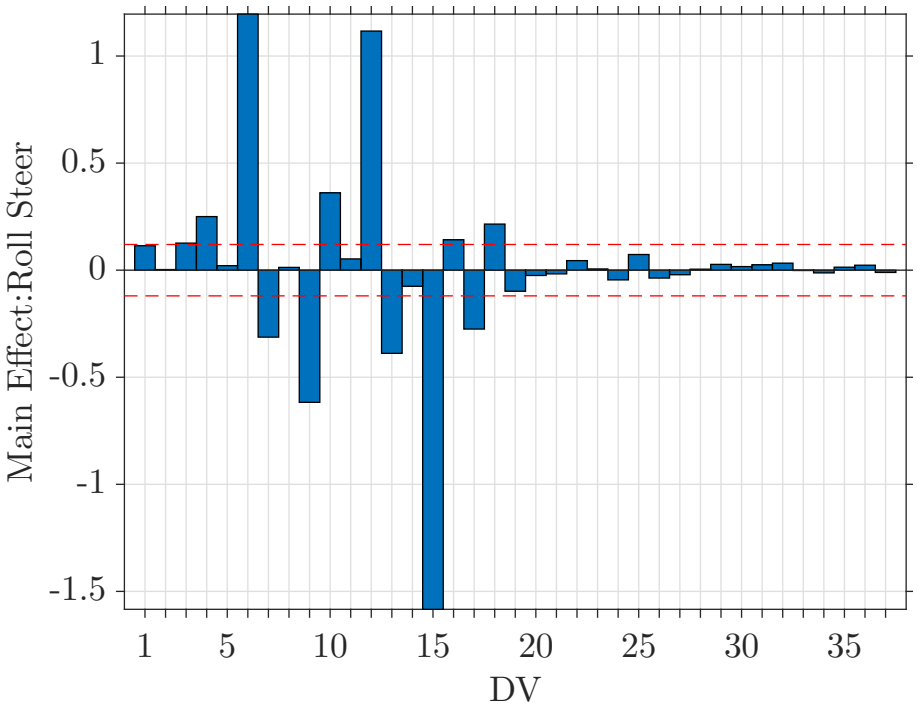

Figure 80: Main Effect: Roll Steer.

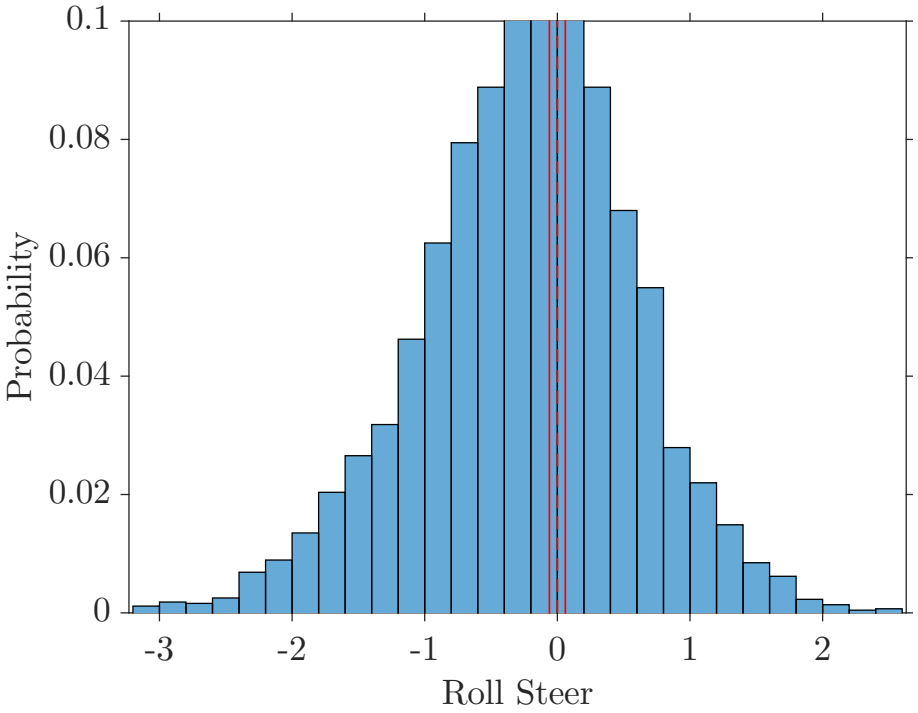

Figure 81: Histogram: Roll Steer.

A.2.4 Roll Camber

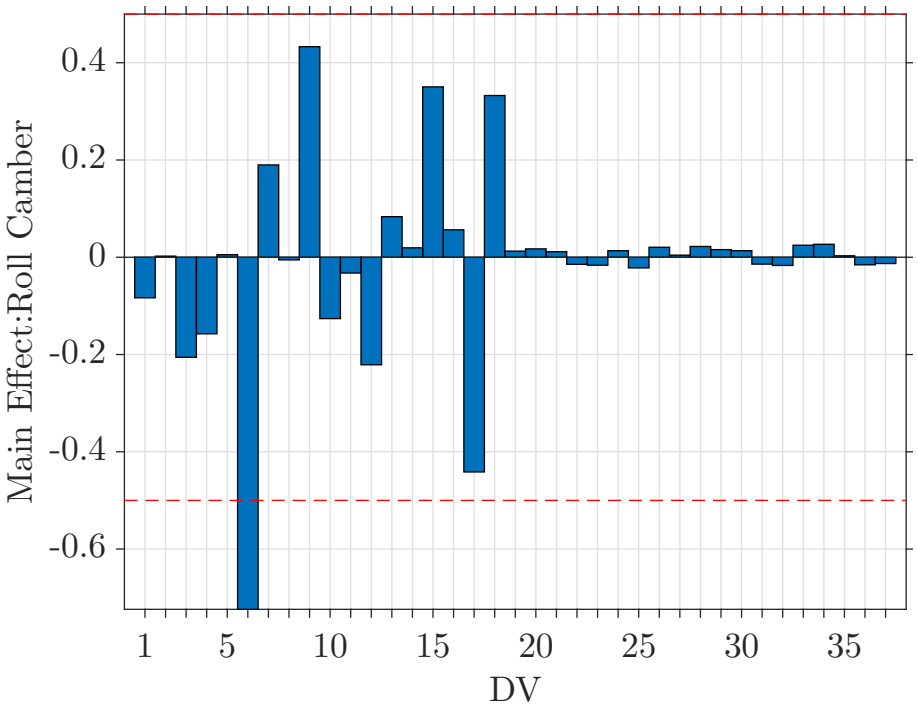

Figure 82: Main Effect: Roll Camber.

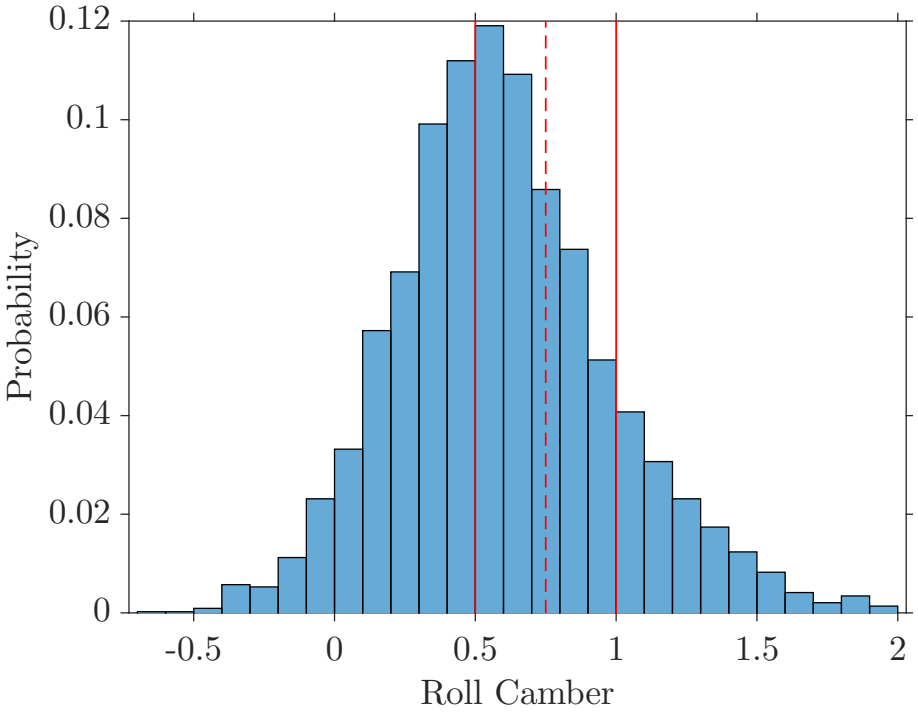

Figure 83: Histogram: Roll Camber.

A.2.5 Lateral WC Compliance

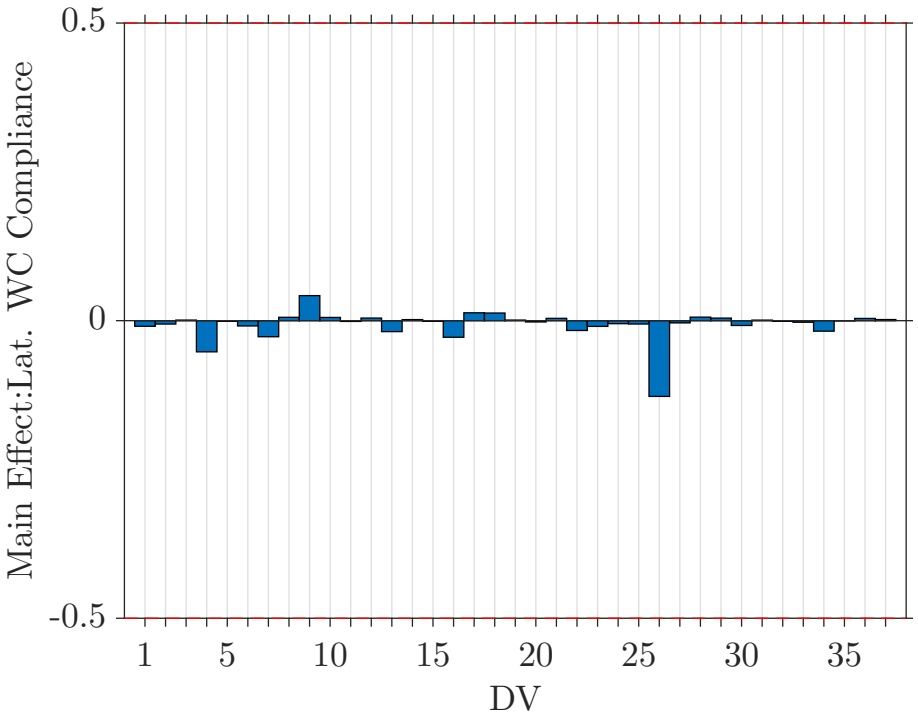

Figure 84: Main Effect: Lateral WC Compliance.

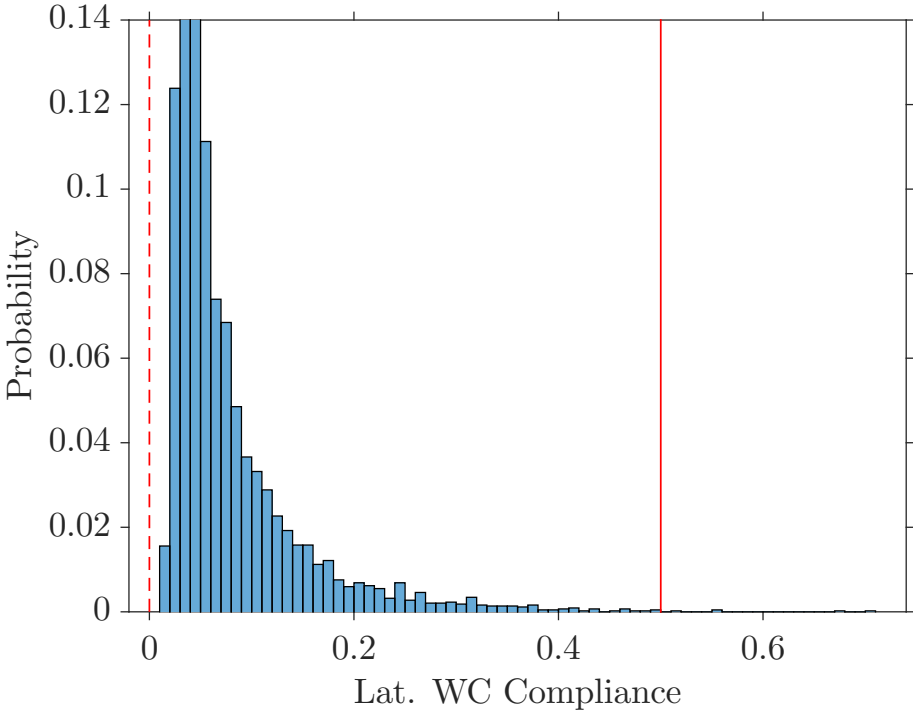

Figure 85: Histogram: Lateral WC Compliance.

A.2.6 Lateral TP Compliance

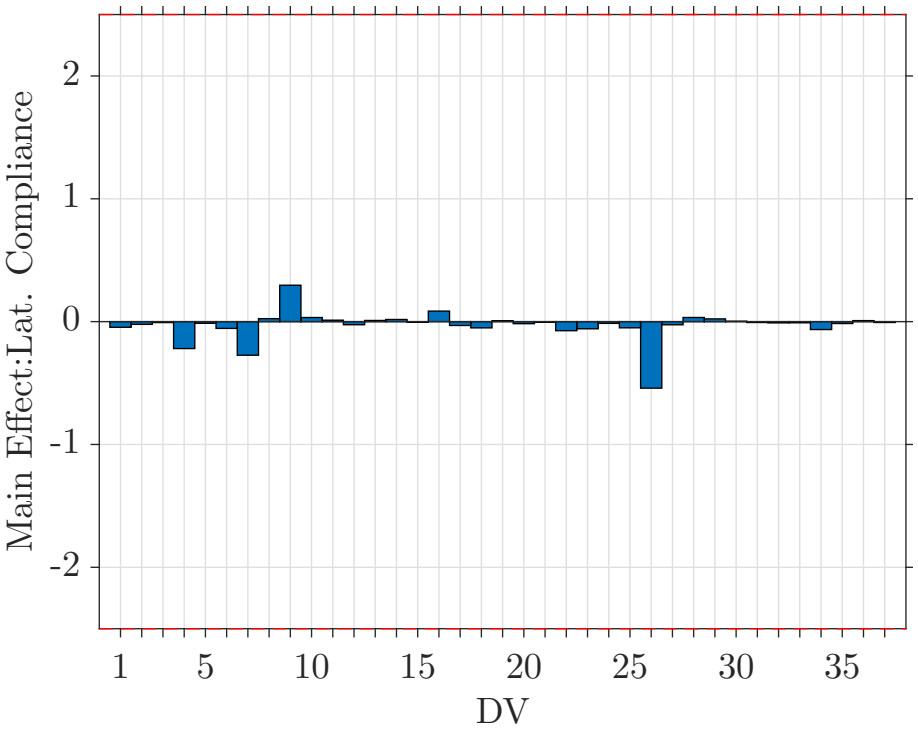

Figure 86: Main Effect: Lateral TP Compliance.

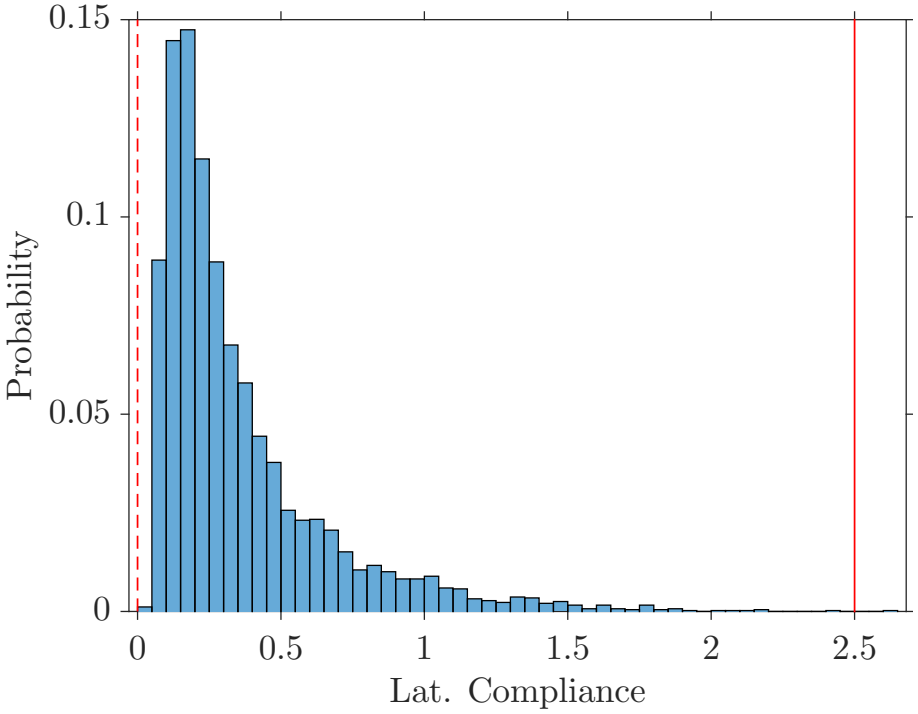

Figure 87: Histogram: Lateral TP Compliance.

A.2.7 Lateral TP Steer

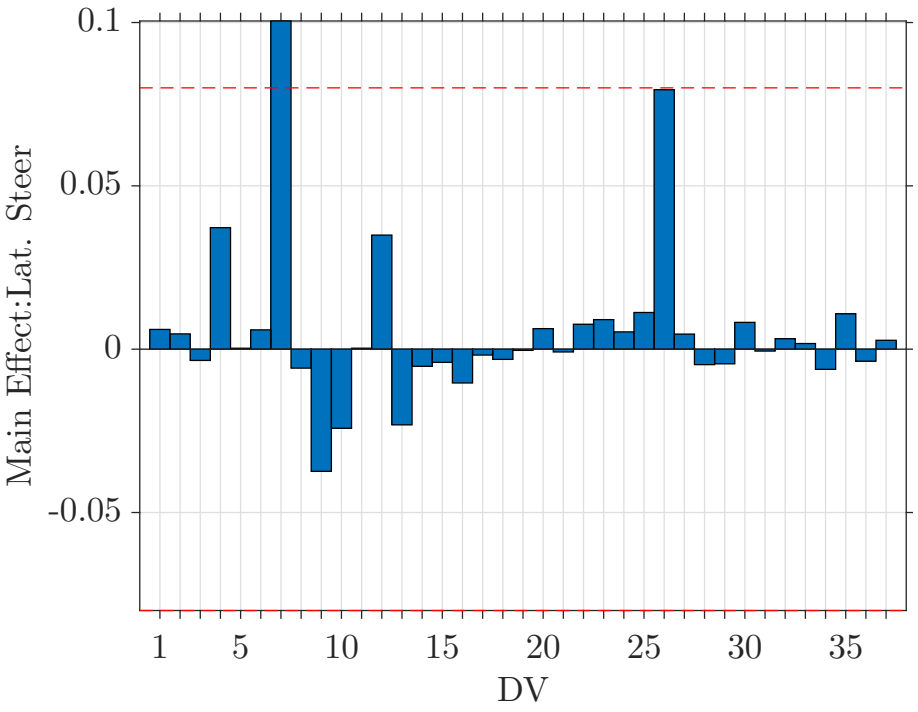

Figure 88: Main Effect: Lateral TP Steer.

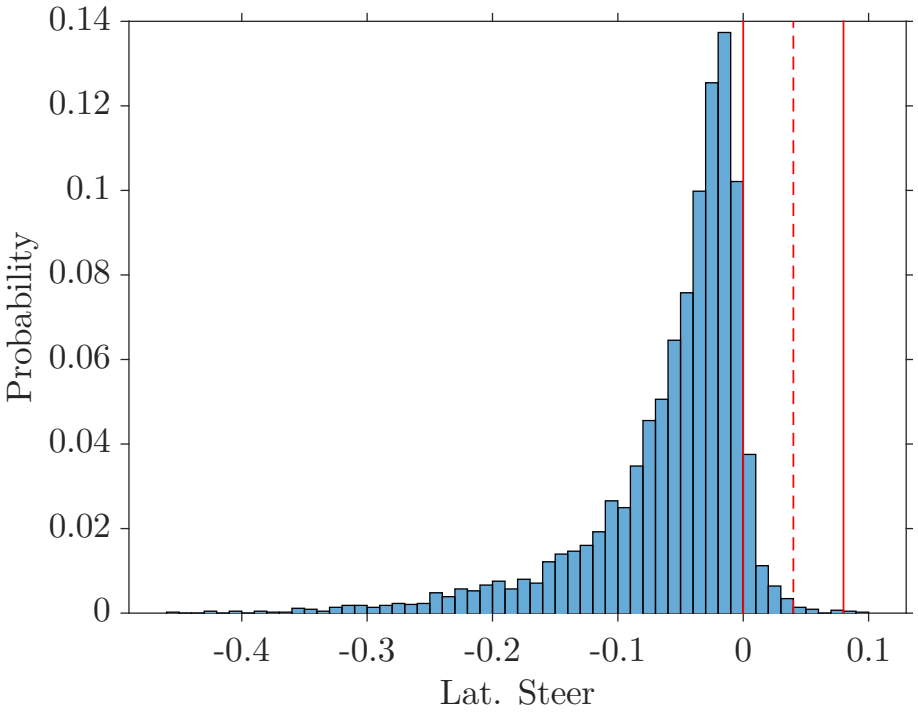

Figure 89: Histogram: Lateral TP Steer.

A.2.8 Lateral TP Camber

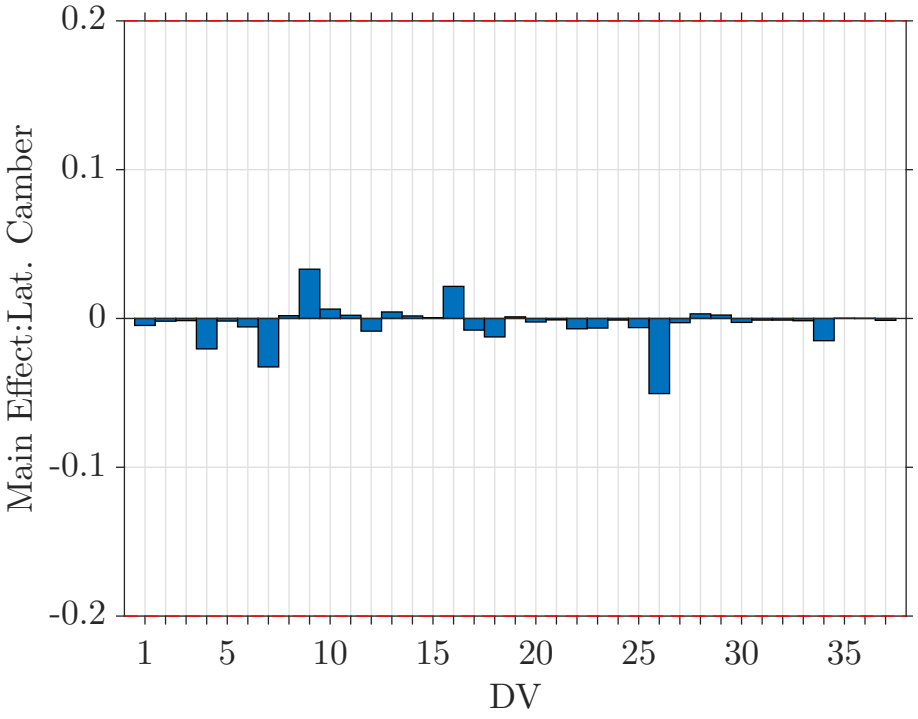

Figure 90: Main Effect: Lateral TP Camber.

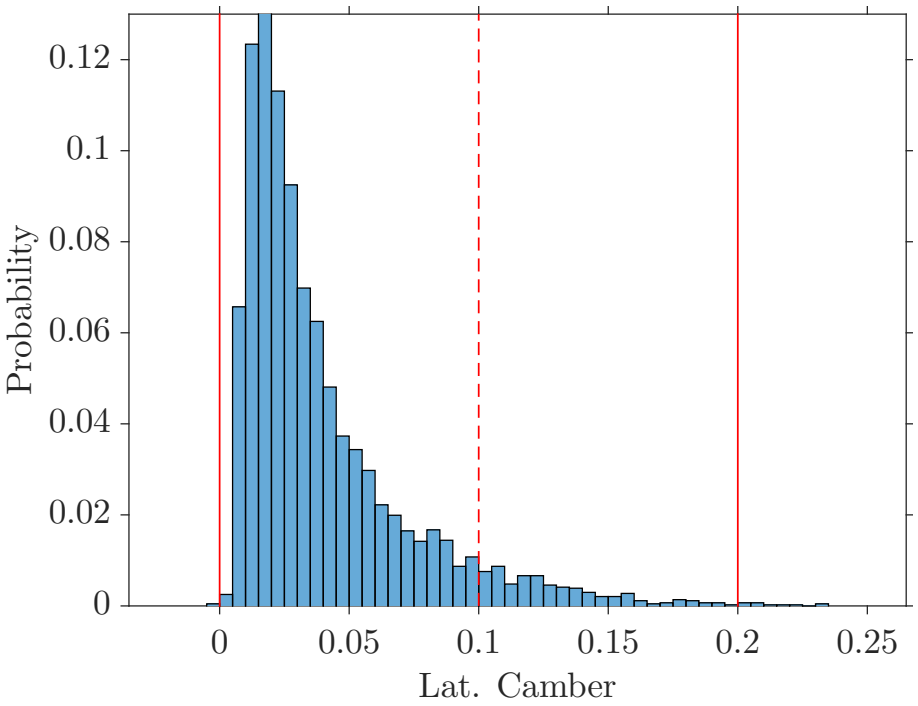

Figure 91: Histogram: Lateral TP Camber.

A.2.9 Longitudinal Compliance

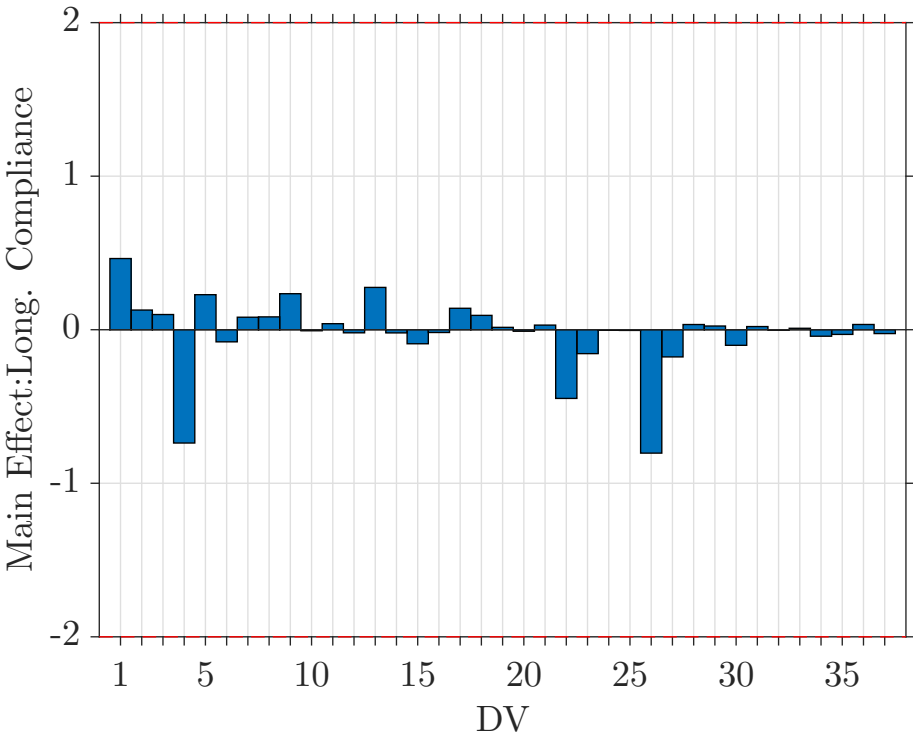

Figure 92: Main Effect: Longitudinal Compliance.

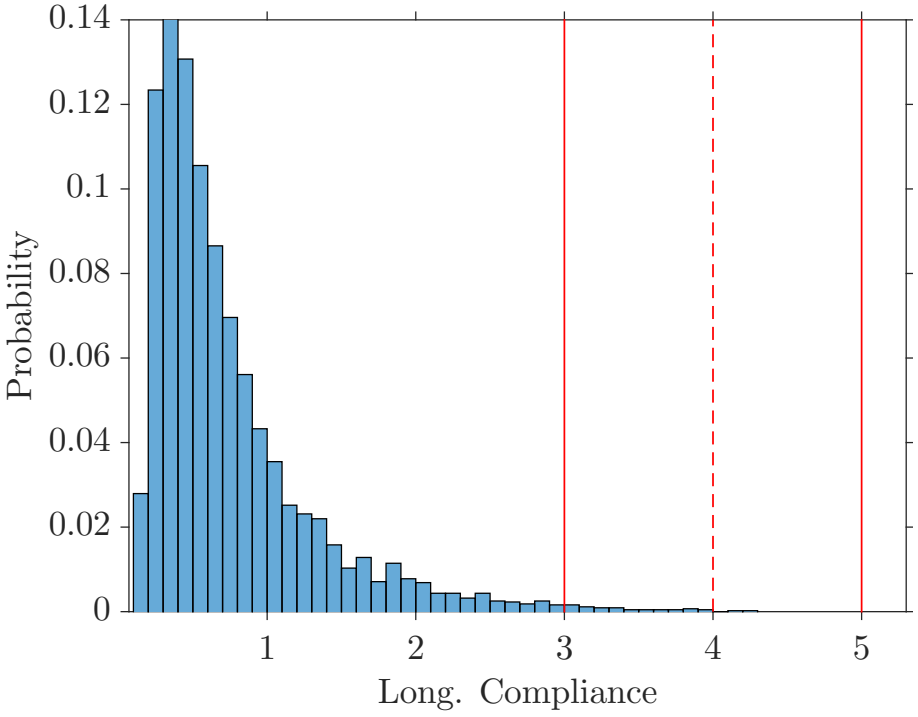

Figure 93: Histogram: Longitudinal Compliance.

A.2.10 Longitudinal Steer

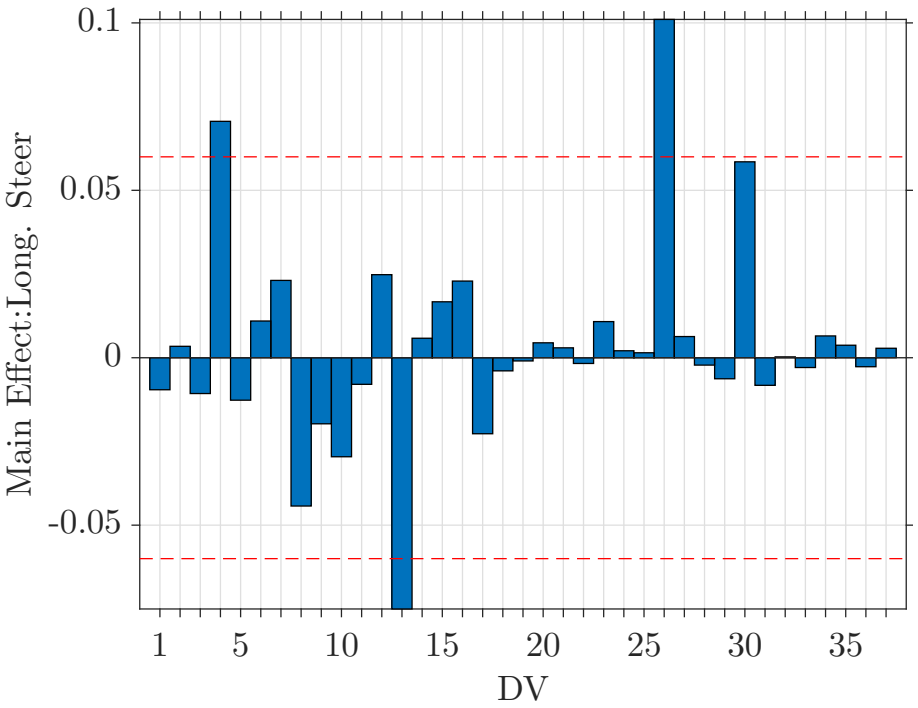

Figure 94: Main Effect: Longitudinal Steer.

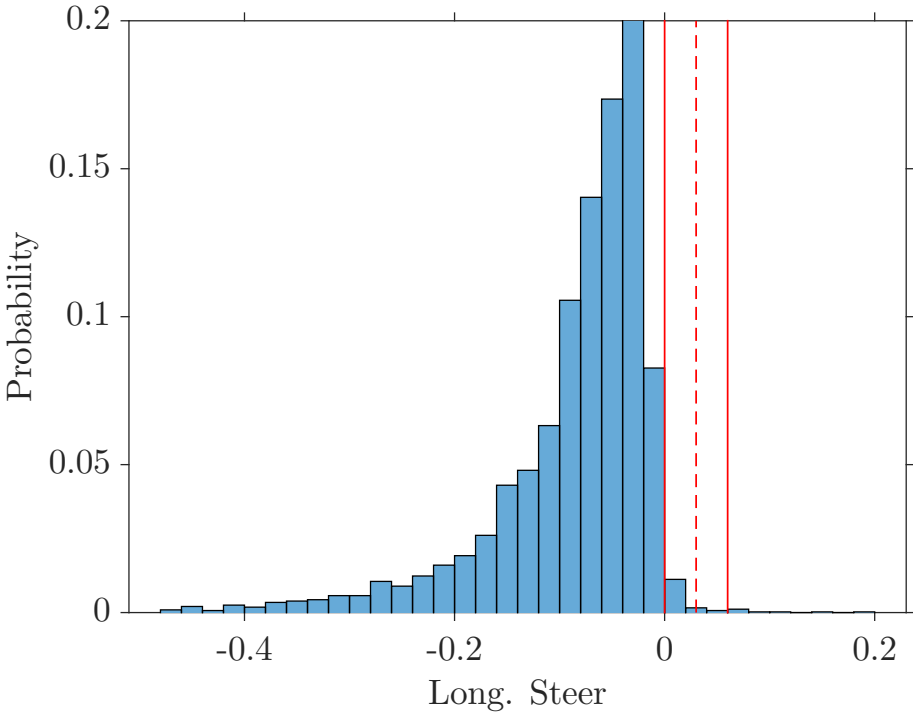

Figure 95: Histogram: Longitudinal Steer.

A.2.11 Longitudinal Camber

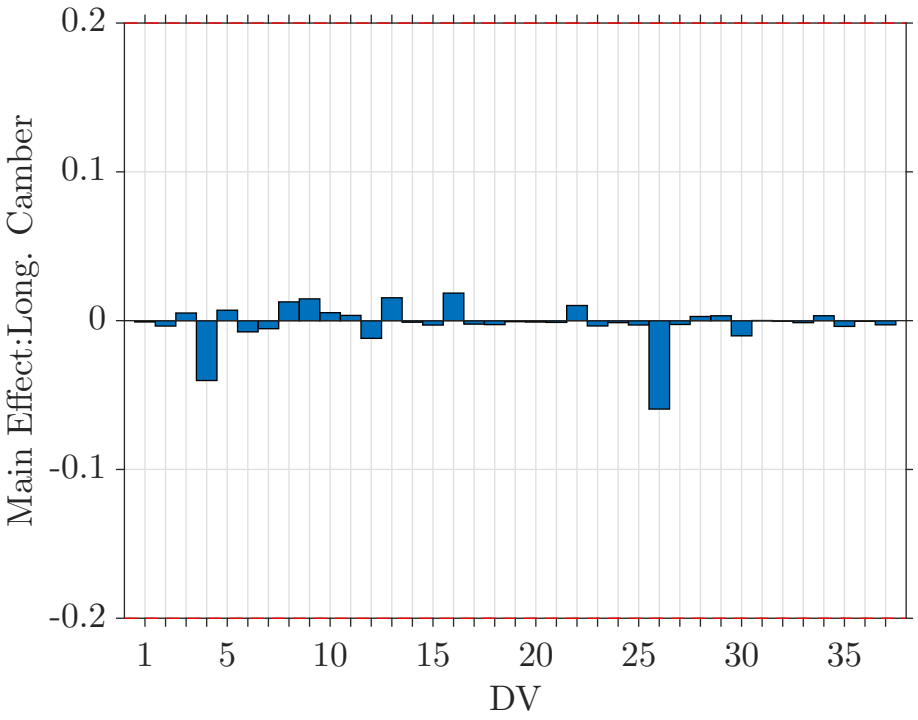

Figure 96: Main Effect: Longitudinal Camber.

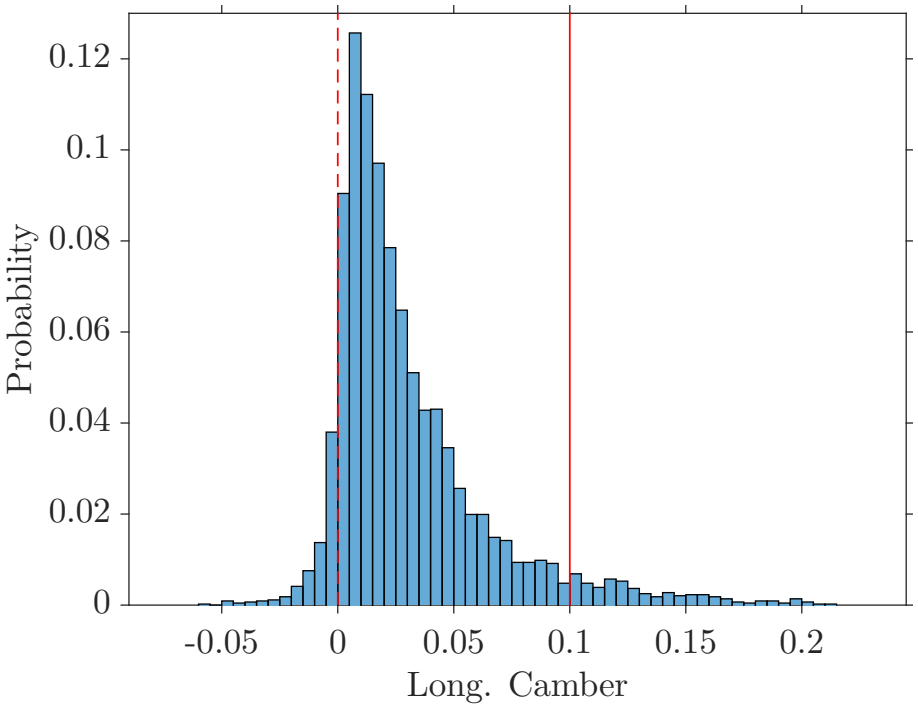

Figure 97: Histogram: Longitudinal Camber.

A.2.12 Overturning Moment Steer

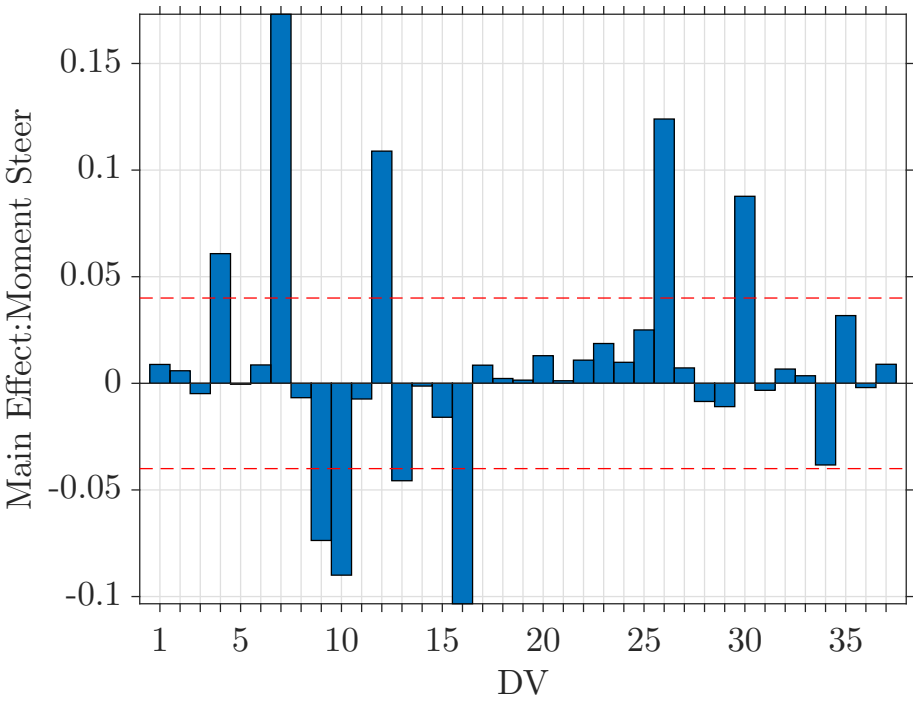

Figure 98: Main Effect: Overturning Moment Steer.

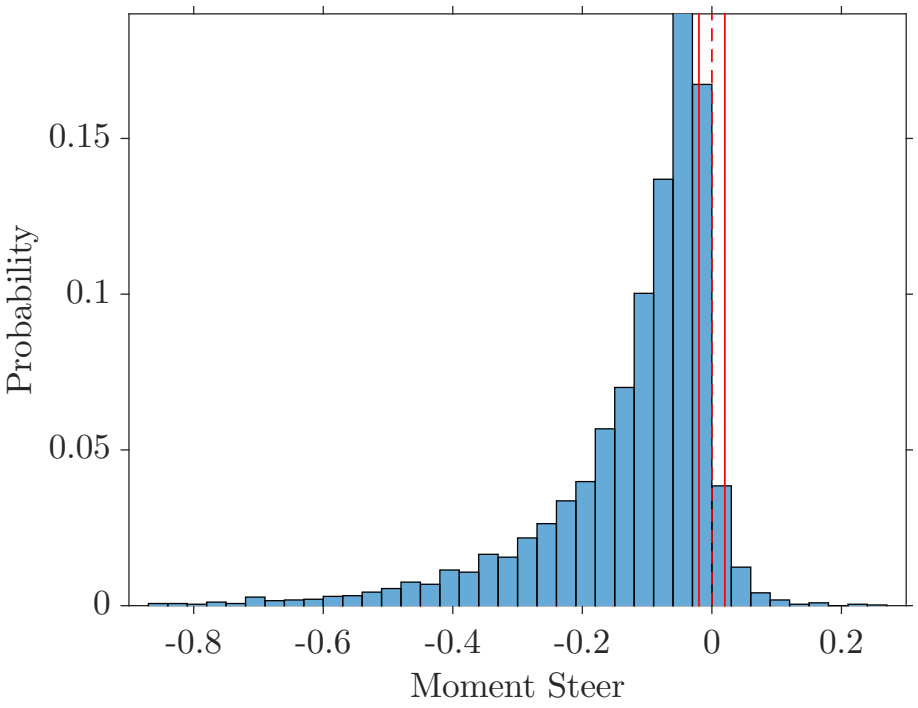

Figure 99: Histogram: Overturning Moment Steer.

A.2.13 Overturning Moment Camber

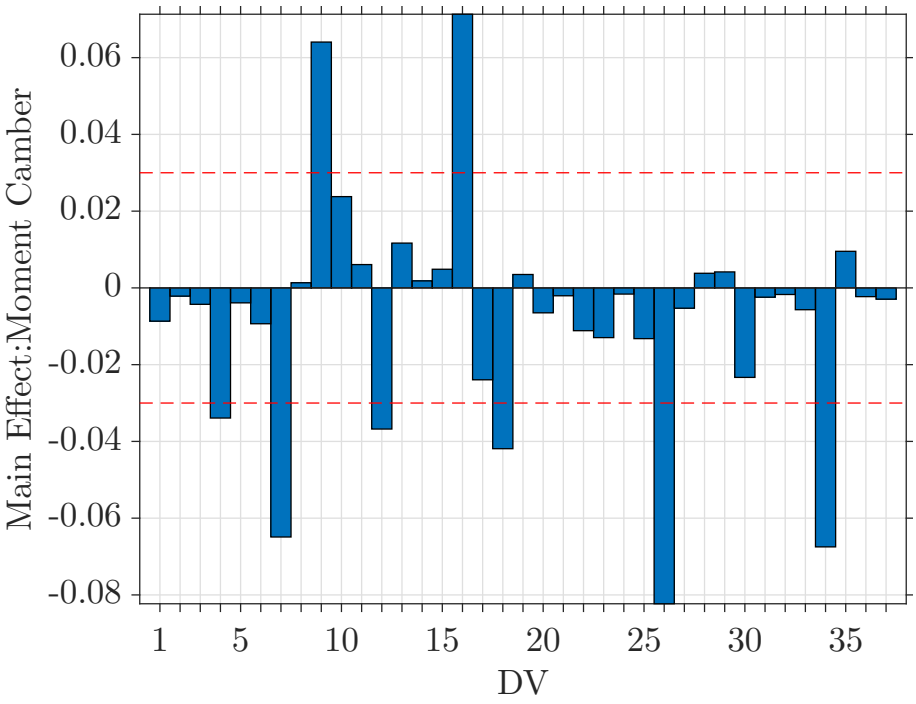

Figure 100: Main Effect: Overturning Moment Camber.

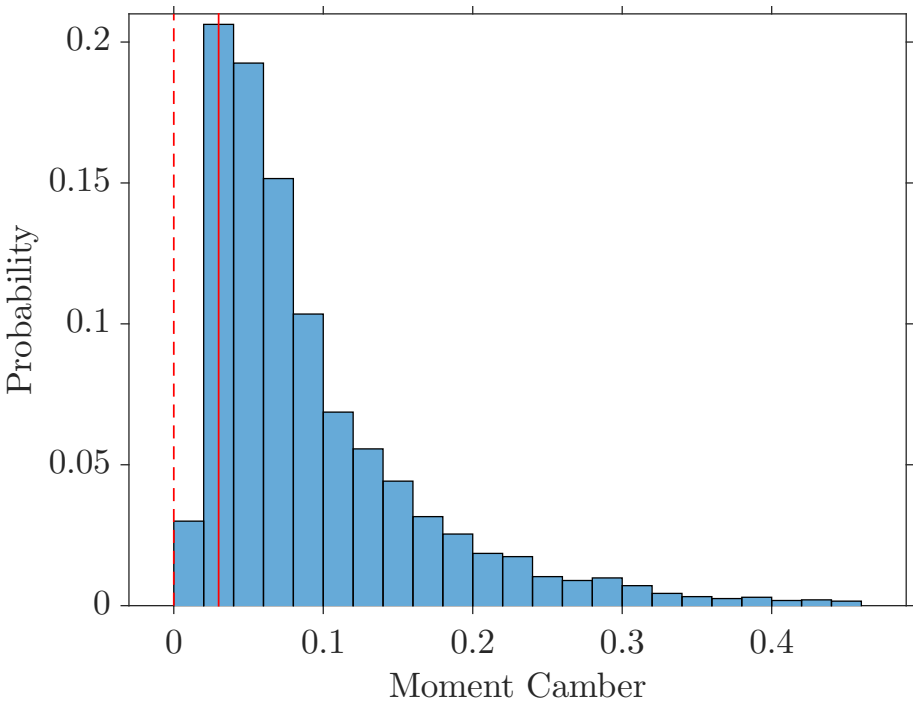

Figure 101: Histogram: Overturning Moment Camber.

A.2.14 Aligning Torque Steer

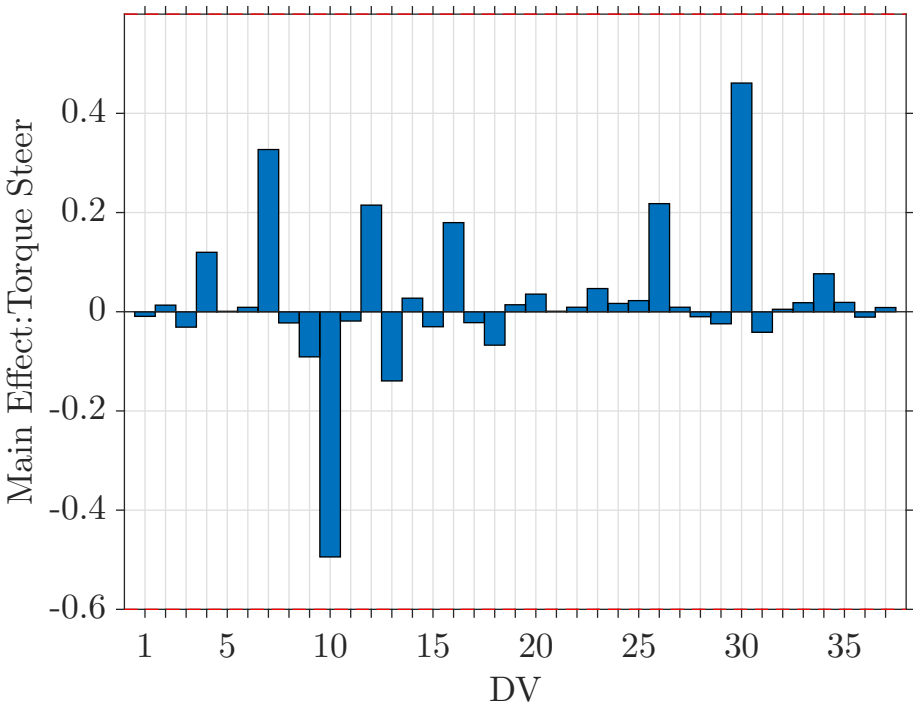

Figure 102: Main Effect: Aligning Torque Steer.

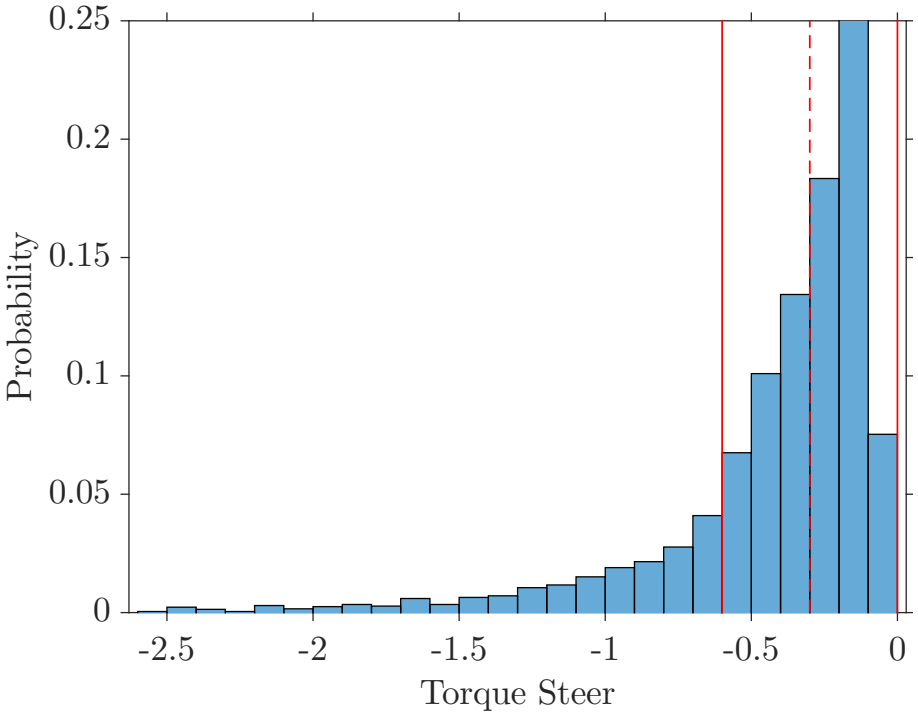

Figure 103: Histogram: Aligning Torque Steer.

Appendix B MATLAB Scripts

B.1 MATLAB Code: Static 1 - stat1.m